

1

## 2 *Response to Review #1*

3 We thank reviewer #1 for the review, the insightful comments to the paper and for his/her  
4 endurance to read the long paper.

5 We will respond to the review point by point. The reviewer's comments are included in bold  
6 italics.

7 ***I think this is a standard paper describing a reanalysis product. It is likely to be useful to***  
8 ***the scientific community; however, it is a bit difficult to read, partly owing to its length.***

9 We appreciate the reviewer's concern that the paper is long. However, we prefer to present  
10 all considered species in one paper because they were produced by the CAMS system in one  
11 combined assimilation experiment.

12 ***The paper should be accepted for publication once the authors address a series of points,***  
13 ***detailed in the specific comments and technical comments. They largely concern***  
14 ***quantification and/or clarification of statements made.***

15 ***Specific comments:***

16 ***L. 32: Indicate why ozone at the surface cannot be improved by the assimilation.***

17 The surface values could potentially be changed by the following processes: (i) direct addition  
18 of observation increments close to the surface, (ii) the impact of non-surface observations or  
19 the observation of other species by means of the model backward error co-variances and (iii)  
20 the downward transport of ozone from levels where the assimilation changed the ozone fields.

21 We think that the impact of any of these three factors was eliminated at the lowest model  
22 levels by the strength of the ozone dry deposition and titration with NO near the surface.

23 CAMSiRA did not assimilate any surface observations nor satellite retrievals for the lower  
24 troposphere. Only total columns and stratospheric profile data were assimilated. The  
25 background error co-variances calculated with the NMC method did not provide enough  
26 impact for strong non-local vertical influence, which would have led to an alteration at  
27 surface. Also, species-to-species back-ground error correlation were not implemented in the  
28 applied 4D-VAR method.

29 We added in the abstract:

30 “ ... because of the strong impact of surface processes such as dry deposition and titration  
31 with nitrogen monoxide (NO), which were both not changed by the assimilation. “

32 We add in the conclusion section when we discussed the reasons for the small influence  
33 (L1147)

34 “ ... nor that the vertical correlations in the model background errors were strong enough to  
35 cause a correction of the surface levels based on the levels above. “

36 ***L. 56: Quantify the “sufficient accuracy”.***

37 We can not quantify this rather general statement but we changed it as follows:

38 “ .. with an accuracy sufficient to have an impact during the assimilation. “

39 ***L. 58: Provide details of the surface properties.***

40 We clarified the statement by replacing “surface properties” with “surface albedo”.

41 ***L. 109: List the key species.***

42 We changed the text as follows:

43 “... the aerosol variables and key chemical species such as ozone, HNO<sub>3</sub>, N<sub>2</sub>O<sub>5</sub>, NO, NO<sub>2</sub>,  
44 PAN and SO<sub>2</sub> only”.

45 ***L. 208: Why did you use scenario 8.5 instead of another one?***

46 The scenario was chosen by the producers of the MACCITY data set (Granier et al. ,2011)

47 We added “... obtained in the MACCity emissions ...”

48 ***L. 286-287: Did you use the averaging kernels for data other than MOPITT? Explain your  
49 choices.***

50 We add

51 “For the ozone retrieval averaging kernels were not used because they were not provided or  
52 did not improve the analysis. For example, the high vertical resolution of the MLS ozone  
53 retrievals in the stratosphere made the use of AK not necessary. “

54

55 ***The L. 291: The data used are flagged “good” or not flagged “bad”?***

56 Yes, this is the case. The retrieval data include a quality flag given by the providers

57 ***L. 375: Does the decrease in the burden indicate a positive result from the assimilation?***

58 Yes, because there is a better agreement with the MOPITT total column retrievals.

59 ***L. 397: Explain in the text why you do not assimilate MOPITT observations over the Arctic.***

60 Larger biases and errors in the retrievals occur at high latitudes because of low thermal  
61 contrast. It is a recommendation by the data providers not to assimilate data in high latitudes.

62 We added: "... because of the higher biases of the MOPITT data in this region."

63 ***L. 451: Why is there only a little effect on the surface? Why are there no changes between***  
64 ***CR and CAMSiRa from the assimilation?***

65 See our response above

66 ***L. 471: Is it reasonable to calculate a linear trend? What assumptions do you make?***

67 It is a valid to comment to question the underlying assumption (i.e. a linearity) for any type of  
68 trend analysis. A detailed trend analysis is beyond the scope of the paper. However, the  
69 linearity of the trend seems not an unreasonable choice when looking at the graphs. Our focus  
70 is the comparison of trends of different data sets using a unified but simple approach.

71 We will add:

72 "... and, for reasons of simplicity, only the linear ..."

73 We also point out that linear trends are often expressed in units of %/yr in the paper. We  
74 concede that this unit is technically not consistent with a linear trend. We obtain the liner  
75 trend as percentage by normalising the linear trend (e.g. Tg/year) with the average of the  
76 quantity over the whole period, i.e. all years.

77 We add at line 361

78 "The linear trend is as expressed as percentage with respect to the mean of the burden over the  
79 whole period."

80 ***L. 516: Provide references for this statement.***

81 We added the following reference:

82 (Eskes et al., 2015).

83 Eskes, H., Huijnen, V., Arola, A., Benedictow, A., Blechschmidt, A.-M., Botek, E., Boucher,  
84 O., Bouarar, I., Chabrillat, S., Cuevas, E., Engelen, R., Flentje, H., Gaudel, A., Griesfeller, J.,  
85 Jones, L., Kapsomenakis, J., Katragkou, E., Kinne, S., Langerock, B., Razinger, M., Richter,  
86 A., Schultz, M., Schulz, M., Sudarchikova, N., Thouret, V., Vrekoussis, M., Wagner, A., and  
87 Zerefos, C.: Validation of reactive gases and aerosols in the MACC global analysis and  
88 forecast system, *Geosci. Model Dev.*, 8, 3523-3543, doi:10.5194/gmd-8-3523-2015, 2015.

89

90 ***L. 523: Is the comparison with MACCRA and CAMSiRA within the errors of these***  
91 ***datasets?***

92 Unfortunately, we cannot provide error estimates of the global burden of the two analysis sets.

93 ***L. 535: Why is there an exaggeration of the sea salt emission?***

94 As pointed out in the supplement, sea salt emissions were close to the median of the AeroCom  
95 models. They were only at the high end of the values given in Boucher et al. (2015)

96 We amend the text as follows:

97 “The simulated sea salt emissions of C-IFS were within the reported range in the literature  
98 (see supplement). This suggests that the loss processes of sea salt were underestimated in C-  
99 IFS in comparison to other models.”

100 ***L. 594: Discuss why this seems unrealistic.***

101 We add the following

102 “ ..., given that the global SO<sub>2</sub> emission are only less than 2% of the total aerosol emissions  
103 (see supplement)”

104 ***L. 662: Quantify the trends. Explain (or remind the reader) how you test for significance.***  
105 ***Same for L. 751 and L. 757.***

106 The significance of the linear trends was estimated at the 95 confidence interval. We now  
107 repeat this information in each section.

108 ***L. 674: Provide further details of the artificial accumulation of sulphate by the***  
109 ***assimilation.***

110 We added:

111 “The increase in sulphate was probably caused by underestimated loss processes for sulphate  
112 and SO<sub>2</sub> in the free and upper troposphere away from the emissions sources. The relative  
113 increase in sulphate with respect to the other aerosol species could not be corrected by the  
114 assimilation of AOD.”

115 *L. 767: Why is this remarkable? Because unexpected? Please avoid subjective comments.*

116 We replace the statement with:

117 “Despite its simplicity, the Cariolle scheme in CR reproduced the...”

118 *L. 852-865: What is the fidelity of the GOZCARDS dataset?*

119 The standard error of the GOZCARDS data set is given as part of the data set. The values of  
120 the error are in the range of 10-20 ppb on the considered region, which is about 1%. However  
121 this error does not reflect biases. As we already mention in the text, the inter-comparison of  
122 different satellite retrievals by Tegtmeier et al. (2013) shows that MLS is biased low above 5  
123 hPa (5-10%) and ACE-FTS is biased high above 10 hPa and biased low below 10 hPa with  
124 respect to the multi-instrument-mean. Since ACE-FTS contributes more to the GOZCARDS  
125 product in this region, we assume that the GOZCAD biases are controlled by the ACE-FTS  
126 biases.

127 We will quantify the biases in the text:

128 “ACE-FTS is biased high (5-10%) above 10 hPa and biased low (5-10%) below 10 hPa  
129 against the median of various retrievals. “

130 We corrected all technical comments.

|131

132

## 133 *Response to Review #2*

134

135 We thank reviewer #2 for the review, the insightful comments to the paper and for his/her  
136 endurance to read the long paper.

137 We will respond to the review point by point. The reviewer's comments are included in bold  
138 italics

139 *Major comments;*

140 *1. An important advantage of this study is the simultaneous analysis of trace gases and*  
141 *aerosols within the same data assimilation framework. However, it is unfortunate that their*  
142 *interactions were not considered in the current setting. More discussions on their potential*  
143 *would still be useful. I suggest discussing this topic in an additional section, for instance,*  
144 *how much changes in trace gas concentration can be expected using the analyzed aerosol*  
145 *fields, and if these changes bring further improvements in the trace gas analysis (and vice*  
146 *versa). Although the paper is already very long, presenting several sensitivity calculation*  
147 *results could be helpful.*

148 We fully agree that interactions between chemistry and aerosol within a data assimilation  
149 frame work is an important topic. However, its study will be more the focus of ongoing and  
150 future work and it is not the result of the work presented here. In the current version of the  
151 manuscript we mention the prospects in the conclusion section (L 1155).

152 In the CAMSiRA (and MACCRA) no interaction between aerosol, chemistry and  
153 meteorology was simulated. The only potential interaction would be the impact of the  
154 tropospheric ozone assimilation on CO and vice versa. As reported in Inness et al. (2015) the  
155 applied system does not show a strong inter-species synergy, in particular as no NO<sub>2</sub>  
156 retrievals were assimilated in CAMSiRA. A further explanation for the lack of synergies is  
157 that no adjoint and tangent linear formulation of the chemistry scheme was applied and that  
158 no species-to-specie background error covariances were considered in our 4D-VAR approach.

159 In the next version of the CAMS system, the impact on assimilated aerosols and ozone in the  
160 radiation scheme, the impact of aerosol on photolysis rates and on some heterogeneous  
161 reaction (N<sub>2</sub>O<sub>5</sub>, HO<sub>2</sub>) will be considered.

162 To clarify that the assimilation system used for the paper does not present these interactions to  
163 a large extent, we add the following statement in section 2.4 (C-IFS data assimilation).

164 “A further potential interaction between the assimilated species could be introduced by the  
165 adjoint and tangent linear representations of the chemical mechanism and the aerosol module  
166 as part of the 4D-VAR approach. The applied tangent linear and adjoint formulation of C-IFS  
167 accounts only for transport processes and not the sources and sinks of atmospheric  
168 composition. Because of this limitation and the lack of aerosol-chemistry-meteorology  
169 feedbacks in the C-IFS version used in this study, interactions among species and with the  
170 meteorology as part of the assimilation are not represented in CAMSiRA. “

171

172 ***2. As the system was developed at meteorological operational centers, the authors may want***  
173 ***to discuss more about the contribution of the CAMS interim reanalysis to meteorological***  
174 ***and climate activities. This discussion would be useful to many readers in understanding***  
175 ***how the composition and aerosol reanalysis will be helpful in wide research fields.***

176 In the current version of the manuscript we mention applications of the re-analysis of  
177 atmospheric composition, such as boundary condition for regional models and trace-gas  
178 climatologies in the introduction and in the conclusions.

179 We can report that new trace-gas climatologies for ozone and aerosol were compiled from  
180 CAMSiRA and implemented in the new cycle of the operational ECMWF NWP model. In  
181 particular the reduced ozone bias in the upper stratosphere and mesosphere led to an improved  
182 skill in temperature forecasts in this region. See  
183 <https://software.ecmwf.int/wiki/display/FCST/Implementation+of+IFS+Cycle+43r1>

184 A report/paper is in preparation but not yet ready to be cited.

185 An other application of CAMSiRA is the analysis of trends, which we demonstrate on the  
186 example of CO surface data (Figure 6). Finally, the evaluation of model runs would be a new  
187 application for AC re-analysis data. However, we would leave it (within the scope of the  
188 paper) to the reader to decide if there is enough confidence that CAMSiRA is well suited for  
189 this purpose.

190 ***3. In Section 3, the differences in CO between the systems are primarily explained by***  
191 ***surface emissions. There could also be clear differences in OH and natural CO sources by***  
192 ***oxidation, which may explain the CO differences.***

193 When discussing the global patterns of the differences between CAMSiRA and CR we  
194 actually come to the conclusion (L 337) that “ ... global chemical loss and production of CO  
195 as well as problems with the large scale transport. ... “ and less the CO emissions itself are  
196 the reason for the biases of the model.

197 We find it difficult to distinguish with the discussed model runs to clarify in detail if  
198 emissions and distribution of CO precursor species such as VOCs and CH<sub>4</sub> or a reduced CO  
199 lifetime because of higher OH values are more likely the reasons for the identified CO biases.  
200 In any case we conclude that the CO emissions are not the sole reason for the CO biases.

201 We mention this in the conclusion of the paper (L 1128) but will refine the statement to:

202 “However, the rather zonally homogeneous CO differences between CR and CAMSiRA  
203 suggest that not only biases in the fire emissions but also of the CO lifetime and chemical  
204 production as well as the CO transport need to be investigated further. “

205

206 *Specific comments:*

207 ***L. 394: “Owing to the hemispheric...”. This sentence is not clear.***

208 We reformulate as follows:

209 “Because of the hemispheric influence, i.e. the hemispheric reduction in CO, the CO trend in  
210 CR over Eastern China became negative in the middle troposphere.”

211

212 ***L.404-407: It is surprising that, even after correcting the concentration by data  
213 assimilation, the influence of different emission data is so large. Does this mean that the  
214 observational constraints are insufficient to remove the influence of a priori model errors?  
215 Further discussions would be helpful.***

216 In the current approach the surface emissions are not changed by the assimilation of CO  
217 observations. This has been identified as a topic for future developments in the conclusions  
218 (see L 1185).

219 The missing total agreement with the observations at the time of the analysis is also caused by  
220 the relative size of the observation and background error statistic. The background error for  
221 CO is calculated using an ensemble of forecasts, which only accounts for the variability in the



222 transport (winds) and not for the uncertainty of the emissions. The background error at the  
223 surface is therefore most likely underestimated leading to an “over-confidence” in the model  
224 as part of the assimilation process.

225 We will add at line (L 274, Section C-IFS data assimilation)

226 “However, the ensemble did not account for the uncertainty of the emissions, which leads to  
227 an underestimation of the background error for CO.”

228 And we will add in the section on recommendations (L 1187)

229 “A promising development is to enable the correction of emissions with the C-IFS data  
230 assimilation system based on observations of atmospheric composition. This could also  
231 improve the analysis of tropospheric ozone as ozone precursor emissions would be corrected.  
232 An intermediate step in this direction is to better account for the emission uncertainty in the  
233 model background error statistics. “

234 ***L. 437-440: How does the bias vary with year?***

235 The data coverage of the MOZAIC/IAGOS data varies a lot so that a robust conclusion for the  
236 year-to-year variability would be difficult to obtain. However, we discuss the agreement of  
237 the trends for surface CO observations in section 3.4. and show a good correspondents in the  
238 observed, modelled (CR) and assimilated trends (CAMSiRA).

239 A conclusion of the discussion of the inter-annual variability of the CO burdens (section 3.2)  
240 over Europe and North-America is that there is better agreement between CR and CAMSiRA  
241 at the end of the period. This could indicate that the biases of the anthropogenic emissions  
242 decrease from 2003 to 2015.

243 ***L. 798-799: “However, the change of...” This sentence is not clear***

244 We reformulate as follows:

245 “It is not caused by the change of the assimilated MLS version (from V2 to V3.4) because this  
246 took place already at the beginning of 2013 (see Table 2).”

247

248 ***L. 1008-1010: How long was the spin-up period?***

249 The MACCRA was started on the 1.12.2002 (Inness et al. 2013)

250 We add “ ...and the short spin-up period of only 1 month”

251

252

253

255 **The CAMS interim Reanalysis of Carbon Monoxide, Ozone**  
256 **and Aerosol for 2003–2015**

257 **J. Flemming<sup>1</sup>, A. Benedetti<sup>1</sup>, A. Inness<sup>1</sup>, R. Engelen<sup>1</sup>, L. Jones<sup>1</sup>, V. Huijnen<sup>2</sup>, S.**  
258 **Remy<sup>3</sup>, M. Parrington<sup>1</sup>, M. Suttie<sup>1</sup>, A. Bozzo<sup>1</sup>, V.-H. Peuch<sup>1</sup>, D. Akritidis<sup>4</sup> and E.**  
259 **Katragkou<sup>4</sup>**

260 [1] European Centre for Medium-Range Weather Forecasts, Reading, UK

261 [2] Royal Netherlands Meteorological Institute, De Bilt, The Netherlands

262 [3] Laboratoire de météorologie dynamique, UPMC/CNRS, Paris, France

263 [4] Department of Meteorology and Climatology, Aristotle University of Thessaloniki, School  
264 of Geology, Thessaloniki, Greece

265

266

267

268 Correspondence to: J. Flemming (Johannes.Flemming@ecmwf.int)

269

270

271

272

273

274 **Abstract**

275 A new global reanalysis data set of atmospheric composition (AC) for the period 2003–2015  
276 has been produced by the Copernicus Atmosphere Monitoring Service (CAMS). Satellite  
277 observations of total column (TC) carbon monoxide (CO) and aerosol optical depth (AOD) as  
278 well as several TC and profile observation of ozone have been assimilated with the Integrated  
279 Forecasting System for Composition (C-IFS) of the European Centre for Medium-Range  
280 Weather Forecasting. Compared to the previous MACC reanalysis (MACCRA), the new  
281 CAMS interim reanalysis (CAMSiRA) is of a coarser horizontal resolution of about 110 km  
282 compared to 80 km but covers a longer period with the intent to be continued to present day.  
283 This paper compares CAMSiRA against MACCRA and a control experiment (CR) without  
284 assimilation of AC retrievals. CAMSiRA has smaller biases than CR with respect to  
285 independent observations of CO, AOD and stratospheric ozone. However, ozone at the  
286 surface could not be improved by the assimilation because of the strong impact of surface  
287 processes such as dry deposition and titration with nitrogen monoxide (NO), which were both  
288 not changed by the assimilation. –The assimilation of AOD led to a global reduction of sea  
289 salt and desert dust as well as an exaggerated increase in sulphate. Compared to MACCRA,  
290 CAMSiRA had smaller biases for AOD, surface CO and TC ozone as well as for upper  
291 stratospheric and tropospheric ozone. Finally, the temporal consistency of CAMSiRA was  
292 clearly better than the one of MACCRA. This was achieved by using a revised emission data  
293 set as well as by applying a careful selection and bias-correction of the assimilated retrievals.  
294 CAMSiRA is therefore better suited than MACCRA for the study of inter-annual variability  
295 than MACCRA as demonstrated for trends in surface CO.

296

## 297 1 Introduction

298 Exploiting the multitude of satellite observations of atmospheric composition (AC) is a key  
299 objective of the Copernicus Atmosphere Monitoring Service (CAMS). For its global  
300 component CAMS uses the four-dimensional variational (4D-VAR) data assimilation  
301 technique to combine satellite observations with chemistry-aerosol modelling to obtain a  
302 gridded continuous representation (analysis) of the mass mixing ratios of atmospheric trace  
303 gases and aerosols.

304 The global CAMS system is built on the heritage of the EU-funded GEMS (Hollingsworth et  
305 al., 2008) and series of MACC projects at the European Centre for Medium-Range Weather  
306 Forecasts (ECMWF). During these projects the Integrated Forecasting System (IFS) of  
307 ECMWF was extended by modules for atmospheric chemistry, aerosols and greenhouse gases  
308 in such a way that the 4D-VAR data assimilation system, which had been developed for the  
309 analysis of the meteorological fields, could be used for the assimilation of AC retrievals.

310 Assimilating satellite AC retrievals into an AC model has advantages to the sole use of the  
311 AC retrievals because of their specific limitations. First, only a small subset of the trace gases  
312 or only total aerosol is directly observable with an accuracy sufficient to have an impact  
313 during the assimilation. ~~sufficient accuracy.~~ Second, AC satellite retrievals have incomplete  
314 horizontal coverage because of the orbital cycle, viewing geometry, the presence of clouds  
315 and other factors such as surface albedo properties. Third, the vertical distribution of the trace  
316 species can often not or only rather coarsely be retrieved from the satellite observations, while  
317 the measurement sensitivity towards the surface is generally low.

318 The AC analyses are used to (i) initialise AC model forecasts and (ii) for the retrospective  
319 analysis (reanalysis) of AC for air quality and climate studies. The reanalysis of the  
320 meteorological fields has been an important activity at ECMWF (ERA-40, Uppala et al.,  
321 2005, ERA interim Dee et al., 2011) and other meteorological centres such as NCEP (CFSR,  
322 Saha et al., 2010, JMA (JRA-55, JRA-25, Onogi et al., 2007) and NASA/DAO (MERRA,  
323 Rienecker, et al., 2011). An important application of these reanalysis data sets is the  
324 estimation of the inter-annual variability and the trends of climate variables over the last  
325 decades up to the present day. The complete spatial and temporal coverage makes the trend  
326 analysis of reanalyses more robust and universal than the trend analysis of individual  
327 observing systems. However, constructing a data set which is suited for this purpose is a  
328 complex task because of the developing and changing observing system, which can introduce

329 spurious trends and sudden shifts in the reanalysis data record. Careful quality control of the  
330 assimilated observations and techniques (e.g. Dee et al., 2004) to address inter-instrument  
331 biases are applied to mitigate this problem.

332 Most meteorological reanalyses contain stratospheric ozone but other trace gases, apart from  
333 water vapour, are not included. In the last decade chemical and aerosol data assimilation has  
334 matured (Bocquet et al., 2015) and dedicated reanalysis data sets for AC have emerged. The  
335 Multi-Sensor-Reanalysis of total ozone (van der A et al., 2015) for 1970–2012 used ground  
336 based Brewer observations to inter-calibrate satellite retrievals. The MERRAero reanalysis  
337 (2002–present, <http://gmao.gsfc.nasa.gov/reanalysis/merra/MERRAero/>) assimilated AOD  
338 retrievals from the two Moderate Resolution Imaging Spectroradiometer (MODIS)  
339 instruments in the GOCART aerosol module of the GEOS-5 model system using the  
340 meteorological variables of the MERRA meteorological analysis. Its next version, the  
341 MERRA2 reanalysis, is a joint meteorological and aerosol reanalysis covering the period  
342 from 1979 to present. Miyazaki et al. (2015) put together a tropospheric chemistry reanalysis  
343 using a Kalman filter approach for the years 2005–2012. They use the CHASER Chemical  
344 transport model (CTM) to assimilate retrievals of tropospheric ozone and CO profiles, NO<sub>2</sub>  
345 tropospheric columns and HNO<sub>3</sub> stratospheric columns. Their approach tackles two specific  
346 challenges of AC data assimilation. First, they not only correct atmospheric concentrations  
347 but also alter the surface emissions which control the tracer distributions to a large extent.  
348 Second, the Kalman filter develops co-variances of the errors between observed and un-  
349 observed species, which are used to correct un-observed species based on the observations  
350 increments.

351 The MACC reanalysis (MACCRA) of reactive gases (Inness et al., 2013) and aerosols for the  
352 period 2003–2012 is an AC reanalysis that covers tropospheric and stratospheric reactive  
353 gases and aerosols as well as the meteorological fields in one consistent data set. MACCRA  
354 has proved to be a realistic data set as shown in several evaluation studies for reactive gases  
355 (Elguindi et al., 2010, Inness et al., 2013, Katragkou et al., 2015 and Gaudel et al., 2015) and  
356 aerosols (Cesnulyte et al., 2014 and Cuevas et al., 2015, ). MACCRA is widely used, for  
357 example, as boundary condition for regional models (Schere et al., 2012, Im et al., 2014,  
358 Giordano et al., 2015), to construct trace gas climatologies for the IFS radiation schemes  
359 (Bechtold et al., 2009), to estimate aerosol radiative forcing (Bellouin et al., 2013), as input to

360 solar radiation schemes for solar energy applications and to report the current state of aerosol  
361 and CO as part of the climate system (Benedetti et al., 2014., Flemming and Inness, 2014).

362 CAMS is committed to produce a comprehensive high-resolution AC reanalysis in the next  
363 years. The CAMS interim Reanalysis (CAMSiRA) presented here has an interim status  
364 between MACCRA and this planned analysis data set. It was produced at a lower horizontal  
365 resolution (110 km) than the resolution of MACCRA (80 km), and the number of archived  
366 AC fields was limited to the aerosol variables and selected chemical species such as ozone,  
367 HNO<sub>3</sub>, N<sub>2</sub>O<sub>5</sub>, NO, NO<sub>2</sub>, PAN and SO<sub>2</sub>selected key species only.

368 The reasons for producing CAMSiRA before the more comprehensive reanalysis are as  
369 follows: The MACCRA for reactive gases was produced using a coupled system consisting of  
370 the IFS and the MOZART-3 (Kinnison et al., 2007) chemical transport model (CTM) as  
371 described in Flemming et al. (2009). This coupled system was replaced by the much more  
372 computationally efficient on-line coupled model C-IFS (Flemming et al., 2015), which uses  
373 the chemical mechanism CB05 of the TM5 CTM (Huijnen et al., 2010). With the  
374 discontinuation of the coupled system it was not possible to extend the MACC reanalysis to  
375 the present day. For the AC monitoring service of CAMS it is however important to be able to  
376 compare the present conditions with previous years in a consistent way. Another motivation  
377 for producing CAMSiRA was that the aerosol module used for the MACCRA had undergone  
378 upgrades (Morcrette et al., 2011) in recent years. Finally, MACCRA suffered from small but  
379 noticeable shifts because of changes in the assimilated observations, the emission data and the  
380 bias correction approach. These spurious shifts undermine the usefulness of the MACCRA for  
381 the reliable estimation of trends. The lessons learnt from the evaluation of CAMSiRA will  
382 feed into the setup of the planned CAMS reanalysis.

383 Reanalyses of AC are generally less well-constrained by observations than meteorological  
384 reanalyses because of the aforementioned limitations of the AC observations and because of  
385 the strong impact of the emission, which are in many cases not constrained by observations. It  
386 is therefore good scientific practice to investigate the impact of the AC assimilation by  
387 comparing the AC reanalysis to a control experiment that did not assimilate AC observations.  
388 The control run (CR) to CAMSiRA was carried out using the same emission data as well as  
389 the meteorological fields produced by CAMSiRA.

390 The purpose of this paper is firstly to document the model system, the emissions and the  
391 assimilated observations used to produce CAMSiRA, and to highlight the differences to the

392 setup of the MACCRA. As the emissions are an important driver for variability of AC, a  
393 presentation of the totals and the inter-annual variability of the emission data used in  
394 CAMSiRA and CR is given in a supplement to the paper.

395 In the remainder of the paper, CO, aerosol as well as tropospheric and stratospheric ozone of  
396 CAMSiRA, CR and MACCRA are inter-compared and evaluated with independent  
397 observations in a separate section for each species. The comparison of CAMSiRA with  
398 MACCRA has the purpose to report progress and issues of CAMSiRA for potential users of  
399 the data sets. The comparison of CAMSiRA with CR shows the impact of the data  
400 assimilation and is helpful to better understand deficiencies of the C-IFS model and its input  
401 data.

402 Each section starts with a discussion of the spatial differences of CAMSiRA, CR and  
403 MACCRA of the considered species. Next, the temporal variability is investigated using time  
404 series of monthly mean values averaged over selected regions. We present global burdens and  
405 discuss changes in the speciation of the aerosol fields introduced by the assimilation. Finally,  
406 the three data sets are compared against independent observations, which were not used in the  
407 assimilation. A summary and recommendations for future AC reanalysis will be given in the  
408 last section.

409



## 410 **2 Description of CAMSiRA setup**

### 411 **2.1 Overview**

412 CAMSiRA is a data set of 6 hourly reanalyses of AC for the period 2003–2015. A 3 hourly  
413 data set consistent with the AC analysis is available from forecasts linking the analyses. The  
414 horizontal resolution is about 110 km on a reduced Gaussian grid (T159) and the vertical  
415 discretisation uses 60 levels from the surface to a model top of 0.1 hPa. Total columns of CO  
416 (TC CO) of the Measurements Of Pollution In The Troposphere (MOPITT) instrument,  
417 MODIS AOD and several ozone TC and stratospheric profile retrievals (see Table 2) were  
418 assimilated together with meteorological in-situ and satellite observations.

419 The description of MACCRA for reactive gases can be found in Inness et al. (2013).  
420 Important commonalities and differences between the two AC reanalyses are given in Table  
421 1.

422 The control run is a forward simulation of C-IFS in monthly segments. The meteorological  
423 simulation is relaxed using the approach by Jung et al. (2008) to the meteorological reanalysis  
424 produced by the CAMSiRA. The emission input fields are the same as used for CAMSiRA.

### 425 **2.2 C-IFS model**

426 The model C-IFS is documented and evaluated in Flemming et al. (2015). C-IFS applies the  
427 chemical mechanism CB05, which describes tropospheric chemistry with 55 species and 126  
428 reactions. Stratospheric ozone chemistry in C-IFS is parameterized by the “Cariolle-scheme”  
429 (Cariolle and Dèquè, 1986 and Cariolle and Teyssède, 2007). Chemical tendencies for  
430 stratospheric and tropospheric ozone are merged at an empirical interface of the diagnosed  
431 tropopause height in C- IFS. C-IFS benefits from the detailed cloud and precipitation physics  
432 of the IFS for the calculation of wet deposition and lightning NO emission. Wet deposition  
433 modelling for the chemical species is based on Jacob (2000) and accounts for the sub-grid  
434 scale distribution of clouds and precipitation. Dry deposition is modelled using pre-calculated  
435 monthly-mean dry deposition velocities following Wesely (1989) with a superimposed  
436 diurnal cycle. Surface emissions and dry deposition fluxes are applied as surface boundary  
437 conditions of the diffusion scheme. Lightning emissions of NO were calculated based on  
438 convective precipitation (Meijer et al., 2001).

439 The aerosol module (Morcrette et al., 2009) is a bulk/bin scheme simulating desert dust, sea  
440 salt at 80% relative humidity (RH), hydrophilic and hydrophobic organic carbon and black  
441 carbon as well as sulphate aerosol based on the LMDZ aerosol model (Reddy et al., 2005).  
442 Sea salt and desert dust are represented in 3 size-bins. The radii ranges of the dust bins are  
443 0.030–0.55, 0.55–0.9 and 0.9–20  $\mu\text{m}$  (DD1, DD2, and DD3) and of the sea salt at 80% RH  
444 bins 0.03–0.5, 0.5–5 and 5–20  $\mu\text{m}$  (SS1, SS2, and SS3). There is no consideration of the  
445 aerosol growth, which would transfer aerosol mass from one size bin to another. Hygroscopic  
446 growth of hydrophilic species is taken into account in the computation of the aerosol optical  
447 properties only. Following the emission release, the aerosol species are subject to wet and dry  
448 deposition and the largest size bins of sea salt and dust also to sedimentation. The chemical  
449 source of sulphate is modelled by climatological conversion rates using a  $\text{SO}_2$  tracer, which is  
450 independent of the  $\text{SO}_2$  simulated in CB05. The  $\text{SO}_2$  tracer is driven by prescribed  $\text{SO}_2$  and  
451 DMS emissions. Its loss is simulated by wet and dry deposition as well as the climatological  
452 chemical conversion to  $\text{SO}_4$ .

453 The aerosol and chemistry modules used to simulate source and sink terms are not coupled.  
454 Also, wet and dry deposition are modelled with different parameterisations but with the same  
455 meteorological input such as precipitations fields. Aerosol and chemistry have in common  
456 that they are advected and vertically distributed by diffusion and convection in the same way.  
457 A proportional mass fixer as described in Diamantakis and Flemming (2014) is applied for all  
458 tracers in C-IFS.

### 459 **2.3 Emission data sets**

460 This section only references the origin of the emission data. The emitted totals and the linear  
461 trends of the anthropogenic, biomass burning and natural emissions as well as the modelled  
462 desert dust and sea salt emissions used in CAMSiRA and CR are presented in a supplement.

463 The anthropogenic surface emissions for the chemical species were taken from the MACCity  
464 inventory (Granier et al., 2011), which covers the period 1960–2010. MACCity emissions are  
465 based on the ACCMIP (Lamarque et al., 2013) inventory but have improved seasonal  
466 variability. The changes from 2000–2005 and for 2010 are obtained [in the MACCity data](#)  
467 using the representative concentration pathways (RCP) scenarios version 8.5. For the  
468 production of CAMSiRA the MACCity data set was extended to 2015 by also applying the  
469 RCP 8.5 scenario. The anthropogenic CO emissions were increased following Stein et al.

470 (2014). Time series of the anthropogenic CO emissions for Europe, North America, East Asia  
471 (see Table 3) and the globe are shown in Figure S2 of the supplement.

472 The anthropogenic emissions of organic matter, black carbon and aerosol precursor SO<sub>2</sub> are  
473 retrieved from AEROCOM data base, which is compiled using EDGAR and SPEW data  
474 (Dentener et al., 2006). In contrast to the anthropogenic gas emissions, the aerosol  
475 anthropogenic emissions did not account for trends but only for the seasonal cycle.

476 The biogenic emissions for the chemical species were simulated off-line by the MEGAN2.1  
477 model (Guenther et al., 2006) for the 2000–2010 period (MEGAN-MACC, Sindelarova et al.,  
478 2014). For the remaining years 2011–2015 a climatology of the MEGAN-MACC data was  
479 put together. Natural emissions from soils and oceans for NO<sub>2</sub>, DMS and SO<sub>2</sub> were taken  
480 from [Precursors of ozone and their Effects in the Troposphere \(POET\)](#) database for 2000  
481 (Granier et al., 2005; Olivier et al., 2003).

482 Daily biomass burning emissions for reactive gases and aerosols were produced by the Global  
483 Fire Assimilation System (GFAS) version 1.2, which is based on satellite retrievals of fire  
484 radiative power (Kaiser et al., 2012). This is an important difference with respect to the  
485 MACCRA, which used an early version of the GFED 3.1 data from 2003 until the end 2008  
486 and daily GFAS v1.0 data from 2009 to 2012. The GFED 3.1 is on average 20% lower than  
487 GFAS v1.2 (Inness et al., 2013). Time series of the biomass burning CO emissions for  
488 Tropical Africa, South America and Maritime South East Asia (see Table 3) and the globe are  
489 shown in Figure S3 of the supplement.

## 490 **2.4 C-IFS data assimilation**

491 C-IFS uses an incremental 4D-VAR algorithm (Courtier et al., 1994), which minimizes a cost  
492 function for selected control variables to combine the model and the observations in order to  
493 obtain the best possible representations of the atmospheric fields. The mass mixing ratios of  
494 O<sub>3</sub>, CO and total aerosol are incorporated into the ECMWF variational analysis as additional  
495 control variables and are minimized together with the meteorological control variables. The  
496 assimilation of satellite retrieval of the chemical species and total aerosol optical depth is  
497 documented in Inness et al. (2015) and Benedetti et al. (2009). The assimilation of aerosol  
498 differs from the assimilation of CO and ozone because only the total aerosol mass can be  
499 constrained by the observations and information about the speciation must be obtained from  
500 the model.

501 The assimilation of AOD retrievals uses an observation operator that translates the aerosol  
502 mass mixing ratios and humidity fields of C-IFS to the respective AOD (550 nm) values using  
503 pre-computed optical properties. Total aerosol mass mixing ratio is included in the 4D-VAR  
504 cost function and the analysis increments are repartitioned into the individual aerosol  
505 components according to their fractional contribution to the total aerosol mass. This is an  
506 approximation which is assumed to be only valid over the 12 hour of the assimilation  
507 window. In reality, the relative fraction of the aerosol components is not conserved during the  
508 whole assimilation procedure because of differences in the efficiency of the removal  
509 processes. Aerosol components with a longer atmospheric lifetime will retain relatively longer  
510 the change imposed by the increments and may thereby change the relative contributions.

511 ~~The background error statistics for the chemical species and for total aerosol are univariate in~~  
512 ~~order to minimize the feedback effects of the chemical fields on the meteorological variables.~~  
513 ~~Correlations between the background errors of different chemical species are also not~~  
514 ~~accounted for (Inness et al., 2015).~~

515 In the ECMWF data assimilation system the background error covariance matrix is given in a  
516 wavelet formulation (Fisher, 2004, 2006). This allows both spatial and spectral variations of  
517 the horizontal and vertical background error covariances. The background errors for AC are  
518 constant in time.

519 The background errors for ozone are the same as the ones used for MACCRA (Inness et al.,  
520 2013). Only the vertical correlations of the ozone background errors have been modified and  
521 restricted to  $\pm 5$  levels around a model level, to avoid correlations between the lower  
522 troposphere and upper tropospheric and stratospheric levels that affected near-surface ozone  
523 adversely. The background errors of total aerosol for both MACCRA and CAMSiRA were  
524 calculated using the method described in Benedetti and Fisher (2008). The aerosol  
525 background errors for CAMSiRA were updated using a more recent C-IFS model version.  
526 The background errors for CO are newly calculated for the CAMSiRA from an ensemble of  
527 C-IFS forecast runs (Inness et al., 2015). However, the ensemble did not account for the  
528 uncertainty of the emissions, which leads to an underestimation of the background error. This  
529 may limit the correcting impact of the observations in the assimilation process.

530 The background error statistics for the chemical species and for total aerosol are univariate in  
531 order to minimize the feedback effects of the chemical fields on the meteorological variables.

532 Correlations between the background errors of different chemical species are also not  
533 accounted for (Inness et al., 2015).

534 A further potential interaction between the assimilated species could be introduced by the  
535 adjoint and tangent linear representations of the chemical mechanism and the aerosol module  
536 as part of the 4D-VAR approach. The applied tangent linear and adjoint formulation of C-IFS  
537 accounts only for transport processes and not the sources and sinks of atmospheric  
538 composition in this study. Because of this limitation and the lack of aerosol-chemistry-  
539 meteorology feedbacks in C-IFS, interaction among species and with the meteorology as part  
540 of the assimilation procedure are not represented in CAMSiRA.

## 543 **2.5 Assimilated observations**

544 Table 2 shows the AC composition data sets for CO, ozone and AOD that were assimilated in  
545 CAMSiRA. The time line of the assimilation for the different retrievals is shown in Figure 1.  
546 CO is assimilated from MOPITT V5 TIR only whereas the MACCRA assimilated the V4 TIR  
547 product and additionally IASI TC CO retrievals after April 2008. The biases between the  
548 retrievals (George et al., 2015) of the two instruments in mid and higher latitudes could not be  
549 reconciled with the variational bias correction and led to a discontinuity in the time series of  
550 CO in MACCRA, which consequently could not be used for trend analyses (see Figure 4  
551 below). It was therefore decided to only use the MOPITT V5 CO data set in CAMSiRA  
552 because it covers the whole period from 2003–2015. The MOPITT V5 product has better long  
553 term stability and a smaller SH bias than V4 (Deeter et al., 2013). V4 suffered from a positive  
554 temporal bias drift and a positive bias in SH.

555 An additional ozone data set in CAMSiRA were the Michelson Interferometer for Passive  
556 Atmospheric Sounding (MIPAS) ozone profiles, which were assimilated from 2005 until the  
557 end of the ENVISAT mission in April 2012. After the end of 2012 the version of the  
558 assimilated Microwave Limb Sounder (MLS) data set changed from V2 to V3.4. Information  
559 about the differences between the two versions can be found in  
560 [https://mls.jpl.nasa.gov/data/v3\\_data\\_quality\\_document.pdf](https://mls.jpl.nasa.gov/data/v3_data_quality_document.pdf)

561 Averaging kernels were used for the calculation of the model's first-guess fields in the  
562 observation operators for the MOPITT data. For the ozone retrieval averaging kernels were  
563 not used because they were not provided or did not improve the analysis. For example, the  
564 high vertical resolution of the MLS ozone retrievals in the stratosphere made the use of AK  
565 not necessary.

566

567 The AC satellite retrievals were thinned to a horizontal resolution of  $1^\circ \times 1^\circ$  by randomly  
568 selecting an observation in the grid box to avoid oversampling and correlated observation  
569 errors. Variational quality control (Andersson and Järvinen, 1999) and background quality  
570 checks were applied. Only 'good' data were used in the analysis and data flagged as 'bad' by  
571 the data providers were discarded.

572 Variational bias correction (Dee, 2004, McNally et al., 2006, Auligné et al., 2007, Dee and  
573 Uppala, 2009) was applied to the MODIS AOD data, as well as to ozone column data from  
574 the Ozone Monitoring Instrument (OMI), the SCanning Imaging Absorption spectroMeter for  
575 Atmospheric CHartographY (SCIAMACHY) and the Global Ozone Monitoring Experiment 2  
576 (GOME-2). The partial column of the Solar Backscatter Ultraviolet Radiometer 2 (SBUV/2),  
577 MLS and MIPAS were used to anchor the bias correction. Experience from the MACC  
578 reanalysis had shown that it was important to have an anchor for the bias correction to avoid  
579 drifts in the fields (Inness et al., 2013).

580

### 581 **3 Carbon monoxide**

582 Global CTMs tend to underestimate the observed CO values (Shindell et al., 2006) but data  
583 assimilation (Inness et al., 2013 and 2015, Miyazaki et al., 2015, Gaubert et al., 2016) of  
584 satellite retrieval is able to successfully reduce the biases of the simulated CO fields. The  
585 correct representation of vertical CO profiles by the assimilation remains a challenge (Gaudel  
586 et al., 2015). An important next step will be the correct representation of the global CO trends  
587 by means of CO reanalyses such as CAMSiRA.

#### 588 **3.1 Spatial patterns of total column CO**

589 Figure 2 shows the seasonal mean of TC CO over the period 2003–2015 of CAMSiRA and  
590 the differences with CR and MACCRA (2003–2012). Overall, the assimilation of TC CO in  
591 CAMSiRA led to an increase in the northern hemisphere (NH) and a decrease in the Southern  
592 hemisphere (SH) and most of the tropics. CAMSiRA was about 2–5% higher than CR in NH  
593 and up to 20% lower in the SH. The reduction was especially large in the tropical and sub-  
594 tropical outflow regions of the biomass burning regions in South America, Central Africa and  
595 Maritime South East Asia. The largest reduction in these regions occurred in DJF. The largest  
596 negative bias of CR with respect to CAMSiRA occurred over NH in December–February  
597 (DJF) and March–May (MAM). Overall the zonal patterns of the biases throughout all  
598 seasons were rather uniform indicating an underestimation of the hemispheric CO gradient in  
599 CR and could point to deficiencies in the simulation of the global chemical loss and  
600 production of CO as well as problems with the large scale transport. Biases in the amount of  
601 the emissions seem to play a smaller role for the problem with the hemispheric gradient.

602 However, more CO emission related differences occurred in September–November (SON)  
603 and to a smaller extent in June–August (JJA), when CR had (i) higher values in the biomass  
604 burning regions and the respective outflow regions in Central Africa, Maritime South East  
605 Asia and South America and (ii) lower values in the outflow regions of the emissions in North  
606 America and East Asia in the Eastern and Western Northern Pacific. This suggests that GFAS  
607 biomass burning emissions were too high whereas the anthropogenic emissions in North  
608 America and East Asia were too low. On the other hand, CR had higher values than  
609 CAMSiRA in South Asia, which indicates that the anthropogenic emissions are too high in  
610 India.

611 Compared to MACCRA, CAMSiRA was up to 10% higher in the Northern high latitudes and  
612 up to 20% higher above the tropical biomass burning regions and above the parts of East  
613 Asia. The differences over the biomass burning regions can be attributed to the different  
614 biomass burning emissions data sets (see section 2.3). Over the oceans in NH and the tropics,  
615 apart from biomass burning outflow regions, CAMSiRA CO is slightly lower (3%) than  
616 MACCRA. The differences in the NH high latitudes are mainly caused by the reduction in  
617 MACCRA CO in this region introduced by the assimilation of IASI CO retrieval after 2008  
618 (see also Figure 4 below).

619 Figure 3 shows the average zonal mean cross section of the average CO mass mixing ratio of  
620 CAMSiRA and the relative difference to CR and MACCRA. The overestimation of CR in the  
621 tropics and SH extratropics was found throughout the troposphere. It was most pronounced in  
622 relative terms at about 500 hPa. Stratospheric CO in CAMSiRA was much lower than in  
623 MACCRA. This might be an improvement as Gaudel et al. (2015) report an overestimation in  
624 the MACCRA over this region. In the upper troposphere CAMSiRA had higher CO than  
625 MACCRA most notably in the tropics and SH where values are up to 40% higher. CO was  
626 lower in the mid and lower troposphere in SH and higher in NH. These differences in the  
627 vertical distribution might be caused by (i) a more consistent modelling approach of the  
628 stratosphere-troposphere exchange with the on-line coupled C-IFS, (ii) the fact that C-IFS  
629 CB05 has a very different chemistry treatment compared to MOZART and (iii) updated  
630 background error statistics for CO (see Table 1).

### 631 **3.2 Inter-annual variability of CO burden**

632 Figure 4 shows time series of the monthly mean CO burden from CAMSiRA, MACCRA and  
633 CR for selected areas (see Table 3). Then modelled global CO burden (CR) was reduced by  
634 the assimilation by about 3% at the start and by about 7% at the end of the period. CAMSiRA  
635 showed a stepwise decrease of the global CO burden from 2008 and 2009 which corresponds  
636 to a significant (95% confidence level) negative linear trend of -0.86%/yr over the whole  
637 period. The linear trend is as expressed as percentage with respect to the mean of the burden  
638 over the whole period. This figure is in good agreement with the results of Worden et al.  
639 (2013) who estimates trends of -1% per year for both the globe and NH over the last decade  
640 by studying different satellite-based instruments. CR also showed the largest decrease in the



641 period from 2007–2009 but the CO burden increased slightly after that period. The resulting  
642 linear trend of CR was still negative (-0.36%/yr) but less strong than the trend of CAMSiRA.

643 The higher global CO burdens of CR with respect to CAMSiRA originated mainly from the  
644 tropics and the SH mid-latitudes, which are strongly influenced by biomass burning emissions  
645 in tropical Africa and South America. CO was reduced by the assimilation in CAMSiRA  
646 especially after the start of the biomass burning season. The reduction of the biomass burning  
647 emissions of -7.4%/yr (see supplement Table S1) over South America led to a significant  
648 negative trend of the CO burden of -1.23%/yr in CAMSiRA and -0.83%/yr in CR over that  
649 region. The overestimation of CR with respect to CAMSiRA increased slightly during the  
650 period.

651 2015 was an exceptional year because the global CO burden reached the highest values in the  
652 whole period for both CAMSiRA and CR despite the overall decadal negative trend. The  
653 increase was caused by exceptionally high biomass burning emissions in Indonesia because of  
654 El Niño related dry conditions. The El Niño controlled inter-annual variability of CO over  
655 Maritime South East Asia was reproduced in a very similar way in CAMSiRA and CR but the  
656 assimilation reduced the burden by about 1 Tg (10%).

657 In the regions of high anthropogenic emissions the temporal variability at a monthly scale was  
658 very similar between CR and CAMSiRA. Both in North America and Europe CR  
659 underestimated the CO maximum of CAMSiRA in early spring by less than 5% up to the year  
660 2010 but the biases almost disappeared in later years. This means that the negative total CO  
661 trend in these regions was larger in CAMSiRA, which contains the MOPITT observations,  
662 than in CR. It could indicate that the anthropogenic emissions were biased low at the  
663 beginning of the period but less so towards the end. Over East Asia the difference between  
664 CR and CAMSiRA was generally very small indicating a high degree of realism of the  
665 emissions in the area. A further explanation for this agreement is the fact that this area covers  
666 both the underestimation of CAMSiRA by CR in NH mid-latitudes and the overestimation in  
667 the tropics. Both CAMSiRA and CR had a negative but not a significant trend over East Asia.

668 Stroden et al. (2016) also find good agreement between MOPITT-based and modelled  
669 negative trends for the 2000-2010 period of total column CO over Europe and North America  
670 but disagreement in the ~~in-the~~ sign of the trend over Eastern China, where their model, using  
671 MACCity emissions, simulates a positive trend but MOPITT has a negative trend. Over  
672 Eastern China also CR (2003-2015) had a small positive linear trends whereas CAMSiRA had

673 a negative trend but both trends were not statistically significant. The positive trend over  
674 Eastern China in CR was mainly driven by directly emitted CO at the surface. ~~Because~~ ~~Owing~~  
675 ~~to the of the~~ hemispheric influence, i.e. the hemispheric reduction in CO, the CO trend in CR  
676 over Eastern China became negative in the middle troposphere, ~~where the MOPITT~~  
677 ~~sensitivity to CO is highest.~~

678 In the Arctic, which is influenced by the long-range transport from North America, Europe  
679 and Asia (Emmons et al., 2015), no MOPITT observations were assimilated (see Table 2)  
680 because of the higher biases of the MOPITT data in this region. –Also in this region the  
681 variability of the CR and CAMSiRA CO burden matched well but the bias was much reduced  
682 after 2012.

683 The time series of the global CO burden of CAMSiRA and MACCRA agree better than  
684 CAMSiRA and CR. The global burden of MACCRA is slightly lower than in CAMSiRA  
685 (1%) until 2010 but starts to exceed CAMSiRA in 2011 and 2012. Hence, larger differences  
686 occur at the beginning and end of the MACCRA period.

687 The CO burden of MACCRA above the biomass burning regions of South America and  
688 Tropical Africa was lower than CAMSiRA for the period 2003–2010. This is most likely  
689 because of the use of the GFED biomass burning emissions until 2008, which are on average  
690 20% lower than GFAS, which was used for CAMSiRA . In the years 2011–2012 MACCRA  
691 had higher values, which even led to a reversal in the sign of the trend over the two regions in  
692 MACCRA in comparison to CAMSiRA. MACCRA and CAMSiRA agreed well above the  
693 anthropogenic source regions. Only from 2008 onwards MACCRA was slightly lower which  
694 led to enhanced negative trends.

695 Over the Arctic, CAMSiRA is higher from 2008 whereas MACCRA was higher at the start.  
696 This is consistent with the respective trends over Europe and North America. All data sets  
697 showed a step-like reduction the CO burden at mid-2008 but it was most pronounced in  
698 MACCRA.

699

### 700 **3.3 Evaluation with MOZAIC/IAGOS aircraft CO observations**

701 Measurements of OZone, water vapour, carbon monoxide and nitrogen oxides by in-service  
702 Airbus aircraft (MOZAIC) and In-service Aircraft for a Global Observing System (IAGOS)

703 are subsequent programmes of AC observations mounted on commercial aircraft. The  
704 MOZAIC CO data have an accuracy of  $\pm 5$  ppbv, a precision of  $\pm 5\%$ , and a detection limit of  
705 10 ppbv (Nédélec et al., 2003). De Laat et al. (2014) compare MOZAIC/IAGOS profile with  
706 the MOPITT v5 NIR retrievals, which were assimilated in CAMSiRA. They find good  
707 agreement and no drift of the biases of the two data sets in their study period 2002–2010.

708 We use the CO profiles obtained during take-off and landing to evaluate the CO fields  
709 averaged over airports in different regions from 2003–2012. The number of MOZAIC/IAGOS  
710 CO profiles fluctuated considerably over the years. They have decreased from 2003–2014 by  
711 about 50% and certain airports had many more observations than others. Since the aircraft  
712 used in MOZAIC were based in Frankfurt, the majority of the CO profiles were observed at  
713 this airport. Therefore the observations from Frankfurt dominate the European mean values.  
714 Observations from Tokyo and other Japanese cities were the largest contribution to the mean  
715 over East Asia. Atlanta, Toronto and Vancouver had the largest number of observation in the  
716 North American domain. Windhoek had by far the largest number of observations in Tropical  
717 Africa and Caracas in South America. The mean of Maritime South East Asia sea salt is  
718 mainly calculated from observations over Jakarta and Kuala Lumpur in 2005, 2006, and 2012  
719 with an unbalanced coverage of the difference months.

720 Profiles of the mean relative bias of CAMSiRA, MACCRA and CR against MOZAIC/IAGOS  
721 CO observations for different regions (see Table 3) averaged over the period 2003–2012 are  
722 shown in Figure 5. We discuss here only the annual biases since the seasonal relative biases  
723 did not differ to a large extent from the annual relative biases.

724 All three data sets underestimated the observed CO values throughout the troposphere in  
725 Europe, North America and East-Asia. At the surface and the lower PBL up to 900 hPa, i.e.  
726 where the highest CO concentrations are observed, CAMSiRA and CR had a relative biases  
727 of about -10% in Europe and North America and up to -20% in East Asia, whereas MACCRA  
728 had larger relative biases of -20 –30% at this level and the largest biases occurred in DJF. On  
729 the other hand, MACCRA had smaller biases than CAMSiRA and CR in the middle and  
730 upper troposphere. The smaller biases of MACCRA may be caused by the more realistic  
731 simulation of the chemical CO production by the MOZART chemical mechanism as well as  
732 by the change in the CO background error statistic. The assimilation of MOPITT in  
733 CAMSiRA reduced the biases relative to CR in the troposphere over Europe and North

734 America but had only little effect at the surface. Over East Asia the assimilation did not lead  
735 to changes between CR and CAMSiRA.

736 Whereas CR had the largest underestimation in NH it was generally higher than CAMSiRA  
737 and MACCRA in the tropics. This led to better agreement with the MOZAIC observation in  
738 South America and Tropical Africa but also to an overestimation of 20–30% in Maritime  
739 South East Asia. The limited number of observations in that region makes this result less  
740 robust. MACCRA and CAMSiRA showed little differences over South America and Tropical  
741 Africa. The 10% negative bias of MACCRA and CAMSiRA in Tropical Africa is consistent  
742 with the 10% underestimation of MOPITT v5 against MOZAIC/IAGOS over Windhoek  
743 reported by de Laat et al. (2014, their Figure 3). Over MSEA below 700hPa CAMSiRA and  
744 MACCRA overestimated CO whereas MACCRA underestimated the observations. This  
745 could be the consequence of the different fire emissions and the different chemistry schemes  
746 but the limited number of available profiles makes this result less representative.

#### 747 **3.4 Evaluation with NOAA GMD surface observations**

748 NOAA Global Monitoring Division (GMD) network of flask CO surface observations  
749 (Novelli and Masarie, 2010) has a good global coverage, which also includes the high  
750 latitudes of SH and NH, to observe the background concentrations. The tropical stations  
751 represent the maritime background because they are mainly located on islands in the tropical  
752 oceans. The station density is higher in North America and Europe. The uncertainty of the  
753 NOAA/GMD CO observations is estimated to be 1–3 ppm (Novelli et al., 2003).

754 We calculated the mean and, for reasons of simplicity, only the linear trend at each station for  
755 the period 2003–2014 or 2003–2012 (MACCRA). The overall bias averaged over all stations  
756 of CAMSiRA and CR was 3.0 ppb for the whole period but CAMSiRA had a slighter lower  
757 RMSE (13 ppb) than CR (15 ppb). For the 2003–2012 period MACCRA had a bias of 6 ppb  
758 whereas CAMSiRA and CR had a bias of 3.1 and 3.9 ppb respectively.

759 Figure 6~~Figure–6~~ shows the zonal means of the observed averages and the corresponding  
760 model values at station location as well as the median of the estimated linear trend from the  
761 observations and the model results. The graphs were constructed by calculating the mean  
762 concentrations and median trends of all stations in 15° wide latitude bins. The errors bars  
763 indicate the range of the observed values in the latitude bin.

764 In the SH high and mid-latitudes the typical observed annual mean surface concentration was  
765 50 ppbv. The background levels started to rise in the SH extra tropics and reached a  
766 maximum of 145 ppbv in the NH mid- latitudes. The values then decreased to about 130 ppb  
767 in the Arctic. The general structure of the zonal variation was well represented by all data  
768 sets. CR overestimated the SH mid and high values by 15 ppb whereas CAMSiRA and  
769 MACCRA had a bias of 7 ppb. In the tropics CAMSiRA had slightly lower (3 ppb) values  
770 than the observations whereas MACCRA and CR overestimated by about 5 ppb. CAMSiRA  
771 had the highest values of all three data sets in the NH mid-latitudes but still underestimated  
772 the mean of the observations by 7 ppb. However the observed means at the station locations  
773 in this latitude band varied in a range of about 100 ppb. CR had a slightly larger  
774 underestimation than CAMSiRA. MACCRA underestimated the observations by more than  
775 20 ppb in the mid and high latitudes. The reduction towards the NH high latitudes in CR and  
776 CAMSiRA was similar to the observations.

777 The observations in the SH showed essentially no linear trend in the 2003–2014 period.  
778 Starting in the tropics a negative linear trend gradually occurred which reached values of  
779 about -2.2 ppb/yr in the NH mid- and high latitudes. CAMSiRA and CR had a small but still  
780 significant (~~95% confidence level~~) negative trend in SH of -0.3 and -0.5 ppb/yr respectively.  
781 The negative trends of CAMSiRA and CR started to become more pronounced from 20°S  
782 onwards. The trend in CAMSiRA was generally stronger than the trend in CR. This meant a  
783 better fit with the observed trends in the tropics for CR and a better fit in the NH mid- and  
784 high latitudes for CAMSiRA. In this region the median of the trends was -2.1ppb/yr for  
785 CAMSiRA and -2.0 ppb/yr for CR. While the trends of CAMSiRA and CR agreed reasonably  
786 well with the observations, MACCRA suffered from unrealistically strong negative trends in  
787 the mid- and high latitudes of both hemispheres. This negative trend in MACCRA was caused  
788 by the reduction in the values related to assimilation of IASI data from 2008 onwards (Inness  
789 et al., 2013).

790  
791

## 792 **4 Aerosols**

793 In contrast to the assimilation of individual chemical gases, the assimilation of AOD  
794 observations is “underdetermined” because different combinations of the aerosol components  
795 can led to the same extinction, i.e. AOD value. A further complicating factor is that each

796 aerosol component has different optical properties, which depend on relative humidity for the  
797 hydrophilic components such as sea salt, sulphate and organic matter. The correction of the  
798 speciation of the assimilated aerosol mass mixing ratio fields is therefore a big challenge  
799 despite good success in reproducing independent AOD observations with the aerosol analysis  
800 ([Eskes et al. , 2015](#)).

#### 801 **4.1 Global aerosol burden, speciation and AOD**

802 In this section the global averages of burdens and AOD are presented. Spatial patterns of  
803 AOD will be discussed in section 4.2. Global area-weighted averages of AOD at 550nm and  
804 the total global burden in Tg for the different aerosol components are shown in Figure 7. The  
805 figure also shows the median of the global AOD average and burdens simulated by the  
806 models of the AeroCom inter-comparison study (Kinne et al., 2006 and Textor et al., 2006).  
807 CR had the highest total global average aerosol burden of 46 Tg compared to MACCRA and  
808 CAMSiRA, which had both 33 Tg. This number was very similar to the AeroCom median of  
809 29 Tg.

810 The global sea salt burden was about twice as high in CR (15.1 Tg) than in CAMSiRA (8.3  
811 Tg), and it was 16.1 Tg for MACCRA. In comparison, the median of the sea salt burden from  
812 the AeroCom models is 6.3 Tg. Another study of different emission schemes by Spada et al.  
813 (2013) found sea salt burdens in the range from 5.0 to 7.2 Tg. In the light of these studies as  
814 well as the applied correction by the assimilation in CAMSiRA, the simulated sea salt burden  
815 of CR ~~as well as the assimilated burden of MACCRA~~ appears to be too high. The simulated  
816 sea salt emissions of C-IFS were ~~at the upper end of, but still within,~~ the reported range in the  
817 literature (see supplement). This suggests that the ~~high sea salt burden of CR can not entirely~~  
818 ~~be explained by exaggerated emissions. The underestimation of the~~ loss processes of sea salt  
819 were underestimated in C-IFS in comparison to other models.~~with respect to other models~~  
820 ~~must have a played an important role too.~~ On the other hand, the high sea salt burden of  
821 MACCRA was probably likely caused by an exaggeration of the sea salt emission with an  
822 earlier version of the emissions module.

823 The desert dust burden in CR was 27 Tg, which was higher than the AeroCom median of 20  
824 Tg. It was strongly reduced by the assimilation in CAMSiRA to 18 Tg. MACCRA had an  
825 even lower desert dust burden of 12 Tg because of the underestimation of the desert dust  
826 emissions scheme used in MACCRA. As in the case of the sea salt, the underestimation of the

827 desert dust loss by deposition and sedimentation may play an important role in the  
828 overestimation of dust burden in CR.

829 The strongest relative change in the global burden by the assimilation occurred for sulphate,  
830 which was 1.2 Tg in CR but was 4.7 Tg in CAMSiRA and 3.3 Tg in MACCRA. The  
831 respective AeroCom median value is 2 Tg. Because of the larger extinction per unit mass of  
832 sulphate, this increase in sulphate had a large impact on total AOD, which will be discussed  
833 further below.

834 The organic matter and black carbon burden of CR (0.2 Tg and 2.0 Tg) was increased by the  
835 assimilation to 0.36 Tg and 2.4 Tg respectively. The values agreed reasonably well with the  
836 AeroCom median of 0.21 Tg and 1.76 Tg.

837 In contrast to the global burden, CR had the lowest global AOD average of 0.13. CAMSiRA  
838 and MACCRA had values of 0.16 and 0.18. The values for CR were close to the median of  
839 the AeroCom models (0.12) but the two reanalyses had a higher value than the highest global  
840 average AOD value of the AeroCom models of 0.15.

841 The largest fraction of the CAMSiRA AOD came from sulphate, which was strongly  
842 increased by the assimilation. The contribution of sulphate AOD to total AOD was 13% in  
843 CR and 43% in CAMSiRA. Sulphate was also the largest AOD contribution in MACCRA.  
844 The global average of sulphate AOD of CR (0.018) was about half of the AeroCom median  
845 (0.034), which could suggest an underestimation in the global sulphate burden and AOD in  
846 CR. On the other hand, global sulphate AOD of CAMSiRA was 0.06, which was higher than  
847 the highest value of the AeroCom model ensemble (0.051).

848 As already discussed for the respective burdens, global desert dust AOD and sea salt AOD  
849 were strongly reduced in CAMSiRA compared to CR. In CR sea salt and desert dust AOD  
850 contributed each about 30% to the total AOD, whereas in CAMSiRA the contribution was  
851 reduced to 15% and 19%. The reduction of sea salt by the assimilation was reasonable as the  
852 sea salt burden was above the reported range by Textor (2006) and Spada et al. (2012).  
853 However, the reduction in sea salt was compensated by the increase in sulphate, which  
854 became the most important contribution to total AOD over many parts of the oceans.

855 The global sea salt burden of MACCRA was higher than in CAMSiRA but similar to CR.  
856 However, a different distribution of the mass within the size classes meant that the resulting  
857 sea salt AOD of MACCRA was 20% higher than CR. MACCRA had the lowest desert dust

858 burden but differences in the size distribution towards smaller particles meant that the  
859 resulting AOD was slightly higher than CR and 20% higher than CAMSiRA. Black carbon  
860 and organic matter AOD and burden were similar among CAMSiRA, CR and MACCRA.

861

862

## 863 **4.2 Spatial patterns of AOD**

864 Figure 8 shows the annual mean of total AOD and AOD for desert dust, sea salt, sulphate,  
865 black carbon and organic matter for period 2003–2015 from CAMSiRA and the differences  
866 with CR and MACCRA (2003–2012). The global maxima of the total AOD (>0.5) in  
867 CAMSiRA were found over areas of desert dust emissions such as the Sahara, the Arabian  
868 Peninsula and the deserts of Central Asia. High emissions of black carbon and organic matter  
869 from biomass burning sources in tropical Africa and anthropogenic sources in Eastern China  
870 and Northern India also produced to AOD maxima on the global scale.

871 The increase of the global average AOD in CAMSiRA with respect to CR by the assimilation  
872 (see section 4.1) occurred in most parts of the globe, in particular over the areas of industrial  
873 activity in North America, Europe and East Asia (20–30%) as well as in the polar regions (>  
874 50%), where AOD is generally low. The differences between CR and CAMSiRA, although  
875 varying in magnitude, exhibit similar spatial patterns in all seasons, with the largest  
876 differences occurring throughout NH in MAM. As discussed in section 4.1 the increase is  
877 mostly caused by a wide-spread increase in sulphate AOD. Sulphate AOD was increased in  
878 relative terms more strongly over the oceans and higher latitudes. In areas of higher modelled  
879 sulphate AOD such as the North America, Europe and Northern Asia and the Arctic the  
880 contribution to total AOD changed from 40% to 90%, which made sulphate the by far the  
881 most abundant aerosol species in these areas as well as over the Antarctic, which seems  
882 unrealistic given that the global SO<sub>2</sub> emission were only less than 2% of the total aerosol  
883 emissions (see supplement).

884 The identified reduction of global desert dust in CAMSiRA with respect to CR was mainly  
885 confined to the main desert dust region, where AOD was reduced by to 0.2. As total AOD  
886 was dominated by desert dust, total AOD was strongly reduced in these regions, whereas total  
887 AOD of CAMSiRA was always higher than CR in the other parts of the globe. The largest  
888 relative reduction of desert dust AOD occurred in the remote outflow regions from Australia,



889 Tropical Africa and Eurasia. The reduction of desert dust occurred throughout all seasons  
890 with the largest reduction in JJA.

891 The strongest reduction in sea salt occurred in CAMSiRA with respect to CR occurred over  
892 the oceans proportional to the sea salt AOD. Because of the increase in sulphate, the sea salt  
893 reduction led only to a small reduction of total AOD over the area of the highest sea salt  
894 emissions in the North Atlantic in DJF and over the Southern Ocean in JJA and MAM. The  
895 contribution of sea salt AOD to total AOD over most of the ocean was changed from more  
896 than 80% in CR to 50% in CAMSiRA in mid- and high latitudes of SH and to 30% over the  
897 rest of the maritime area by the assimilation.

898 Black carbon and organic matter AOD were reduced in CAMSiRA over tropical Africa where  
899 biomass burning is the largest source on the global scale and also the CO biomass burning  
900 emissions were too high. The black carbon and organic matter AOD values were higher in  
901 CAMSiRA away from the sources where values are generally low. The differences of black  
902 carbon and organic matter AOD between CAMSiRA and CR showed a strong reduction  
903 directly over the areas of intense fire emission in tropical Africa and boreal forest of NH and  
904 an increase in the adjacent outflow regions. This could indicate that the GFAS emissions, as  
905 in the case of CO (see section 3.1), were too high but the atmospheric residence times of the  
906 aerosol species were too short.

907 Compared to CAMSiRA, MACCRA AOD values were up to 50% (-0.2– -0.3) lower in the  
908 desert dust dominated areas over the Sahara and Central Asia. The largest differences over  
909 North-Africa occurred in JJA and MAM and are an indication that MODIS AOD retrievals  
910 are not available over this regions because of their bright surface (Hsu et al., 2013). The  
911 higher AOD values of CAMSiRA than MACCRA in the desert dust regions might be an  
912 improvement as Cuevas et al. (2015) reported a general underestimation with respect to  
913 AERONET observations in the dust dominated regions of MACCRA.

914 On the other hand, sea salt AOD over all oceans was much higher in MACCRA than  
915 CAMSiRA and it even exceeded the high sea salt AOD of CR. Despite the higher sea salt  
916 AOD, the total AOD of MACCRA over the oceans was lower than in CAMSiRA because of  
917 the overall smaller sulphate AOD in maritime regions.

918 In the regions of boreal fire emissions MACCRA was lower during the JJA fire season as well  
919 as in the South American fire season in SON. For the rest of the globe the CAMSiRA, was

920 about 0.05 lower than the MACCRA, which meant a large relative reduction (>50%) in  
921 particular over the oceans.

922 The differences between MACCRA and CAMSiRA can mainly be explained with the  
923 changes in the underlying modelling approach and the emissions since the same MODIS  
924 AOD retrievals were assimilated in both reanalyses. Differences in the back ground error  
925 statistics may have contributed to the differences, particularly in the high latitudes.

926 Figure 9 shows a zonally averaged cross section of the total aerosol mixing ratio of  
927 CAMSiRA and its relative differences of CR and MACCRA. The highest zonal average  
928 occurred over the southern ocean because of the continuous sea salt production, and over the  
929 latitudes of the regions with large desert dust and anthropogenic emissions. Despite the  
930 mostly higher AOD values, CAMSiRA had lower mass mixing ratios than CR throughout the  
931 troposphere with the largest relative differences occurring over the SH mid-latitudes and in  
932 the region of intense convection in the tropics. This is related to a change in the speciation,  
933 which was discussed in section 4.1. CAMSiRA had up to 90% higher values in the  
934 stratosphere and Antarctica. The higher aerosol mixing ratios of CAMSiRA in the upper  
935 troposphere were dominated by sulphate aerosol. MACCRA mixing ratios were considerably  
936 higher in relative terms than CAMSiRA throughout the troposphere with the exception of NH  
937 extra-tropical mid- troposphere, caused by the lower dust emissions in MACCRA, and the SH  
938 and tropical stratosphere related to high sulphate concentrations in CAMSiRA.

### 939 **4.3 Inter-annual variability of AOD**

940 Figure 10 shows time series of average AOD from CAMSiRA, CR and MACCRA for  
941 different regions. To better distinguish the impact of sea salt, the regional AOD is averaged  
942 over land points only. The global average AOD time series are shown separately for land and  
943 sea points.

944 CR and CAMSiRA did not have any significant (95% confidence level) trends in AOD over  
945 the whole globe or any of the considered regions. There was a good agreement between  
946 CAMSiRA and CR in their inter-annual variability with respect to specific years with higher  
947 maxima over South and North America as well as over Maritime South East Asia and North-  
948 Africa. This demonstrates that despite biases the model was able to reproduce the variability  
949 related to fire emissions and wind driven desert dust suspension. A large relative difference

950 between CR and CAMSiRA occurred in the Arctic. The CAMSiRA and MACCRA AOD  
951 values were almost twice as high as CR and had a much more pronounced seasonality.

952 In contrast to the lack of significant trends in CR and CAMSiRA, MACCRA had significant  
953 positive trend over all sea points leading to an increase over 10 years, which was as large as  
954 the seasonal variation over all sea points. Averaged over all land points, the seasonal variation  
955 is much larger than over sea. The agreement in AOD in the monthly means time series was  
956 generally high but MACCRA also showed a significant increasing trend, which was not  
957 present in the other two data sets. Most of this trend in MACCRA was caused by dust AOD,  
958 which increased by 3.7%/yr, and by sea salt AOD, which increased by 1.7%/yr over sea  
959 points. We consider this trend in MACCRA as spurious. It is probably likely caused by an  
960 accumulation of aerosol mass, which could not be corrected by the assimilation. A reason for  
961 the mass accumulation could be the fact that the MACCRA model did not apply a global mass  
962 fixer.

963 Even if CR and CAMSiRA did not show significant trends in total AOD, sulphate AOD of  
964 CAMSiRA increased significantly by 0.55%/yr and both CR and CAMSiRA had a positive  
965 trend in sea salt AOD of 0.3%/yr. This suggests an artificial accumulation of sulphate by the  
966 assimilation because considering that the SO<sub>2</sub> emissions for the aerosol sulphate precursor  
967 (SO<sub>2</sub>) were constant. The increase in sulphate was likely caused by underestimated loss  
968 processes for sulphate and SO<sub>2</sub> in the free and upper troposphere away from the emissions  
969 sources. The relative increase in sulphate with respect to the other aerosol species could not  
970 be corrected by the assimilation of AOD.

#### 971 **4.4 Evaluation with AERONET AOD observations**

972 The AOD at 550 nm was evaluated with observations of the AErosol RObotic NETwork  
973 (AERONET) network. The AERONET is a network of about 400 stations measuring spectral  
974 AOD aerosol with ground based sun-photometers (Holben et al., 1998). The stations are  
975 mostly located over land with a high number of stations situated in North America and  
976 Europe. The global number of stations contributing observations for the evaluation increased  
977 from about 60 in 2003 to about 250 in 2014 before it reduced strongly to only a couple of  
978 stations at the end of 2015.

979 Figure 11 shows time series of the monthly biases of CAMSiRA, MACCRA and CR for the  
980 globe and different regions. Over North America, an area with a high density of AERONET

981 stations, CR underestimated AOD in general by 0.05 on average. On the other hand, the two  
982 analyses overestimated AOD by about 0.02 but CAMSiRA has marginally smaller biases than  
983 MACCRA. In South America a similar pattern was found only that the average  
984 underestimation of CR and overestimation of CAMSiRA and MACCRA was -0.05 and 0.05  
985 respectively. The overestimation of CAMSiRA and MACCRA and the underestimation of CR  
986 over America leads to the conclusion that the assimilated MODIS retrievals were biased high  
987 against the AERONET observations in this region as also pointed out in Levy et al. (2010).  
988 The underlying model does not seem to be the cause of the overestimation in CAMSiRA.

989 Over Europe CAMSiRA had the smallest biases and MACCRA overestimated slightly  
990 whereas CR underestimated the observations. The bias of CR was -0.07 at the beginning of  
991 the period and almost zero at the end. More research is needed to understand this trend in the  
992 bias, which is also apparent in CAMSiRA and MACCRA, but it might be caused by the  
993 reduced number of available stations.

994 MACCRA had the lowest biases over South East Asia because of small biases in Northern  
995 India and Indochina. It was higher, as almost everywhere, than CAMSiRA and CR.  
996 CAMSiRA underestimated the observations in this region by about 0.05. The underestimation  
997 by CR was bigger and showed a pronounced seasonal cycle. The largest negative biases  
998 occurred at the time of the seasonal minimum in DJF.

999 The performance for desert dust and sea salt was more difficult to evaluate with AERONET  
1000 stations in a robust way because only few stations are available in these regions. The average  
1001 bias over Africa showed a strong reduction of the CR peak values, which occurred because of  
1002 desert dust outbreaks, by the assimilation. A good example of the successful reduction of dust  
1003 by the assimilations was Lake Argyle (16.11.S, 128.75E) in Australia (Figure 11, left).

1004 The AOD AERONET observations over the oceans show generally an overestimation of all  
1005 runs, in particular for MACCRA. The bias of the MODIS retrievals with respect to  
1006 AERONET (Shi et al., 2011) may be a reason for this overestimation. The comparison with  
1007 AOD observation at Mauna Loa Station (19.54 N, 155.58 W, not shown) in the Eastern  
1008 Pacific suggests that the low AOD values of CR reproduced the observations best, although  
1009 still overestimating them. At Nauru Station (0.52 ° S, 166.9 ° E, Figure 11, right) in the  
1010 Western Pacific CAMSiRA match the observations well whereas CR underestimated and  
1011 MACCRA overestimated them.

## 1012 **5 Stratospheric ozone**

1013 The experience from the assimilation of TC and stratospheric profiles retrievals (Inness et al.,  
1014 2013, van der A et al., 2015 and Levefer et al., 2015) shows that these observations are  
1015 sufficient to constrain stratospheric ozone in the reanalysis. Because almost the same ozone  
1016 retrievals were assimilated in CAMSiRA as in MACCRA (see Table 2) most of the  
1017 differences in the ozone analyses can be attributed to differences in the ozone simulation of  
1018 the assimilating model. For CAMSiRA the Cariolle parameterization (Cariolle and Teysse re,  
1019 2007) of stratospheric ozone chemistry and the chemical mechanism CB05 for the  
1020 troposphere were used. The tropospheric and stratospheric chemical scheme of the MOZART  
1021 CTM (Kinnison et al., 2007) was used for MACCRA.

### 1022 **5.1 Spatial patterns of TC ozone**

1023 Figure 13 shows the seasonal average TC ozone from CAMSiRA and the difference between  
1024 this data set and CR and MACCRA. The differences between CAMSiRA and CR had a  
1025 meridional pattern. The assimilation in CAMSiRA increased the total ozone columns in the  
1026 tropics and subtropics by up to 25 DU (8%) and it decreased them by 50–70 DU in the NH  
1027 mid and high latitudes. The largest reduction occurred in DJF and MAM. Also over  
1028 Antarctica the assimilation led to lower values in austral winter (JJA), when TC ozone was  
1029 reduced by up to 30 DU.

1030 CAMSiRA was about 3–5 DU (1%) lower than MACCRA throughout the globe. Larger  
1031 differences of up to 10 DU (2%) were located mainly over tropical land areas. Their shape  
1032 suggest that they were partially caused by differences in tropospheric ozone (see section 6.1).  
1033 On the seasonal scale, CAMSiRA was about 10 DU lower over Antarctica and the Arctic in  
1034 the respective spring seasons MAM and SON.

1035 Figure 14 shows the average ozone partial pressure cross section of CAMSiRA and the  
1036 relative differences with CR and MACCRA. The tropospheric part of the figure will be  
1037 discussed in section 6.1. The overestimation of CR in the high latitudes of NH and SH was  
1038 located predominately in the mid and upper stratosphere at around 20 hPa. The  
1039 underestimation in the tropics had the largest values at around 50 hPa.

1040 In the lower and middle stratosphere, i.e. from 70 to 20 hPa, CAMSiRA and MACCRA  
1041 differed by less than 5%. Larger differences occurred above 10 hPa where MACCRA was up  
1042 to 30% higher than CAMSiRA.

## 1043 **5.2 Inter-annual variability of TC ozone**

1044 Figure 15 shows area-weighted averages of the monthly TCs for the whole globe, the tropics,  
1045 SH and NH mid-latitudes, Antarctica and the Arctic.

1046 In the tropics, CAMSiRA had a significant (95% confidence level) trend of +0.15%/yr.  
1047 Although the period of 13 years is too short to estimate total ozone trends with respect to  
1048 ozone recovery it is worth noticing that the number is in good agreement with the estimate of  
1049 the ozone trend for the period 1995–2013 by Coldewey-Egbers et al. (2014, see their figure  
1050 1), which varies in the tropics between 0.5 to 1.5%/decade. No trends could be found in CR,  
1051 probably because the climatological approach applied in the Cariolle scheme is not able to  
1052 simulate long-term trends. The tropical trend in MACCRA was 0.25%/yr, which seems too  
1053 high and there was also a significant trend in the SH mid-latitudes of 0.65%/yr.

1054 The seasonal range, i.e. the difference between annual maximum and minimum, of TC ozone  
1055 in CAMSiRA increased from 10 DU in the tropics to up 150 DU in the Arctic and 100 DU in  
1056 Antarctica. As already mentioned in section 5.1, CR was 20% higher than CAMSiRA in NH  
1057 mid-latitudes and Antarctica. However, the inter-annual variability agreed reasonably well  
1058 between CAMSiRA and CR in SH and MH high and mid-latitudes. For example, the reduced  
1059 Arctic ozone spring in 2011 (Manney et al., 2011) and the year-to-year differences in mid-  
1060 latitudes found in CAMSiRA were well reproduced by CR.

1061 The ozone hole in Austral spring is the most important feature of seasonal variability over  
1062 Antarctica. Despite its simplicity, the Cariolle scheme in CR reproduced the Remarkably CR,  
1063 which uses the Cariolle scheme, reproduced the ozone loss during the ozone hole periods with  
1064 respect to minimum value and inter-annual variability of TC ozone very well without  
1065 assimilating any observations. 2015, 2003 and 2006 were the years with the deepest ozone  
1066 holes and 2011, 2013 and 2004 with the shallowest ozone hole both in CAMSiRA and CR.  
1067 On the other hand, CR overestimated the average TC ozone during winter by about 30 DU.

1068 There was generally good agreement between CAMSiRA and MACCRA over all parts of the  
1069 globe but MACCRA was on average about 5–10 DU (2%) higher than CAMSiRA. The strong  
1070 positive trend of MACCRA in the tropics together with a significant positive trend in the SH  
1071 mid-latitudes led to increasing differences of the global average at the end of the MACC  
1072 period. Larger difference between MACCRA and CAMSiRA occurred in winter (JJA) over

1073 Antarctica, when MACCRA was up to 25 DU lower than CAMSIRA. The depth of the ozone  
1074 hole was slightly deeper in CAMSiRA than in MACCRA.

### 1075 **5.3 Evaluation with total ozone retrievals from Dobson sun-photometers**

1076 Ozone TCs are observed from the ground with Dobson, Brewer, Point Filter and FTIR  
1077 spectrometers. The Dobson instruments provide the longest and best spatial coverage and we  
1078 use this data set to evaluate the TC of CAMSiRA, MACCRA and CR. The Dobson  
1079 instruments of the WOUDC network are well calibrated and their precision is 1% (Basher,  
1080 1982). Factors that influence the accuracy of the Dobson spectrometer are the temperature  
1081 dependency of the ozone absorption coefficient and the presence of SO<sub>2</sub>.

1082 Figure 16 shows time series of the monthly bias against the Dobson photometer observations  
1083 for different regions. Observations of about 50–60 stations were available until 2013 but the  
1084 number of stations dropped steadily to about 10 Stations at the end of 2015. CAMSiRA  
1085 overestimated the observations in the tropics and the mid-latitudes of both hemisphere on  
1086 average by 2 DU whereas the mean bias of MACCRA was about 5 DU larger. In Antarctica  
1087 and the Arctic the biases showed a more pronounced seasonal cycle mostly between -10 and  
1088 20 DU.

1089 The biases of MACCRA increased in the tropics and the SH-mid latitudes from 2003 to 2008  
1090 whereas CAMSiRA and CR did not show an obvious change in the biases until 2012. The  
1091 variability of the bias of CAMSiRA amplified at the start of 2013 in NH. As this change in  
1092 the bias is not seen at individual stations reporting until the end of 2015, we conclude that the  
1093 change is caused by the reduction in the number of stations available after 2013. It is not  
1094 caused by ~~However,~~ the change of the assimilated MLS data set version (from V2 to V3.4)  
1095 because this took place already at the beginning of 2013 (see Table 2).

1096 The biases of CR were much larger than the ones of CAMSiRA, and they had a strong  
1097 seasonal cycle. In the tropics CR underestimated the TC by 10 DU in DJF and 0 DU in MAM.  
1098 The NH biases were positive and varied between 20–50 DU and in the Arctic between 20–70  
1099 DU. Over Antarctica CR overestimated the observation by 40–60 DU in JJA but the bias was  
1100 close to zero or even slightly negative during the time of the ozone hole.

#### 1101 **5.4 Evaluation with ozone sondes in the stratosphere**

1102 The global network of ozone sondes is the most comprehensive independent data set for the  
1103 evaluation of the 3D ozone fields from the surface to about 10 hPa, which is the level with the  
1104 highest stratospheric ozone volume mixing ratios. The observation error of the sondes is about  
1105  $\pm 5\%$  in the range between 200 and 10 hPa and  $-7$ – $-17\%$  below 200 hPa (Beekmann et al.,  
1106 1994, Komhyr et al., 1995 and Steinbrecht et al., 1996). The number of soundings varied for  
1107 the different stations used here. Typically, the sondes are launched once a week but in certain  
1108 periods such as during ozone hole conditions launches are more frequent. Sonde launches are  
1109 carried out mostly between 9 and 12 hours local time. The global distribution of the launch  
1110 sites is even enough to allow meaningful averages over larger areas such North America,  
1111 Europe, the tropics, the Arctic and Antarctica.

1112 Figure 17 shows the profiles of the relative biases of CAMSiRA, MACCRA and CR over the  
1113 tropics, Antarctica, the Arctic and the NH and SH mid-latitudes for the period 2003–2012. All  
1114 available observations were included in the average.

1115 In the tropics, CAMSiRA had a relative bias of mostly below 10% in most of the stratosphere.  
1116 MACCRA underestimated the ozone sondes strongly (up to 30%) in the lower stratosphere  
1117 but the relative bias of MACCRA was similar or slightly smaller than the bias of CAMSiRA  
1118 in most parts of the stratosphere, i.e. in the pressure range from 70 to 20 hPa. CR  
1119 underestimated the ozone sondes by up to 20% in the stratosphere up to 30 hPa. The largest  
1120 underestimation of CR occurred in the lower and mid stratosphere, where the maximum in  
1121 ozone partial pressure is located. In the upper stratosphere above 20 hPa, where the maximum  
1122 of ozone volume mixing ratio is located, the relative biases of all data sets were smaller than  
1123 in the levels below. CR had almost no bias whereas MACCRA overestimated by up 10%.

1124 Over the Arctic and NH mid-latitudes CAMSiRA and MACCRA agreed well with the sondes  
1125 in the whole stratosphere with relative biases below 5%. The absolute biases of CAMSiRA  
1126 were slightly smaller than the biases of MACCRA in particular in the lower stratosphere and  
1127 upper troposphere. CR overestimated the ozone observations by up to 25% in the stratosphere  
1128 and upper troposphere over the Arctic and up to 20% in the NH mid-latitudes. The relative  
1129 biases of CR tended to be slightly smaller in the mid stratosphere (50 hPa) than in the upper  
1130 and lower stratosphere.



1131 Over SH-mid latitudes and Antarctica the annual biases in the stratosphere were slightly  
1132 smaller in CAMSIRA than MACCRA but for both reanalyses they were below 10%. As over  
1133 the Arctic, the absolute tropospheric biases, with the exception of the surface values, were  
1134 smaller in MACCRA since CAMSIRA showed an underestimation of about 10%. CR had a  
1135 stronger underestimation in the lower and upper stratosphere.

1136 As the process of the ozone-hole formation cannot easily be demonstrated with annual means,  
1137 Figure 18 shows the monthly mean profile from August to November over Neumayer Station  
1138 (70.7° S, 8.3° W). The two reanalysis agreed very well with the observations: vertical level  
1139 and magnitude of the ozone profile at the end of the austral winter in August, the ozone  
1140 depletion in September and October and the closure of the ozone hole starting in the upper  
1141 stratosphere were well captured because of the assimilation of TC and limb-sounders profiles.

1142 In contrast, CR showed a strong overestimation in August in the middle and lower  
1143 stratosphere. Ozone in the upper stratosphere in September was underestimated in CR  
1144 because of an exaggerated depletion whereas ozone was overestimated in the lower  
1145 stratosphere. In the following months CR ozone remained too high in the lower stratosphere  
1146 and too low in the upper troposphere but the resulting TCs matched the observations in a  
1147 reasonable way (see Figure 16)

## 1148 **5.5 Evaluation with the GOZCARDS ozone product in the upper stratosphere**

1149 Ozone sondes do not provide accurate measurements above 10 hPa. The ozone bias profiles  
1150 shown in Figure 17 indicate higher values of MACCRA in the upper stratosphere and  
1151 mesosphere, i.e. from above 10 hPa to the model top of 0.1 hPa. Although the ozone mass in  
1152 this region is relatively small, the high values of the mixing ratios have a large impact on the  
1153 radiative transfer and the associated heating rates. To investigate the biases in that region we  
1154 used the Global OZone Chemistry And Related trace gas Data records for the Stratosphere  
1155 (GOZCARDS) product (Froidevaux et al., 2015). It consists of merged SAGE I, SAGE II,  
1156 HALOE, UARS and Aura MLS, and ACE-FTS data from late 1979 to 2012. SAGE II is used  
1157 as the primary reference in the merging procedure for the instruments. For most of the  
1158 CAMSIRA period, i.e. from 2004 onwards, Aura MLS and ACE-FTS are the dominating  
1159 instruments in the upper stratosphere. Tegtmeier et al. (2013) showed that ozone retrievals  
1160 from various instruments show a considerable spread in the upper stratosphere. ACE-FTS is

1161 biased high (5-10%) above 10 hPa and biased low ~~below (5-10%) below~~ 10 hPa against the  
1162 median of various retrievals.

1163 Figure 19 shows cross sections of the GOZCARDS product and relative bias of CAMSiRA,  
1164 MACCRA and CR in the vertical range from 50–0.3 hPa. In the region from 10–5 hPa  
1165 MACCRA had a positive bias of 10–15% in the tropics and mid-latitudes, which has already  
1166 been reported in Inness et al. (2013). About half of the 10 DU higher TCs in MACCRA  
1167 compared to CAMSiRA were caused by this overestimation in the levels above 10 hPa. The  
1168 biases of CAMSiRA in that region were smaller and vary between 2.5 and -2.5%. CAMSiRA  
1169 underestimated the GOZCARDS data between 5 and 1 hPa by up to 7%, whereas MACCRA  
1170 slightly overestimated. In the lower mesosphere MACCRA underestimated the ozone  
1171 concentrations by up to 30%.

1172 CR had very similar biases as CAMSiRA above 5 hPa in the tropics and mid-latitudes. This  
1173 means that the assimilation of observations had already little influence in this region even if  
1174 no increments were added during the CAMSiRA assimilation above 1 hPa. Below 10 hPa the  
1175 cross section of the bias shows the already discussed strong overestimation of CR in the mid  
1176 and higher latitudes, which was largest in relative terms at around 20–15 hPa and the  
1177 underestimation in the tropics, which was largest at around 50 hPa.

## 1178 **6 Tropospheric ozone**

1179 Correcting tropospheric ozone by the assimilation of TC and stratospheric ozone profiles  
1180 remains a challenge because the observations are dominated by the high stratospheric mixing  
1181 ratios (Wagner et al., 2015). The modelled ozone fields as well as the specification of the  
1182 vertical background error correlation have therefore a large impact on the analysed  
1183 tropospheric ozone fields (Inness et al., 2015).

### 1184 **6.1 Spatial patterns of ozone at 850 hPa**

1185 We focus the discussion of the seasonal spatial patterns of monthly mean tropospheric ozone  
1186 mole fraction to the 850 hPa pressure level values but we also discuss tropospheric ozone at  
1187 500 and 200 hPa in the section 6.2 and comparisons with ozone sondes for different  
1188 tropospheric layers in section 6.3. Figure 20 shows the seasonal means of CAMSiRA and the  
1189 differences with CR and MACCRA at 850 hPa. Extratropical NH ozone values of CAMSiRA  
1190 were mostly in the range from 35–55 ppb. The season of the maximum was MAM, when  
1191 values were about 20 ppb higher than in the seasonal minimum in DJF. Regional maxima of

1192 over 60 ppb were situated over the East Asia and the Arabian Peninsula. JJA was the season  
1193 when the highest values occurred over the areas of the regional maxima. In this season an  
1194 additional regional maxima occurred over tropical Africa. The SH values were generally  
1195 below 35 ppb. The seasonal maximum was in Austral spring (SON) and the minimum in  
1196 Austral summer and late autumn (SON).

1197 CR was about 2–4 ppb higher than CAMSiRA in most parts of the globe. Only in the higher  
1198 latitudes of SH as well as over the biomass burning regions in Africa, South America and  
1199 Maritime South East Asia, CAMSiRA was up to 4 ppb lower than CR. The biggest large-  
1200 scale reduction by the assimilation in NH occurred in DJF and the biggest increase in SH in  
1201 SON. The largest absolute increases of CAMSiRA of up to 10 ppb occurred over the Southern  
1202 end of the Arabian Peninsula at the time of the seasonal maximum in JJA. This was the only  
1203 local maximum in CAMSiRA that was increased by the assimilation.

1204 Tropospheric ozone was the only considered species for which the differences between  
1205 CAMSiRA and MACCRA were larger than the difference between CAMSiRA and CR. This  
1206 indicates the importance of the chemistry model parameterization and the limitations of the  
1207 data assimilation in this respect. In the extra-tropics of NH and SH, CAMSiRA was 2–5 ppb  
1208 lower than MACCRA with an increasing difference towards the poles. The largest difference  
1209 occurred in NH summer in JJA. CAMSiRA was up to 10 ppb lower than MACCRA over the  
1210 continents in the tropics. On the other hand, CAMSiRA had higher values than MACCRA  
1211 over the tropical oceans, the Sahara as well as at the location of the strong maximum over the  
1212 Arabian Peninsula, which was not present in MACCRA. The strong land-sea contrast in the  
1213 differences could be caused by (i) a different efficiency of deposition over the oceans, (ii) the  
1214 discussed differences in biomass burning emissions and (iii) differences in the chemistry  
1215 treatment (e.g. the isoprene degradation scheme).

1216 The vertical distribution (see Figure 14) of the mean ozone partial pressure in the troposphere  
1217 shows that CAMSiRA was lower than CR in the whole troposphere apart from the tropical  
1218 upper troposphere, where it was up to 10% higher, as well as below 500 hPa in the SH  
1219 troposphere. Compared to MACCRA, CAMSiRA was up to 20% higher in the middle and  
1220 upper troposphere in the tropics and subtropics but increasingly lower towards the surface.

## 1221 **6.2 Inter-annual variability**

1222 Estimating and understanding tropospheric ozone trends have been studied widely in the  
1223 literature, as reviewed in Cooper et al. (2014) and Monks et al. (2015). Factors that influence  
1224 the inter-annual variability and trends of tropospheric ozone are changes in anthropogenic and  
1225 biomass burning emissions, the stratosphere-troposphere exchange and the variability of the  
1226 meteorological fields. The observed trends vary strongly because these different factors are  
1227 not uniform in space and time. Trends are often confined to specific seasons or levels.  
1228 Positive trends are more common than negative trends and are found over Europe and North  
1229 America during spring (Cooper et al., 2014).

1230 Figure 21 shows time series of average ozone volume mixing ratios over selected regions  
1231 and pressure levels at 850, 500 and 200 hPa. It is beyond the scope of the paper to investigate  
1232 the robustness of the trends in CAMSiRA in detail. But it is worth noting that there were only  
1233 positive trends in the considered region at 850, 500 and 200 hPa in CAMSiRA. The trends  
1234 varied between 0-1.1%/yr, with a global mean of 0.5%/yr. Many of these trends were  
1235 significant (95% confidence level). CR also had mostly positive but much smaller trends with  
1236 a global mean of 0.17%/yr. The only significant trend in CR of 0.35%/yr was found over  
1237 East-Asia and the corresponding trend in CAMSiRA had the same value. Focusing over  
1238 Eastern China, Verstraeten et al. (2015) find a trend of about 1.2%/yr between 2005 and 2010,  
1239 which is considerably larger than the trend in CAMSiRA and CR.

1240 The time series in Figure 21 show that the higher values in NH of CR with respect to  
1241 CAMSiRA occurred in the entire troposphere. In the lower and mid troposphere CAMSiRA  
1242 was lower than CR especially during the seasonal minimum. In the tropics, CR and  
1243 CAMSiRA agreed well at 850 hPa, CR was slightly higher at 500 hPa and about 5 ppb lower  
1244 than CAMSiRA at 200 hPa. At this level CAMSiRA had a significant trend of 0.95%/yr in the  
1245 tropics, which was not present in CR. More detailed studies are needed to confirm the  
1246 realness of this upper tropospheric trend in CAMSiRA.

1247 A more detailed inspection of the time series shows that from the start of 2013 CR and  
1248 CAMSiRA agree to a higher degree than before in the middle and upper part of the troposphere  
1249 in NH. The agreement is most likely caused by a reduced correction by the assimilation in the  
1250 NH troposphere in this period. In early 2013 the assimilated MLS ozone retrieval switched  
1251 from version V2 to the NRT V3.4 product (see Table 2), which had different levels and

1252 observations errors. The discontinuation of the MIPAS in spring 2012 do not seem to be the  
1253 reason for this behaviour.

1254 The year-to-year variability of tropospheric ozone from MACCRA did often not resemble that  
1255 of CAMSiRA. In NH at 850 hPa (most prominently seen in the Arctic) MACCRA had  
1256 increasing values until 2008 after which they dropped to the values of CAMSiRA. This drift  
1257 of MACCRA and the associated negative trends are not realistic (as confirmed in section 6.3).  
1258 They were caused by applying the variational bias correction scheme to MLS data in  
1259 MACCRA (see Inness et al. 2013 for more details). The agreement between CAMSiRA and  
1260 MACCRA increases with increasing height in the extra-tropics but in the tropics MACCRA  
1261 showed a much stronger trend at 200 hPa than CAMSiRA.

### 1262 **6.3 Evaluation with ozone sondes in the troposphere**

1263 Figure 22 show time series of seasonal biases in pressure ranges representing the lower,  
1264 middle and upper troposphere from 6 different ozone sonde sites. The selected stations had at  
1265 least one observations for each month of the 2003-2105 period and are examples for Europe  
1266 (De Bilt), North America (Huntsville), the tropics (Nairobi), the Arctic (Ny-Ålesund) and  
1267 Antarctica (Neumayer Station). To present South-Asia we chose Hong Kong Observatory,  
1268 which had complete cover from 2003-2012. These individual time series depend on the  
1269 specific characteristics of the individual stations and are therefore less representative than the  
1270 averages over the gridded data sets shown in section 6.2.

1271 In the lower troposphere (950-700 hPa) over DeBilt, Huntsville and Nairobi, CR and  
1272 CAMSiRA had seasonal biases in the mostly in the range of -7-7 ppb. In the polar regions at  
1273 Neumayer Station and Ny-Ålesund both CR and CAMSiRA underestimated the observations.  
1274 At all locations CAMSiR was lower in the lower troposphere than CR, which meant that  
1275 CAMSiRA had mostly a larger absolute bias than CR. At Hong Kong Observatory both  
1276 CAMSiRA and CR overestimated the observations with biases in the range between 0-10 ppb.

1277 In the middle troposphere the absolute biases of CAMSiRA and CR were of the same  
1278 magnitude but of different signs. In the upper troposphere CR overestimated the observations  
1279 by about 10 ppb whereas the bias of CAMSiRA remained below 5 ppb. The overestimation of  
1280 CR is probably likely caused by the influence of the stratosphere where CR was too high (see  
1281 section 5.4). Over Nairobi the biases of CR and CAMSiRA were very similar in all levels but  
1282 CAMSiRA had overall lower biases in the lower troposphere. In the pressure range 400-300

1283 hPa in the tropics the impact of stratospheric biases on CR is less strong because of the higher  
1284 tropopause height in this region.

1285 The biases for all three data sets at Ny-Ålesund, Hunstville and Hong Kong Observatory  
1286 showed a pronounced seasonality in the middle and upper troposphere. At Huntsville the  
1287 spring maximum was especially overestimated, i.e. it occurred 2-3 month too early. At Ny-  
1288 Ålesund the overestimation was caused by too high values in summer and autumn. Over  
1289 Hong Kong Observatory the pronounced observed spring maximum was not well reproduced.

1290 As already discussed in section 6.2, the characteristics of the bias of CAMSiRA changed at  
1291 the start of 2013 mainly in the upper parts of the NH troposphere but also throughout the  
1292 troposphere over higher latitudes. In this period the CAMSiRA biases resembles much more  
1293 the bias of CR which often mean an increase in the average values, which could cause a  
1294 spurious enhancement of positive trends.

1295 At Neumayer Station CAMSiRA increased in a step-wise manner already at the start of 2012,  
1296 which changed the bias from an underestimation to a slight overestimation together with an  
1297 increased seasonality. This behaviour could be caused by the discontinuation of MIPAS in  
1298 spring 2012 (see Table 2). Although the MIPAS retrievals were only stratospheric profiles,  
1299 the combined assimilation with total column retrievals can trigger a correction in the  
1300 troposphere (Flemming et al., 2011).

1301 MACCRA had a less stable bias than CAMSiRA. In the lower and mid-troposphere biases  
1302 from 2006–2008 were much higher than in the rest of the period, when they resembled more  
1303 the biases of CAMSiRA and CR. This confirms that the discussed inter-annual variability of  
1304 MACCRA seem less realistic than that of CR and CAMSiRA.

1305 It should be noted that both MACCRA and CAMSiRA suffered from larger than typical  
1306 negative biases in the NH in the first half of 2003, which can probably be explained by biases  
1307 in the initial conditions and the short spin-up period of 1 month only.

#### 1308 **6.4 Evaluation with Airbase Ozone surface observations**

1309 The AirBase and EMEP databases host operational air quality observations from different  
1310 national European networks. All EMEP stations are located in rural areas, while Airbase  
1311 stations are designed to monitor pollution at different scales. Stations of the rural regime can  
1312 capture the larger scale signal in particular for O<sub>3</sub>, which is spatially well correlated

1313 (Flemming et al., 2005). Therefore EMEP stations and only rural Airbase stations were used  
1314 in the evaluation to account for the model resolution of C-IFS.

1315 ~~Figure 23~~ [Figure 23](#) shows the average diurnal cycle for each season of the observed values  
1316 and CAMSiRA, CR and MACCRA. CR and CAMSiRA were very similar and matched well  
1317 the shape of the observed diurnal cycle. However there was a constant bias of about 5 ppb in  
1318 MAM and DJF. CR had slightly smaller biases than CAMSiRA in JJA in the afternoon.  
1319 MACCRA had a larger diurnal range because the day-time values were higher than the ones  
1320 of CAMSiRA. This meant smaller day-time biases in MAM and DJF and hence a smaller  
1321 seasonal bias for MACCRA. But it also led to a considerable (10 ppb) day time  
1322 overestimation in JJA and a smaller overestimation in SON as well as a less well fit with the  
1323 shape of the observed diurnal cycle in all seasons.

1324 The winter and spring underestimation of CAMSiRA and CR has already been reported in  
1325 Fleming et al. (2015). To investigate the possible causes of this seasonal bias Figure 24  
1326 shows the average seasonal cycle at the surface at the EMEP-AirBase stations and in the  
1327 lower troposphere (950–750 hPa) over ozone sonde stations. The differences between  
1328 CAMSiRA, CR and MACCRA were more pronounced in the lower troposphere than at the  
1329 surface. This indicates again that the assimilation has little influence on the surface values.  
1330 CR matched the observations in the lower troposphere well in all seasons apart from SON,  
1331 when it overestimated. MACCRA had similar biases as CR but overestimated additionally in  
1332 JJA and especially over southern Europe, as shown in Katragkou et al. (2015). CAMSiRA  
1333 underestimated throughout the year with the exception of SON. As the patterns of the  
1334 seasonal biases were different in the lower troposphere and at the surface, we conclude that  
1335 the winter and spring-time bias at the surface is not predominately caused by tropospheric  
1336 biases. It is more likely that the simulation of surface processes such dry deposition and  
1337 titration by freshly emitted NO are the reasons for this bias at the surface.

## 1338 **7 Summary and conclusions**

1339 CAMSiRA is a new reanalysis data set of aerosol, CO and ozone for the period 2003–2015. It  
1340 has been produced by assimilating satellite retrievals of AOD, TC CO as well as TC and  
1341 stratospheric ozone profile retrievals from various sensors in C-IFS using the ECMWF 4D-  
1342 VAR approach. A similar set of observations was assimilated in MACCRA, a previous  
1343 reanalysis data set for the period 2003–2012. A control run with C-IFS (CR) without the

1344 assimilation of AC observations was carried to infer the impact of the assimilated  
1345 observations.

## 1346 **7.1 CAMSiRA compared to MACCRA**

1347 Compared to its predecessor MACCRA, CAMSiRA had smaller biases of surface and lower  
1348 tropospheric CO as shown by the comparison with MOZAIC/IAGOS CO profiles and  
1349 NOAA-GMD CO flask observations. However, MACCRA had lower CO biases in NH mid  
1350 and upper troposphere with respect to the MOZAIC/IAGOS CO profiles. The biases of TC  
1351 ozone against the WOUDC Dobson sun photometers were reduced from 5–10 DU in  
1352 MACCRA to 0–5 DU in CAMSiRA. The biases of CAMSiRA against AERONET AOD  
1353 observations were lower in most parts of the globe with the exception of South East Asia. A  
1354 larger improvement was the elimination of the positive bias of upper stratospheric ozone in  
1355 MACCRA as shown by the comparison with the GOZCARDS ozone product. CAMSiRA  
1356 also had a better agreement with the shape of the mean observed diurnal cycle of AIRBASE  
1357 ground-level ozone observations in Europe in all seasons but winter and spring time seasonal  
1358 values were still underestimated by 5 ppb. We attribute all the aforementioned differences  
1359 between CAMSiRA and MACCRA, which were mainly improvements, to the change of the  
1360 assimilating model, which was the coupled system IFS-MOZART for MACCRA and C-IFS  
1361 with updated aerosol parameterizations for CAMSiRA.

1362 Progress achieved by changes to the assimilated observations was a noteworthy improvement  
1363 of the temporal consistency of the tropospheric CO and ozone fields in CAMSiRA. The  
1364 assimilation of IASI CO in MACCRA from 2008 onwards had led to a decrease in the TC CO  
1365 values because of the biases against the MOPITT data set, which was assimilated during the  
1366 whole period. Consequently, the MACCRA CO fields in the mid- and high latitudes of both  
1367 hemispheres showed strong negative trends which were not in agreement with linear trends  
1368 estimated from CO flask surface observations. On the other hand, the linear trends of  
1369 CAMSiRA agreed well with the observed trends, which were close to zero in SH and reached  
1370 values of about 2 ppb/yr in the NH mid and high latitudes. The mid and upper tropospheric  
1371 ozone fields of MACCRA suffered from an increase in the period 2004–2008 caused by a  
1372 applying disproportionate application of the inter-instrument bias correction to the MLS  
1373 column retrievals, which was corrected for CAMSiRA (Inness et al., 2015).



1374 A discontinuity in the upper and middle tropospheric ozone field was noted for CAMSiRA  
1375 after January of 2013 and was due to a change in version of the assimilated MLS ozone  
1376 retrievals. Although this change in CAMSiRA did not mean an increase in the bias, it has to  
1377 be considered when trends of tropospheric ozone fields are to be calculated from the  
1378 CAMSiRA data set.

1379 The AOD in CAMSiRA was about 0.01 lower than MACCRA in most parts of the globe,  
1380 mainly because of a 50% lower burden of sea salt in CAMSiRA. CAMSiRA had higher AOD  
1381 values over the desert dust emitting regions in North-Africa and the global desert dust burden  
1382 was higher in CAMSiRA. CAMSiRA had 25% higher AOD contribution by sulphate than  
1383 MACCRA, which is currently under scrutiny.

## 1384 **7.2 CAMSiRA compared to CR**

1385 The comparison with CR showed that the assimilation led to a clear improvement for CO,  
1386 AOD and TC ozone as well as stratospheric and upper tropospheric ozone.

1387 The assimilation of MOPITT CO increased the values in the NH mid-latitudes more in the  
1388 beginning of the period, which could indicate a stronger underestimation of the anthropogenic  
1389 emissions in this period as well as an overestimation of the trend in the emissions. The  
1390 tropical and SH values were reduced by the assimilation, which may indicate an  
1391 overestimation of the biomass burning emissions in this region. However, the rather zonally  
1392 homogeneous CO differences between CR and CAMSiRA suggest that not only biases in the  
1393 fire emissions but also of the CO lifetime and chemical production as well as the CO transport  
1394 need to be investigated further.

1395 The Cariolle scheme for stratospheric ozone, which was used in C-IFS, suffered from a large  
1396 overestimation of NH mid-and high latitude stratospheric ozone (50–100DU) and an  
1397 underestimation in the tropics (-20 DU). These biases were corrected by the assimilation and  
1398 the resulting biases of CAMSiRA were of 5 DU and lower. Also in the SH high-latitudes the  
1399 Cariolle scheme overestimated the mean TCs especially in JJA by up to 30 DU but the depth  
1400 and the year-to-year variability of the ozone hole was well reproduced by CR. Nevertheless,  
1401 CAMSiRA had more realistic TCs and profiles than CR during the annual ozone hole events.

1402 The assimilation had only little impact on the ozone values at the surface and in lower  
1403 troposphere, where the biases of CAMSiRA were sometimes even slightly larger than of CR.  
1404 The small influence could be explained by the fact, that dry deposition velocities and

1405 important ozone precursors such as  $\text{NO}_x$  were not constrained during the assimilation process.  
1406 Also contributing was the fact that no direct tropospheric ozone observations were assimilated  
1407 nor that the vertical correlations in the model background errors were strong enough to cause  
1408 a correction of the surface levels based on the levels above. –The assimilation was more  
1409 beneficial in the upper troposphere, where the stratospheric influence is more important.

1410 CAMSiRA had about 0.05 higher AOD values than CR apart from the desert dust emission  
1411 regions, where the assimilation strongly reduced the modelled values. CAMSiRA tended to  
1412 slightly overestimate the AERONET AOD observations and CR to underestimate but the  
1413 overall biases of CAMSiRA were smaller.

1414 Despite moderate differences in AOD, CR and CAMSiRA had considerable differences in  
1415 the aerosol speciation. The global annual sea salt burden by C-IFS in CR of 15 Tg was  
1416 considerably higher than the result of other modelling studies (Textor et al., 2006 and Spada  
1417 et al., 2012). Less efficient loss processes may have played a large role in this overestimation.  
1418 The assimilation strongly reduced the sea salt burden in CAMSiRA to about half of the value  
1419 in CR. Also the global desert dust burden was reduced by 25% by the assimilation leading to  
1420 lower total AOD values over the desert dust emissions regions of Sahara, Australia and  
1421 Middle Asia. Despite the fact that CAMSiRA had a 30% smaller global aerosol burden, its  
1422 average global AOD was about 10% higher than the one of CAMSiRA. This was caused by a  
1423 strong increase in sulphate in CAMSiRA. The optical properties and assumed size distribution  
1424 of sulphate make extinction more efficient for the same amount of mass. Sulphate became the  
1425 dominant contribution to AOD in the regions away from the main aerosol emissions. The  
1426 strong contribution of sulphate may have partly compensated for the inadequate  
1427 representation of other secondary aerosols in C-IFS. However its magnitude and spread over  
1428 the whole globe seems excessive. It might be caused by the lack of strong loss processes in  
1429 the free troposphere as well as biases in the assimilated observations over the open oceans. As  
1430 the CR underestimates the assimilated AOD, the aerosol mass is increased during the  
1431 assimilation, initially by the same relative amount for all components. However, a longer life-  
1432 time of sulphate causes a longer lasting change compared to the other aerosol species, which  
1433 made sulphate the dominating aerosol. This distortion of the speciation can not be corrected  
1434 by the assimilated MODIS AOD retrievals, which do not contain information about the  
1435 speciation.

### 1436 **7.3 Recommendations for future AC reanalysis**

1437 CAMSiRA is considerable improvement over MACCRA especially with respect to the  
1438 temporal consistency. To further improve on this important aspect, one should make sure that  
1439 consistent input emission data sets and assimilated observations are used. Changes in the  
1440 assimilated observations, such as the version change in the MLS after 2012 should be  
1441 avoided. The use of MEGAN simulated biogenic emissions for the whole period is advisable  
1442 even if no related jumps were detected in this study. To ensure consistency between the  
1443 aerosols and chemistry components, the same SO<sub>2</sub> emissions should be used.

1444 As improvements to lower tropospheric ozone by assimilating current satellite observations  
1445 are difficult to achieve, emphasis needs to be put on the improved simulation of chemistry and  
1446 dry deposition. The assimilation of tropospheric ozone column retrievals as well as of  
1447 tropospheric NO<sub>2</sub> may further help to improve the ground level ozone in the reanalysis.

1448 A prospect is to enable the correction of emissions based on observations of atmospheric  
1449 composition with the C-IFS data assimilation system. This could also improve the analysis of  
1450 tropospheric ozone as ozone precursor emissions would be corrected. An intermediate step in  
1451 this direction is to better account for the emission uncertainty in the model background error  
1452 statistics.

1453 ~~To further develop the C-IFS assimilation system to allow the correction of ozone precursor~~  
1454 ~~emissions could be an important next step towards an improved tropospheric ozone analysis.~~

1455 The high sulphate burden introduced by the assimilation can ~~perhaps~~ be avoided by (i) the  
1456 introduction of more intensive loss processes in the free troposphere, (ii) an increase of the  
1457 organic matter to better represent non-accounted SOA components and (iii) changes to the  
1458 vertical structure of the background errors to avoid the accumulation of aerosol mass away  
1459 from the surface. In general, any modelling improvements for a better speciation will reflect  
1460 in a more realistic aerosol analysis and a better exploitation of the available observations. If  
1461 possible the latest reprocesses MODIS AOD dataset should be used (collection 6).

1462 In CAMSiRA and MACCRA the aerosol and chemistry schemes were independent. A better  
1463 coupling between the two and the meteorological simulation is desirable. For example the use  
1464 of aerosol to modulate photolysis rates and heterogeneous uptake on aerosol as well as the  
1465 simulating the impact on aerosols and ozone within the radiation transfer calculation of IFS  
1466 will be important next steps.

1467

1468

1469

1470 ***Data access***

1471 The CAMSiRA data are freely available. Please contact [copernicus-support@ecmwf.int](mailto:copernicus-support@ecmwf.int)

1472

1473 ***Acknowledgments***

1474 CAMS is funded by the European Union's Copernicus Programme. The GOZCARDS data

1475 were obtained from the NASA Goddard Earth Science Data and Information Services Centre.

1476 We are grateful to the World Ozone and Ultraviolet Radiation Data Centre (WOUDC) for

1477 providing ozone sonde and Dobson-photometer observations. We thank the Global

1478 Atmospheric Watch programme for the provision of CO and ozone surface observations. We

1479 thank the European Environmental Agency for providing access to European ozone

1480 observations in the AirBase data base. We also thank the MOZAIC (Measurements of OZone,

1481 water vapour, carbon monoxide and nitrogen oxides by in-service Airbus aircraft) and

1482 IAGOS (In-Service Aircraft for a Global Observing System) programmes for providing CO

1483 profile observations.

1484

1485

1486 **References**

- 1487 Auligne, T., McNally, A. P., and Dee, D. P.: Adaptive bias correction for satellite data in a  
1488 numerical weather prediction system, *Q. J. Roy. Meteor. Soc.*, 133, 631–642, 2007.
- 1489 Basher, R. E. (1982), Review of the Dobson spectrophotometer and its accuracy, *Global*  
1490 *Ozone Res. Monit. Proj.*, Rep. 13, World Meteorol. Organ., Geneva, Switzerland, Dec.  
1491 (Available at <http://www.esrl.noaa.gov/gmd/ozwv/dobson/papers/report13/report13.html>)
- 1492 Bechtold, P., Orr, A. Morcrette, J.-J., Engelen, R., Flemming, J. and Janiskova, M.:  
1493 Improvements in the stratosphere and mesosphere of the IFS, *ECMWF Newsletter No.* 120–  
1494 Summer, 2009.
- 1495 Beekmann M., Ancellet G., Megie G., Smit H. G. J., and Kley D.: Intercomparison campaign  
1496 for vertical ozone profiles including electrochemical sondes of ECC and Brewer-Mast type  
1497 and aground based UV-differential absorption radar, *J. Atmos. Chem.*, 10, 259–288, 1994.
- 1498 Bellouin, N., Quaas, J., Morcrette, J.-J., and Boucher, O.: Estimates of aerosol radiative  
1499 forcing from the MACC re-analysis, *Atmos. Chem. Phys.*, 13, 2045-2062, doi:10.5194/acp-  
1500 13-2045-2013, 2013.
- 1501 Benedetti, A., Morcrette, J.-J., Boucher, O., Dethof, A., Engelen, R. J., Fisher, M., Flentje, H.,  
1502 Huneus, N., Jones, L., Kaiser, J. W., Kinne, S., Mangold, A., Razinger, M., Simmons, A. J.,  
1503 Suttie, M., and the GEMS-AER team: Aerosol analysis and forecast in the European Centre  
1504 for Medium-Range Weather Forecasts Integrated Forecast System: 2. Data assimilation, *J.*  
1505 *Geophys. Res.*, 114, D13205, doi:10.1029/2008JD011115, 2009.
- 1506 Benedetti, A. Jones, L., Kaiser, J. W., Morcrette, J.-J. and Rémy, S.: [Global climate]  
1507 Aerosols [in “State of the Climate in 2013”]. *Bull. Amer. Meteor. Soc.*, 95 (7), S36-37, 2014.
- 1508 Bhartia, P. K. and Wellemeyer, C.: TOMS-V8 total O<sub>3</sub> algorithm, in: *OMI Ozone Product*  
1509 *ATBD Volume II*, NASA Goddard Space Flight Center, Greenbelt, MD, USA, 2002.
- 1510 Bhartia, P. K., McPeters, R. D., Mateer, C. L., Flynn, L. E., and Wellemeyer, C., Algorithm  
1511 for the estimation of vertical ozone profiles from the backscattered ultraviolet technique, *J.*  
1512 *Geophys. Res.*, 101, 18793–18806, 1996.
- 1513 Bocquet, M., Elbern, H., Eskes, H., Hirtl, M., Žabkar, R., Carmichael, G. R., Flemming, J.,  
1514 Inness, A., Pagowski, M., Pérez Camaño, J. L., Saide, P. E., San Jose, R., Sofiev, M., Vira, J.,  
1515 Baklanov, A., Carnevale, C., Grell, G., and Seigneur, C.: Data assimilation in atmospheric

1516 chemistry models: current status and future prospects for coupled chemistry meteorology  
1517 models, *Atmos. Chem. Phys.*, 15, 5325-5358, doi:10.5194/acp-15-5325-2015, 2015.

1518 Boucher, O.: *Atmospheric Aerosols, Properties and Climate Impacts*, Springer Netherlands,  
1519 10.1007/978-94-017-9649-1, 311p. 2015.

1520 Cariolle, D. and Dèquè, M.: Southern hemisphere medium-scale waves and total ozone  
1521 disturbances in a spectral general circulation model, *J. Geophys. Res.*, 91D, 10825–10846,  
1522 1986.

1523 Cariolle, D. and Teyssèdre, H.: A revised linear ozone photochemistry parameterization for  
1524 use in transport and general circulation models: multi-annual simulations, *Atmos. Chem.*  
1525 *Phys.*, 7, 2183-2196, doi:10.5194/acp-7-2183-2007, 2007.

1526 Cesnulyte, V., Lindfors, A. V., Pitkänen, M. R. A., Lehtinen, K. E. J., Morcrette, J.-J., and  
1527 Arola, A.: Comparing ECMWF AOD with AERONET observations at visible and UV  
1528 wavelengths, *Atmos. Chem. Phys.*, 14, 593-608, doi:10.5194/acp-14-593-2014, 2014.

1529 Coldewey-Egbers, M., Loyola R., D. G., Braesicke, P., Dameris, M., van Roozendaal, M.,  
1530 Lerot, C. and Zimmer, W.: A new health check of the ozone layer at global and regional  
1531 scales, *Geophys. Res. Lett.*, 41, 4363–4372, doi:10.1002/2014GL060212, 2014.

1532 Cooper, O. R., Parrish, D. D., Ziemke, J., Balashov, N. V., Cupeiro, M., Galbally, I. E., Gilge,  
1533 S., Horowitz, L., Jensen, N. R., Lamarque, J.-F., Naik, V., Oltmans, S. J., Schwab, J.,  
1534 Shindell, D. T., Thompson, A. M., Thouret, V., Wang, Y., and Zbinden, R. M.: Global  
1535 distribution and trends of tropospheric ozone: An observation-based review, *Elementa:*  
1536 *Science of the Anthropocene*, 2, 1–28, doi:10.12952/journal.elementa.000029, 2014.

1537 Courtier, P., Thépaut, J.-N., and Hollingsworth, A.: A strategy for operational implementation  
1538 of 4D-Var, using an incremental approach, *Q. J. Roy. Meteorol. Soc.*, 120, 1367–1388, 1994.

1539 Cuevas, E., Camino, C., Benedetti, A., Basart, S., Terradellas, E., Baldasano, J. M.,  
1540 Morcrette, J. J., Marticorena, B., Goloub, P., Mortier, A., Berjón, A., Hernández, Y., Gil-  
1541 Ojeda, M., and Schulz, M.: The MACC-II 2007–2008 reanalysis: atmospheric dust evaluation  
1542 and characterization over northern Africa and the Middle East, *Atmos. Chem. Phys.*, 15,  
1543 3991-4024, doi:10.5194/acp-15-3991-2015, 2015.

1544 Dee, D. P.: Variational bias correction of radiance data in the ECMWF system, in:  
1545 Proceedings of the ECMWF workshop on assimilation of high spectral resolution sounders in  
1546 NWP, Reading, UK, 28 June–1 July 2004, 97–112, 2004.

1547 Dee, D. P. and Uppala, S.: Variational bias correction of satellite radiance data in the ERA-  
1548 Interim reanalysis, *Q. J. Roy. Meteor. Soc.*, 135, 1830–1841, 2009.

1549 Dee, D.P., Uppala, S.M., Simmons, A.J., Berrisford, P., Poli, P., Kobayashi, S., Andrae, U.,  
1550 Balmaseda, M.A., Balsamo, G., Bauer, P., Bechtold, P., Beljaars, A.C.M., van de Berg, L.,  
1551 Bidlot, J., Bormann, N., Delsol, C., Dragani, R., Fuentes, M., Geer, A.J., Haimberger, L.,  
1552 Healy, S.B., Hersbach, H., Hólm, E.V., Isaksen, L., Kållberg, P., Köhler, M., Matricardi, M.,  
1553 McNally, A.P., Monge-Sanz, B.M., Morcrette, J.-J., Park, B.-K., Peubey, C., de Rosnay, P.,  
1554 Tavolato, C., Thépaut, J.-N., Vitart, F.: The ERA-Interim reanalysis: Configuration and  
1555 performance of the data assimilation system, *Quarterly Journal of the Royal Meteorological*  
1556 *Society*, 2011.

1557 Deeter, M.N., MOPITT Version 5 Product User's Guide, Technical Report, NCAR, Boulder,  
1558 USA, [www.acom.ucar.edu/mopitt/v5\\_users\\_guide\\_beta.pdf](http://www.acom.ucar.edu/mopitt/v5_users_guide_beta.pdf) (last access 24.7.2016), 2011.

1559 Deeter, M. N., S. Martínez-Alonso, D. P. Edwards, L. K. Emmons, J. C. Gille, H. M. Worden,  
1560 J. V. Pittman, B. C. Daube, and S. C. Wofsy: Validation of MOPITT Version 5 thermal-  
1561 infrared, near-infrared, and multispectral carbon monoxide profile retrievals for 2000–2011, *J.*  
1562 *Geophys. Res. Atmos.*, 118, 6710–6725, doi:10.1002/jgrd.50272, 2013.

1563 de Laat, A. T. J., Aben, I., Deeter, M., Nédélec, P., Eskes, H., Attié, J.-L., Ricaud, P., Abida,  
1564 R., El Amraoui, L., and Landgraf, J.: Validation of nine years of MOPITT V5 NIR using  
1565 MOZAIC/IAGOS measurements: biases and long-term stability, *Atmos. Meas. Tech.*, 7,  
1566 3783-3799, doi:10.5194/amt-7-3783-2014, 2014.

1567 Dentener, F., Kinne, S., Bond, T., Boucher, O., Cofala, J., Generoso, S., Ginoux, P., Gong, S.,  
1568 Hoelzemann, J. J., Ito, A., Marelli, L., Penner, J. E., Putaud, J.-P., Textor, C., Schulz, M., van  
1569 der Werf, G. R., and Wilson, J.: Emissions of primary aerosol and precursor gases in the years  
1570 2000 and 1750 prescribed data-sets for AeroCom, *Atmos. Chem. Phys.*, 6, 4321-4344,  
1571 doi:10.5194/acp-6-4321-2006, 2006.

1572 Diamantakis, M. and Flemming, J.: Global mass fixer algorithms for conservative tracer  
1573 transport in the ECMWF model, *Geosci. Model Dev.*, 7, 965-979, doi:10.5194/gmd-7-965-  
1574 2014, 2014.

1575 Elguindi, N., Clark, H., Ordóñez, C., Thouret, V., Flemming, J., Stein, O., Huijnen, V.,  
1576 Moinat, P., Inness, A., Peuch, V.-H., Stohl, A., Turquety, S., Athier, G., Cammas, J.-P., and  
1577 Schultz, M.: Current status of the ability of the GEMS/MACC models to reproduce the  
1578 tropospheric CO vertical distribution as measured by MOZAIC, *Geosci. Model Dev.*, 3, 501-  
1579 518, doi:10.5194/gmd-3-501-2010, 2010.

1580 Emmons, L. K., Arnold, S. R., Monks, S. A., Huijnen, V., Tilmes, S., Law, K. S., Thomas, J.  
1581 L., Raut, J.-C., Bouarar, I., Turquety, S., Long, Y., Duncan, B., Steenrod, S., Strode, S.,  
1582 Flemming, J., Mao, J., Langner, J., Thompson, A. M., Tarasick, D., Apel, E. C., Blake, D. R.,  
1583 Cohen, R. C., Dibb, J., Diskin, G. S., Fried, A., Hall, S. R., Huey, L. G., Weinheimer, A. J.,  
1584 Wisthaler, A., Mikoviny, T., Nowak, J., Peischl, J., Roberts, J. M., Ryerson, T., Warneke, C.,  
1585 and Helmig, D.: The POLARCAT Model Intercomparison Project (POLMIP): overview and  
1586 evaluation with observations, *Atmos. Chem. Phys.*, 15, 6721-6744, doi:10.5194/acp-15-6721-  
1587 2015, 2015.

1588 [Eskes, H., Huijnen, V., Arola, A., Benedictow, A., Blechschmidt, A.-M., Botek, E., Boucher,](#)  
1589 [O., Bouarar, I., Chabrilat, S., Cuevas, E., Engelen, R., Flentje, H., Gaudel, A., Griesfeller, J.,](#)  
1590 [Jones, L., Kapsomenakis, J., Katragkou, E., Kinne, S., Langerock, B., Razinger, M., Richter,](#)  
1591 [A., Schultz, M., Schulz, M., Sudarchikova, N., Thouret, V., Vrekoussis, M., Wagner, A., and](#)  
1592 [Zerefos, C.: Validation of reactive gases and aerosols in the MACC global analysis and](#)  
1593 [forecast system, \*Geosci. Model Dev.\*, 8, 3523-3543, doi:10.5194/gmd-8-3523-2015, 2015.](#)

1594

1595 Field, R.D., G.R. van der Werf, and S.S.P. Shen, Human amplification of drought-induced  
1596 biomass burning in Indonesia since 1960, *Nature Geoscience*, 2 (3), 185-188,  
1597 doi:10.1038/ngeo443, 2009.

1598 Flemming, J., Stern, R., and Yamartino, R. J.: A new air quality regime classification scheme  
1599 for O<sub>3</sub>, NO<sub>2</sub>, SO<sub>2</sub> and PM<sub>10</sub> observations sites, *Atmos. Environ.*, 39, 6121–6129, 2005.

1600 Flemming, J., Inness, A., Flentje, H., Huijnen, V., Moinat, P., Schultz, M. G., and Stein, O.:  
1601 Coupling global chemistry transport models to ECMWF's integrated forecast system, *Geosci.*  
1602 *Model Dev.*, 2, 253-265, doi:10.5194/gmd-2-253-2009, 2009.

1603 Flemming, J., Inness, A., Jones, L., Eskes, H. J., Huijnen, V., Schultz, M. G., Stein, O.,  
1604 Cariolle, D., Kinnison, D., and Brasseur, G.: Forecasts and assimilation experiments of the



1605 Antarctic ozone hole 2008, *Atmos. Chem. Phys.*, 11, 1961–1977, doi:10.5194/acp-11-1961-  
1606 2011, 2011.

1607 Flemming J, and Inness, A.: [Global climate] Carbon Monoxide [in “State of the Climate in  
1608 2013”]. *Bull. Amer. Meteor. Soc.*, 95 (7), S43, 2014.

1609 Flemming, J., Huijnen, V., Arteta, J., Bechtold, P., Beljaars, A., Blechschmidt, A.-M.,  
1610 Diamantakis, M., Engelen, R. J., Gaudel, A., Inness, A., Jones, L., Josse, B., Katragkou, E.,  
1611 Marecal, V., Peuch, V.-H., Richter, A., Schultz, M. G., Stein, O., and Tsikerdekis, A.:  
1612 Tropospheric chemistry in the Integrated Forecasting System of ECMWF, *Geosci. Model  
1613 Dev.*, 8, 975-1003, doi:10.5194/gmd-8-975-2015, 2015.

1614 Froidevaux, L., Anderson, J., Wang, H.-J., Fuller, R. A., Schwartz, M. J., Santee, M. L.,  
1615 Livesey, N. J., Pumphrey, H. C., Bernath, P. F., Russell III, J. M., and McCormick, M. P.:  
1616 Global OZone Chemistry And Related trace gas Data records for the Stratosphere  
1617 (GOZCARDS): methodology and sample results with a focus on HCl, H<sub>2</sub>O, and O<sub>3</sub>, *Atmos.  
1618 Chem. Phys.*, 15, 10471-10507, doi:10.5194/acp-15-10471-2015, 2015.

1619 Froidevaux, L., Jiang, Y. B., Lambert, A., Livesey, N. J., Read, W. G., Waters, J. W.,  
1620 Browell, E. V., Hair, J. W., Avery, M. A., McGee, T. J., Twigg, L.W., Sunnicht, G. K.,  
1621 Jucks, K.W., Margitan, J. J., Sen, B., Stachnik, R. A., Toon, G. C., Bernath, P. F., Boone, C.  
1622 D., Walker, K. A., Filipiak, M. J., Harwood, R. S., Fuller, R. A., Manney, G. L., Schwartz, M.  
1623 J., Daffer, W. H., Drouin, B. J., Cofield, R. E., Cuddy, D. T., Jarnot, R. F., Knosp, B.W.,  
1624 Perun, V. S., Snyder, W. V., Stek, P. C., Thurstans, R. P., and Wagner, P. A.: Validation of  
1625 Aura Microwave LimbSounder stratospheric ozone measurements, *J. Geophys. Res.*, 113,  
1626 D15S20, doi:10.1029/2007JD008771, 2008.

1627 Gaubert, B., Arellano Jr. A. F., Barré, J., Worden, H. M., Emmons, L. K., Tilmes, S.,  
1628 Buchholz, R. R., Vitt, F., Raeder, K., Collins, N., Anderson, J. L., Wiedinmyer, C., Martinez  
1629 Alonso, S., Edwards, D. P., Andreae, M. O., Hannigan, J. W., Petri, C., Strong, K. and Jones,  
1630 N.: Toward a chemical reanalysis in a coupled chemistry-climate model: An evaluation of  
1631 MOPITT CO assimilation and its impact on tropospheric composition, *J. Geophys. Res.*  
1632 *Atmos.*, 121, 7310–7343, doi:10.1002/2016JD024863, 2016.

1633 Gaudel, A., Clark, H., Thouret, V., Jones, L., Inness, A., Flemming, J., Stein, O., Huijnen, V.,  
1634 Eskes, H., Nédélec, and P. Boulangerand,D.: On the use of MOZAIC-IAGOS data to assess

1635 the ability of the MACC reanalysis to reproduce the distribution of O<sub>3</sub> and CO in the UTLS  
1636 over Europe. *Tellus B.* 67, 27955. DOI: <http://dx.doi.org/10.3402/tellusb.v67.27955>, 2015.

1637 Giordano, L., Brunner, D., Flemming, J., Hogrefe, C., Im, U., Bianconi, R., Badia, A.,  
1638 Balzarini, A., Baró, R., Chemel, C., Curci, G., Forkel, R., Jiménez-Guerrero, P., Hirtl, M.,  
1639 Hodzic, A., Honzak, L., Jorba, O., Knote, C., Kuenen, J. J. P., Makar, P. A., Manders-Groot,  
1640 A., Neal, L., Pérez, J. L., Pirovano, G., Pouliot, G., San José, R., Savage, N., Schröder, W.,  
1641 Sokhi, R. S., Syrakov, D., Torian, A., Tuccella, P., Werhahn, J., Wolke, R., Yahya, K.,  
1642 Žabkar, R., Zhang, Y., and Galmarini, S.: Assessment of the MACC reanalysis and its  
1643 influence as chemical boundary conditions for regional air quality modelling in AQMEII-2,  
1644 *Atmos. Environ.*, 115, 371–388, 2015.

1645 George, M., Clerbaux, C., Bouarar, I., Coheur, P.-F., Deeter, M. N., Edwards, D. P., Francis,  
1646 G., Gille, J. C., Hadji-Lazaro, J., Hurtmans, D., Inness, A., Mao, D., and Worden, H. M.: An  
1647 examination of the long-term CO records from MOPITT and IASI: comparison of retrieval  
1648 methodology, *Atmos. Meas. Tech.*, 8, 4313-4328, doi:10.5194/amt-8-4313-2015, 2015.

1649 Granier, C., J.F. Lamarque, A. Mieville, J.F. Muller, J. Olivier, J. Orlando, J. Peters, G.  
1650 Petron, G. Tyndall, S. Wallens, POET, a database of surface emissions of ozone precursors,  
1651 available on internet at <http://www.aero.jussieu.fr/projet/ACCENT/POET.php>, 2005.

1652 Granier, C., B. Bessagnet, T. Bond, A. D'Angiola, H.D.v.d. Gon, G.J. Frost, A. Heil, J.W.  
1653 Kaiser, S. Kinne, Z. Klimont, S. Kloster, J.-F. Lamarque, C. Liousse, T. Masui, F. Meleux, A.  
1654 Mieville, T. Ohara, J.-C. Raut, K. Riahi, M.G. Schultz, S.J. Smith, A. Thomson, J.v.  
1655 Aardenne, G.R.v.d. Werf, and D.P.v. Vuuren, Evolution of anthropogenic and biomass  
1656 burning emissions of air pollutants at global and regional scales during the 1980-2010 period,  
1657 *Climatic Change*, 109(1-2), 163-190, doi:10.1007/s10584-011-0154-1, 2011.

1658 Grythe, H., Ström, J., Krejci, R., Quinn, P., and Stohl, A.: A review of sea-spray aerosol  
1659 source functions using a large global set of sea salt aerosol concentration measurements,  
1660 *Atmos. Chem. Phys.*, 14, 1277-1297, doi:10.5194/acp-14-1277-2014, 2014.

1661 Guenther, A. B., Karl, T., Harley, P., Wiedinmyer, C., Palmer, P. I., and Geron, C.: Estimates  
1662 of global terrestrial isoprene emissions using MEGAN (Model of Emissions of Gases and  
1663 Aerosols from Nature), *Atmos. Chem. Phys.*, 6, 3181–3210, doi:10.5194/acp-6-3181-2006,  
1664 2006.

1665 Hao, N., Koukouli, M. E., Inness, A., Valks, P., Loyola, D. G., Zimmer, W., Balis, D. S.,  
1666 Zyrichidou, I., Van Roozendaal, M., Lerot, C., and Spurr, R. J. D.: GOME-2 total ozone  
1667 columns from MetOp-A/MetOp-B and assimilation in the MACC system, *Atmos. Meas.*  
1668 *Tech.*, 7, 2937-2951, doi:10.5194/amt-7-2937-2014, 2014.

1669 Holben B.N., Eck, T.F., Slutsker, I., Tanré, D., Buis, J.P., Setzer, A., Vermote, E., Reagan,  
1670 J.A. . Kaufman, Y., Nakajima, T., Lavenu, F., Jankowiak, I. and Smirnov, A.: AERONET - A  
1671 federated instrument network and data archive for aerosol characterization, *Rem. Sens.*  
1672 *Environ.*, 66, 1-16, 1998.

1673 Hollingsworth, A., Engelen, R.J., Textor, C., Benedetti, A., Boucher, O., Chevallier, F.,  
1674 Dethof, A., Elbern, H., Eskes, H., Flemming, J., Granier, C., Kaiser, J.W., Morcrette, J.-J.,  
1675 Rayner, P., Peuch, V.H., Rouil, L., Schultz, M.G., Simmons, A.J and The GEMS  
1676 Consortium: Toward a Monitoring and Forecasting System For Atmospheric Composition:  
1677 The GEMS Project. *Bull. Amer. Meteor. Soc.*, 89, 1147-1164, 2008.

1678 Hsu N. C., Jeong M.-J., Bettenhausen C, Sayer A.M., Hansell R., Seftor C.S., Huang J., Tsay  
1679 S.-C.: Enhanced Deep Blue aerosol retrieval algorithm: The second generation, *J. Geophys.*  
1680 *Res.*, VOL. 118, 120, doi:10.1002/jgrd.50712, 2013.

1681 Huneus, N., Schulz, M., Balkanski, Y., Griesfeller, J., Prospero, J., Kinne, S., Bauer, S.,  
1682 Boucher, O., Chin, M., Dentener, F., Diehl, T., Easter, R., Fillmore, D., Ghan, S., Ginoux, P.,  
1683 Grini, A., Horowitz, L., Koch, D., Krol, M. C., Landing, W., Liu, X., Mahowald, N., Miller,  
1684 R., Morcrette, J.-J., Myhre, G., Penner, J., Perlwitz, J., Stier, P., Takemura, T., and Zender, C.  
1685 S.: Global dust model intercomparison in AeroCom phase I, *Atmos. Chem. Phys.*, 11, 7781-  
1686 7816, doi:10.5194/acp-11-7781-2011, 2011.

1687 Huijnen, V., Williams, J., van Weele, M., van Noije, T., Krol, M., Dentener, F., Segers, A.,  
1688 Houweling, S., Peters, W., de Laat, J., Boersma, F., Bergamaschi, P., van Velthoven, P., Le  
1689 Sager, P., Eskes, H., Alkemade, F., Scheele, R., Nédélec, P., and Pätz, H.-W.: The global  
1690 chemistry transport model TM5: description and evaluation of the tropospheric chemistry  
1691 version 3.0, *Geosci. Model Dev.*, 3, 445-473, doi:10.5194/gmd-3-445-2010, 2010.

1692 Huijnen V., Wooster, M. J., Kaiser, J. W., Gaveau, D.L.A., Flemming, J., Parrington, M.  
1693 Inness, A., Murdiyarso, D., Main, B. and van Weele, M.: Fire carbon emissions over maritime  
1694 southeast Asia in 2015 largest since 1997, *Scientific Reports*, 6:26886, DOI:  
1695 10.1038/srep26886, 2016.

1696 Im, U., Bianconi, R., Solazzo, E., Kioutsioukis, I., Badia, A., Balzarini, A., Baró, R., Bellasio,  
1697 R., Brunner, D., Chemel, C., Curci, G., Flemming, J., Forkel, R., Giordano, L., Jiménez-  
1698 Guerrero, P., Hirtl, M., Hodzic, A., Honzak, L., Jorba, O., Knote, C., Kuenen, J.J.P., Makar,  
1699 P.A., Manders-Groot, A., Neal, L., Pérez, J.L., Pirovano, G., Pouliot, G., San Jose, R.,  
1700 Savage, N., Schroder, W., Sokhi, R.S., Syrakov, D., Torian, A., Tuccella, P., Werhahn, J.,  
1701 Wolke, R., Yahya, K., Zabkar, R., Zhang, Y., Zhang, J., Hogrefe, C., Galmarini, S.:  
1702 Evaluation of operational on-line-coupled regional air quality models over Europe and North  
1703 America in the context of AQMEII phase 2. Part I: Ozone, Atmospheric Environment, doi:  
1704 10.1016/j.atmosenv.2014.09.042, 2014.

1705 Inness, A., Baier, F., Benedetti, A., Bouarar, I., Chabrilat, S., Clark, H., Clerbaux, C.,  
1706 Coheur, P., Engelen, R. J., Errera, Q., Flemming, J., George, M., Granier, C., Hadji-Lazaro,  
1707 J., Huijnen, V., Hurtmans, D., Jones, L., Kaiser, J. W., Kapsomenakis, J., Lefever, K., Leitão,  
1708 J., Razinger, M., Richter, A., Schultz, M. G., Simmons, A. J., Suttie, M., Stein, O., Thépaut,  
1709 J.-N., Thouret, V., Vrekoussis, M., Zerefos, C., and the MACC team: The MACC reanalysis:  
1710 an 8 yr data set of atmospheric composition, *Atmos. Chem. Phys.*, 13, 4073-4109,  
1711 doi:10.5194/acp-13-4073-2013, 2013.

1712 Inness, A., Blechschmidt, A.-M., Bouarar, I., Chabrilat, S., Crepulja, M., Engelen, R. J.,  
1713 Eskes, H., Flemming, J., Gaudel, A., Hendrick, F., Huijnen, V., Jones, L., Kapsomenakis, J.,  
1714 Katragkou, E., Keppens, A., Langerock, B., de Mazière, M., Melas, D., Parrington, M.,  
1715 Peuch, V. H., Razinger, M., Richter, A., Schultz, M. G., Suttie, M., Thouret, V., Vrekoussis,  
1716 M., Wagner, A., and Zerefos, C.: Data assimilation of satellite retrieved ozone, carbon  
1717 monoxide and nitrogen dioxide with ECMWF's Composition-IFS, *Atmos. Chem. Phys.*, 15,  
1718 5275-5303, doi:10.5194/acp-15-5275-2015, 2015.

1719 Jacob, D.J. H. Liu, C.Mari, and R.M. Yantosca, Harvard wet deposition scheme for GMI,  
1720 Harvard University Atmospheric Chemistry Modeling Group, revised March 2000.  
1721 [http://acmg.seas.harvard.edu/geos/wiki\\_docs/deposition/wetdep.jacob\\_etal\\_2000.pdf](http://acmg.seas.harvard.edu/geos/wiki_docs/deposition/wetdep.jacob_etal_2000.pdf), 2000.

1722 Jung, T., T. N. Palmer, M. J. Rodwell, and S. Serrar: Diagnosing forecast error using  
1723 relaxation experiments. ECMWF Newsletter 82, ECMWF, Shinfield Park, Reading, Berkshire  
1724 RG2 9AX, UK, 2008.

1725 Kaiser, J. W., Heil, A., Andreae, M. O., Benedetti, A., Chubarova, N., Jones, L., Morcrette,  
1726 J.-J., Razinger, M., Schultz, M. G., Suttie, M., and van der Werf, G. R.: Biomass burning

1727 emissions estimated with a global fire assimilation system based on observed fire radiative  
1728 power, *Biogeosciences*, 9, 527-554, doi:10.5194/bg-9-527-2012, 2012.

1729 Katragkou, E., Zanis, P., Tsikerdekis, A., Kapsomenakis, J., Melas, D., Eskes, H., Flemming,  
1730 J., Huijnen, V., Inness, A., Schultz, M. G., Stein, O., and Zerefos, C. S.: Evaluation of near  
1731 surface ozone over Europe from the MACC reanalysis, *Geoscientific Model Development*, 8,  
1732 2299-2314, 2015.

1733 Kinne, S., Schulz, M., Textor, C., Guibert, S., Balkanski, Y., Bauer, S. E., Berntsen, T.,  
1734 Berglen, T. F., Boucher, O., Chin, M., Collins, W., Dentener, F., Diehl, T., Easter, R.,  
1735 Feichter, J., Fillmore, D., Ghan, S., Ginoux, P., Gong, S., Grini, A., Hendricks, J., Herzog,  
1736 M., Horowitz, L., Isaksen, I., Iversen, T., Kirkevåg, A., Kloster, S., Koch, D., Kristjansson, J.  
1737 E., Krol, M., Lauer, A., Lamarque, J. F., Lesins, G., Liu, X., Lohmann, U., Montanaro, V.,  
1738 Myhre, G., Penner, J., Pitari, G., Reddy, S., Seland, O., Stier, P., Takemura, T., and Tie, X.:  
1739 An AeroCom initial assessment – optical properties in aerosol component modules of global  
1740 models, *Atmos. Chem. Phys.*, 6, 1815-1834, doi:10.5194/acp-6-1815-2006, 2006.

1741 Kinnison, D. E., Brasseur, G. P., Walters, S., Garcia, R. R., Marsh, D. R., Sassi, F., Harvey,  
1742 V. L., Randall, C. E., Emmons, L., Lamarque, J. F., Hess, P., Orlando, J. J., Tie, X. X.,  
1743 Randel, W., Pan, L. L., Gettelman, A., Granier, C., Diehl, T., Niemeier, U. and Simmons, A.  
1744 J.: Sensitivity of Chemical Tracers to Meteorological Parameters in the MOZART-3  
1745 Chemical Transport Model. *J. Geophys. Res.*, 112, D03303, doi:10.1029/2008JD010739,  
1746 2007.

1747 Komhyr, W. D., Barnes, R. A., Borthers, G. B., Lathrop, J. A., Kerr, J. B., and Opperman, D.  
1748 P.: Electrochemical concentration cell ozonesonde performance evaluation during STOIC  
1749 1989, *J. Geophys. Res.*, 100, 9231–9244, 1995.

1750 Lamarque, J.-F., Shindell, D. T., Josse, B., Young, P. J., Cionni, I., Eyring, V., Bergmann, D.,  
1751 Cameron-Smith, P., Collins, W. J., Doherty, R., Dalsoren, S., Faluvegi, G., Folberth, G.,  
1752 Ghan, S. J., Horowitz, L. W., Lee, Y. H., MacKenzie, I. A., Nagashima, T., Naik, V.,  
1753 Plummer, D., Righi, M., Rumbold, S. T., Schulz, M., Skeie, R. B., Stevenson, D. S., Strode,  
1754 S., Sudo, K., Szopa, S., Voulgarakis, A., and Zeng, G.: The Atmospheric Chemistry and  
1755 Climate Model Intercomparison Project (ACCMIP): overview and description of models,  
1756 simulations and climate diagnostics, *Geosci. Model Dev.*, 6, 179-206, doi:10.5194/gmd-6-  
1757 179-2013, 2013.

1758 Lefever, K., van der A, R., Baier, F., Christophe, Y., Errera, Q., Eskes, H., Flemming, J.,  
1759 Inness, A., Jones, L., Lambert, J.-C., Langerock, B., Schultz, M. G., Stein, O., Wagner, A.,  
1760 and Chabrillat, S.: Copernicus stratospheric ozone service, 2009–2012: validation, system  
1761 intercomparison and roles of input data sets, *Atmos. Chem. Phys.*, 15, 2269–2293,  
1762 doi:10.5194/acp-15-2269-2015, 2015.

1763 Levelt, P. F., van den Oord, G. H. J., Dobber, M. R., Malkki, A., Visser, H., de Vries, J.,  
1764 Stammes, P., Lundell, J. O. V., and Saari, H.: The ozone monitoring instrument, *IEEE T.*  
1765 *Geosci. Remote*, 44, 1093–1101, 2006.

1766 Levy, R. C., Remer, L. A., Kleidman, R. G., Mattoo, S., Ichoku, C., Kahn, R., and Eck, T. F.:  
1767 Global evaluation of the Collection 5 MODIS dark-target aerosol products over land, *Atmos.*  
1768 *Chem. Phys.*, 10, 10399–10420, doi:10.5194/acp-10-10399-2010, 2010.

1769 Liu, X., Bhartia, P. K., Chance, K., Spurr, R. J. D., and Kurosu, T. P.: Ozone profile retrievals  
1770 from the Ozone Monitoring Instrument, *Atmos. Chem. Phys.*, 10, 2521–2537, 2010,  
1771 <http://www.atmos-chem-phys.net/10/2521/2010/>.

1772 Manney, G., Santee, M. L., Rex, M., Livesey, N. J., Pitts, M. C., Veefkind, P., Nash, R. R.,  
1773 Wohltmann, I., Lehmann, R., Froidevaux, L., Poole, L. R., Schoeberl, M. R., Haffner, D. P.,  
1774 Davies, J., Dorokhov, V., Gernandt, H., Johnson, B., Kivi, R., Kyr o, E., Larsen, N., Levelt, P.  
1775 F., Makshtas, A., McElroy, C. T., Nakajima, H., Parrondo, M. C., Tarasick, D.W., von der  
1776 Gathen, P., Walker, P. K. A., and Zinoviev, N. S.: Unprecedented Arctic ozone loss in 2011,  
1777 Arctic winter 2010/2011 at the brink of an ozone hole, *Nature*, 478, 469–475,  
1778 doi:10.1038/nature10556, 2011.

1779 McNally, A. P., Watts, P. D., Smith, J. A., Engelen, R. J., Kelly, G. A., Thépaut, J.-N., and  
1780 Matricardi, M.: The assimilation of AIRS radiance data at ECMWF, *Q. J. Roy. Meteor. Soc.*,  
1781 132, 935–957, 2006.

1782 Marenco, A., Thouret, V., Nédelec, P., Smit, H. G., Helten, M., Kley, D., Karcher, F., Simon,  
1783 P., Law, K., Pyle, J., Poschmann, G., Von Wrede, R., Hume, C., and Cook, T.: Measurement  
1784 of ozone and water vapour by Airbus in-service air-craft: The MOZAIC airborne programme,  
1785 an overview, *J. Geophys. Res.*, 103, 25631–25642, 1998.

1786 Meijer, E.W., P. F. J. van Velthoven, D. W. Brunner, H. Huntrieser and H. Kelder:  
1787 Improvement and evaluation of the parameterization of nitrogen oxide production by

1788 lightning, *Physics and Chemistry of the Earth, Part C, Volume 26, Issue 8, Pages 577-583,*  
1789 2001.

1790 Miyazaki, K., Eskes, H. J., and Sudo, K.: A tropospheric chemistry reanalysis for the years  
1791 2005–2012 based on an assimilation of OMI, MLS, TES, and MOPITT satellite data, *Atmos.*  
1792 *Chem. Phys.*, 15, 8315-8348, doi:10.5194/acp-15-8315-2015, 2015.

1793 Monks, P. S., Archibald, A. T., Colette, A., Cooper, O., Coyle, M., Derwent, R., Fowler, D.,  
1794 Granier, C., Law, K. S., Mills, G. E., Stevenson, D. S., Tarasova, O., Thouret, V., von  
1795 Schneidemesser, E., Sommariva, R., Wild, O., and Williams, M. L.: Tropospheric ozone and  
1796 its precursors from the urban to the global scale from air quality to short-lived climate forcer,  
1797 *Atmos. Chem. Phys.*, 15, 8889-8973, doi:10.5194/acp-15-8889-2015, 2015.

1798 Morcrette, J.-J., Boucher, O., Jones, L., Salmond, D., Bechtold, P., Beljaars, A., Benedetti, A.,  
1799 Bonet, A., Kaiser, J. W., Razinger, M., Schulz, M., Serrar, S., Simmons, A. J., Sofiev, M.,  
1800 Suttie, M., Tompkins, A. M. and Untch, A.: Aerosol analysis and forecast in the ECMWF  
1801 Integrated Forecast System. Part I: Forward modelling, *J. Geophys. Res.*, 2009.

1802 Morcrette, J. J., Benedetti, A., Jones, L., Kaiser, J. W., Razinger, M., and Suttie, M.:  
1803 Prognostic Aerosols in the ECMWF IFS: MACC vs. GEMS Aerosols, ECMWF Technical  
1804 Memorandum, 659, 2011.

1805 Nedelec, P., Cammas, J.-P., Thouret, V., Athier, G., Cousin, J.-M., Legrand, C., Abonnel, C.,  
1806 Lecoq, F., Cayez, G., and Marizy, C.: An improved infrared carbon monoxide analyser for  
1807 routine measurements aboard commercial Airbus aircraft: technical validation and first  
1808 scientific results of the MOZAIC III programme, *Atmos. Chem. Phys.*, 3, 1551–1564,  
1809 doi:10.5194/acp-3-1551-2003, 2003.

1810 Munro, R., R. Siddans, W. J. Reburn, and B. J. Kerridge, Direct measurements of  
1811 tropospheric ozone distributions from space, *Nature*, 392, 168–171, 1998.

1812 Munro, R., Eisinger, M., Anderson, C., Callies, J., Corpaccioli, E., Lang, R., Lefebvre, A.,  
1813 Livschitz, Y., and Albinana, A. P.: GOME-2 on MetOp, Proc. of The 2006 EUMETSAT  
1814 Meteorological Satellite Conference, Helsinki, Finland, 2006.

1815 Novelli, P.C. and Masarie, K.A.: Atmospheric Carbon Monoxide Dry Air Mole Fractions  
1816 from the NOAA ESRL Carbon Cycle Cooperative Global Air Sampling Network, 1988-2012,  
1817 Version: 2013-08-08, Path: [ftp://aftp.cmdl.noaa.gov/data/trace\\_gases/co/flask/surface/](ftp://aftp.cmdl.noaa.gov/data/trace_gases/co/flask/surface/), 2013.  
1818 (last access 6.5.2016)

1819 Novelli, P. C., Masarie, K. A., Lang, P. M., Hall, B. D., Myers, R. C., and Elkins, J. W.:  
1820 Reanalysis of tropospheric CO trends: effects of the 1997–1998 wildfires, *J. Geophys. Res.*,  
1821 108, 4464, doi:10.1029/2002JD003031, 2003.

1822 Olivier J., J. Peters, C. Granier, G. Petron, J.F. Muller, and S. Wallens: Present and future  
1823 surface emissions of atmospheric compounds, POET report #2, EU project EVK2-1999-  
1824 00011, 2003.

1825 Onogi, K., Tsutsui, J., Koide, H., Sakamoto, M., Kobayashi, S., Hatsushika, H., Matsumoto,  
1826 T., Yamazaki, N., Kamahori, H., Takahashi, K., Kadokura, S., Wada, K., Kato, K., Oyama,  
1827 R., Ose, T., Mannoji, N., and Taira, R.: The JRA-25 Reanalysis, *Q. J. Roy. Meteorol. Soc.*,  
1828 85, 369–432, 2007.

1829 Reddy M. S., Boucher O., Bellouin N., Schulz M., Balkanski Y., Dufresne J.-L., Pham M.:  
1830 Estimates of global multicomponent aerosol optical depth and direct radiative perturbation in  
1831 the Laboratoire de Méte´orologie Dynamique general circulation model, *J. Geophys. Res.*,  
1832 110, D10S16, doi:10.1029/2004JD004757, 2005.

1833 Remer, L. A., Kaufman, Y. J. M, Tanré, D., Mattoo, S., Chu, D. A. M, Martins, J. V., Li, R.-  
1834 R., Ichoku, C., Levy, R. C., Kleidman, R. G., Eck, T. F., Vermote, E. and Holben, B. N.: The  
1835 MODIS Aerosol Algorithm, Products, and Validation *Journal of the Atmospheric Sciences*  
1836 2005 62:4, 947-973, 2005.

1837 Rienecker, M. M., Suarez, M. J., Gelaro, R., Todling, R., Bacmeister, J., Liu, E., Bosilovich,  
1838 M. G., Schubert, S. D., Takacs, L., Kim, G.- K., Bloom, S., Chen, J., Collins, D., Conaty, A.,  
1839 da Silva, A., Gu, W., Joiner, J., Koster, R. D., Lucchesi, R., Molod, A. M., Owens, T.,  
1840 Pawson, S., Pegion, P., Redder, C. R., Reichle, R., Robertson, F. R., Ruddick, A. G.,  
1841 Sienkiewicz, M., and Woollen, J.: MERRA – NASA’s Modern- Era Retrospective, *Anal. Res.*  
1842 *Appl., J. Climate*, 24, 3624–3648, doi:10.1175/JCLID-11-00015.1, 2011.

1843 Saha, S., Moorthi, S., Pan, H. L., Wu, X., Wang, J., Nadiga, S., Tripp, P., Kistler, R.,  
1844 Woollen, J., Behringer, D., Liu, H., Stokes, D., Grumbine, R., Gayno, G., Hou, Y. T.,  
1845 Chuang, H. Y., Juang, H. M. H., Sela, J., Iredell, M., Treadon, R., Kleist, D., Van Delst, P.,  
1846 Keyser, D., Derber, J., Ek, M., Meng, J., Wei, H., Yang, R., Lord, S., Van Den Dool, H.,  
1847 Kumar, A., Wang, W., Long, C., Chelliah, M., Xue, Y., Huang, B., Schemm, J. K., Ebisuzaki,  
1848 W., Lin, R., Xie, P., Chen, M., Zhou, S., Higgins, W., Zou, C. Z., Liu, Q., Chen, Y., Han, Y.,



1849 Cucurull, L., Reynolds, R. W., Rutledge, G., and Goldberg, M.: The NCEP climate forecast  
1850 system reanalysis, *B. Am. Meteorol. Soc.*, 91, 1015–1057, 2010.

1851 Schere, K., Flemming, J., Vautard, R., Chemel, C., Colette, A., Hogrefe, C., Bessagnet, B.,  
1852 Meleux, F., Mathur, R., Roselle, S., Hu, R.-M., Sokhi, R. S., Rao, S. T., and Galmarini, S.:  
1853 Trace gas/aerosol boundary concentrations and their impacts on continental-scale AQMEII  
1854 modeling domains, *Atmos. Environ.*, 53, 38–50, doi:10.1016/j.atmosenv.2011.09.043, 2012.

1855 Schutgens, N. A. J., Nakata, M., and Nakajima, T.: Estimating aerosol emissions by  
1856 assimilating remote sensing observations into a Global transport model, *Remote Sens.*, 4,  
1857 3528–3543, 2012.

1858 Sindelarova, K., Granier, C., Bouarar, I., Guenther, A., Tilmes, S., Stavrou, T., Müller, J.-  
1859 F., Kuhn, U., Stefani, P., and Knorr, W.: Global data set of biogenic VOC emissions  
1860 calculated by the MEGAN model over the last 30 years, *Atmos. Chem. Phys.*, 14, 9317-9341,  
1861 doi:10.5194/acp-14-9317-2014, 2014.

1862 Shi, Y., Zhang, J., Reid, J. S., Holben, B., Hyer, E. J., and Curtis, C.: An analysis of the  
1863 collection 5 MODIS over-ocean aerosol optical depth product for its implication in aerosol  
1864 assimilation, *Atmos. Chem. Phys.*, 11, 557-565, doi:10.5194/acp-11-557-2011, 2011.

1865 Shindell, D.T., Faluvegi, D.S. Stevenson, M.C. Krol, L.K. Emmons, J.-F. Lamarque, G.  
1866 Pétron, F.J. Dentener, K. Ellingsen, M.G. Schultz, O. Wild, M. Amann, C.S. Atherton, D.J.  
1867 Bergmann, I. Bey, T. Butler, J. Cofala, W.J. Collins, R.G. Derwent, R.M. Doherty, J. Drevet,  
1868 H.J. Eskes, A.M. Fiore, M. Gauss, D.A. Hauglustaine, L.W. Horowitz, I.S.A. Isaksen, M.G.  
1869 Lawrence, V. Montanaro, J.-F. Müller, G. Pitari, M.J. Prather, J.A. Pyle, S. Rast, J.M.  
1870 Rodriguez, M.G. Sanderson, N.H. Savage, S.E. Strahan, K. Sudo, S. Szopa, N. Unger, T.P.C.  
1871 van Noije, and G. Zeng: Multi-model simulations of carbon monoxide: Comparison with  
1872 observations and projected near-future changes. *J. Geophys. Res.*, 111, D19306,  
1873 doi:10.1029/2006JD007100, 2006.

1874 Spada, M., Jorba, O., Pérez García-Pando, C., Janjic, Z., and Baldasano, J. M.: Modeling and  
1875 evaluation of the global sea-salt aerosol distribution: sensitivity to size-resolved and sea-  
1876 surface temperature dependent emission schemes, *Atmos. Chem. Phys.*, 13, 11735-11755,  
1877 doi:10.5194/acp-13-11735-2013, 2013.

1878 Stein, O., Schultz, M. G., Bouarar, I., Clark, H., Huijnen, V., Gaudel, A., George, M., and  
1879 Clerbaux, C.: On the wintertime low bias of Northern Hemisphere carbon monoxide in global  
1880 model studies, *Atmos. Chem. Phys.*, 14, 9295–9316, doi:10.5194/acp-14-9295-2014, 2014

1881 Steinbrecht, W., Shwartz, R., and Claude, H.: New pump correction for the Brewer-Mast  
1882 ozonesonde: Determination from experiment and instrument intercomparisons, *J. Atmos.*  
1883 *Ocean. Tech.* 15, 144–156, 1998.

1884 Tegtmeier, S., Hegglin, M. I., Anderson, J., Bourassa, A., Brohede, S., Degenstein, D.,  
1885 Froidevaux, L., Fuller, R., Funke, B., Gille, J., Jones, A., Kasai, Y., Krüger, K., Kyrölä, E.,  
1886 Lingenfelter, G., Lumpe, J., Nardi, B., Neu, J., Pendlebury, D., Remsberg, E., Rozanov, A.,  
1887 Smith, L., Toohey, M., Urban, J., von Clarmann, T., Walker, K. A., and Wang, R. H. J.:  
1888 SPARC Data Initiative: a comparison of ozone climatologies from international satellite limb  
1889 sounders, *J. Geophys. Res.*, 118, 12229–12247, doi:10.1002/2013JD019877, 2013.

1890 Textor, C., Schulz, M., Guibert, S., Kinne, S., Balkanski, Y., Bauer, S., Bernsten, T., Berglen,  
1891 T., Boucher, O., Chin, M., Dentener, F., Diehl, T., Easter, R., Feichter, H., Fillmore, D.,  
1892 Ghan, S., Ginoux, P., Gong, S., Grini, A., Hendricks, J., Horowitz, L., Huang, P., Isaksen, I.,  
1893 Iversen, I., Kloster, S., Koch, D., Kirkevåg, A., Kristjansson, J. E., Krol, M., Lauer, A.,  
1894 Lamarque, J. F., Liu, X., Montanaro, V., Myhre, G., Penner, J., Pitari, G., Reddy, S., Seland,  
1895 Ø., Stier, P., Takemura, T., and Tie, X.: Analysis and quantification of the diversities of  
1896 aerosol life cycles within AeroCom, *Atmos. Chem. Phys.*, 6, 1777–1813, doi:10.5194/acp-6-  
1897 1777-2006, 2006.

1898 Uppala, S., Kallberg, P., Simmons, A. J., Andrae, U., Bechtold, V. D. C., Fiorino, M., Gibson,  
1899 J. K., Haseler, J., Hernandez, A., Kelly, G. A., Li, X., Onogi, K., Saarinen, S., Sokka, N.,  
1900 Allan, R. P., Andersson, E., Arpe, K., Balmaseda, M. A., Beljaars, A. C. M., van de Berg, L.,  
1901 Bidlot, J., Bormann, N., Caires, S., Chevallier, F., Dethof, A., Dragosavac, M., Fisher, M.,  
1902 Fuentes, M., Hagemann, S., Holm, E., Hoskins, B. J., Isaksen, L., Janssen, P. A. E. M., Jenne,  
1903 R., McNally, A. P., Mahfouf, J. F., Morcrette, J. J., Rayner, N. A., Saunders, R. W., Simon,  
1904 P., Sterl, A., Trenberth, K. E., Untch, A., Vasiljevic, D., Viterbo, P., and Woollen, J.: The  
1905 ERA-40 re-analysis, *Q. J. R. Meteorol. Soc.*, 131, 2961–3012, 2005.

1906 Wagner, A., Blechschmidt, A.-M., Bouarar, I., Brunke, E.-G., Clerbaux, C., Cupeiro, M.,  
1907 Cristofanelli, P., Eskes, H., Flemming, J., Flentje, H., George, M., Gilge, S., Hilboll, A.,  
1908 Inness, A., Kapsomenakis, J., Richter, A., Ries, L., Spangl, W., Stein, O., Weller, R., and

1909 Zerefos, C.: Evaluation of the MACC operational forecast system – potential and challenges  
1910 of global near-real-time modelling with respect to reactive gases in the troposphere, *Atmos.*  
1911 *Chem. Phys.*, 15, 14005-14030, doi:10.5194/acp-15-14005-2015, 2015.

1912 Wesely, M.L.: Parameterization of Surface Resistances to Gaseous Dry Deposition in  
1913 Regional-Scale Numerical Models. *Atmos. Environ.*, 23, 1293-1304, 1989.

1914 Worden, H. M., Deeter, M. N., Frankenberg, C., George, M., Nichitiu, F., Worden, J., Aben,  
1915 I., Bowman, K. W., Clerbaux, C., Coheur, P. F., de Laat, A. T. J., Detweiler, R., Drummond,  
1916 J. R., Edwards, D. P., Gille, J. C., Hurtmans, D., Luo, M., Martínez-Alonso, S., Massie, S.,  
1917 Pfister, G., and Warner, J. X.: Decadal record of satellite carbon monoxide observations,  
1918 *Atmos. Chem. Phys.*, 13, 837-850, doi:10.5194/acp-13-837-2013, 2013.

1919 Van der A, R.J.; Allaart, M.A.F.; Eskes, H.J. Multi sensor reanalysis of total ozone. *Atmos.*  
1920 *Chem.Phys.* 2010, 10, 11277–11294.

1921 van der A, R. J., Allaart, M. A. F., and Eskes, H. J.: Extended and refined multi sensor  
1922 reanalysis of total ozone for the period 1970-2012, *Atmos. Meas. Tech.*, 8, 3021-3035,  
1923 doi:10.5194/amt-8-3021-2015, 2015.

1924 Verstraeten, W. W., Neu, J. L., Williams, J. E., Bowman, K. W., Worden, J. R., Boersma, K.  
1925 F.: Rapid increases in tropospheric ozone production and export from China, *Nat. Geosci.*, 8,  
1926 690–695, doi:10.1038/ngeo2493, 2015.

1927 von Clarmann, T., Glatthor, N., Grabowski, U., Höpfner, M., Kellmann, S., Kiefer, M.,  
1928 Linden, A., Mengistu Tsidu, G., Milz, M., Steck, T., Stiller, G. P., Wang, D. Y., Fischer, H.,  
1929 Funke, B., Gil-López, S., and López-Puertas, M.: Retrieval of temperature and tangent  
1930 altitude pointing from limb emission spectra recorded from space by the Michelson  
1931 Interferometer for Passive Atmospheric Sounding (MIPAS), *J. Geophys. Res.*, 108, 4736,  
1932 doi:10.1029/2003JD003602, 2003.

1933 Waters, J.W., Froidevaux, L., Harwood, R. S., Jarnot, R. F., Pickett, H. M., Read, W. G.,  
1934 Siegel, P. H., Cofield, R. E., Filipiak, M. J., Flower, D. A., Holden, J. R., Lau, G. K., Livesey,  
1935 N. J., Manney, G. L., Pumphrey, H. C., Santee, M. L., Wu, D. L., Cuddy, D. T., Lay, R. R.,  
1936 Loo, M. S., Perun, V. S., Schwartz, M. J., Stek, P. C., Thurstans, R. P., Boyles, M. A.,  
1937 Chandra, K. M., Chavez, M. C., Chen, G. S., Chudasama, B. V., Dodge, R., Fuller, R. A.,  
1938 Girard, M. A., Jiang, J. H., Jiang, Y., Knosp, B. W., Labelle, R. C., Lam, J. C., Lee, A. K.,  
1939 Miller, D., Oswald, J. E., Patel, N. C., Pukala, D. M., Quintero, O., Scaff, D. M., Vansnyder,

1940 W., Tope, M. C., Wagner, P. A., and Walch, M. J.: The Earth Observing System Microwave  
 1941 Limb Sounder (EOS MLS) on the Aura Satellite, IEEE T. Geosci. Remote, 44, 1075–1092,  
 1942 2006.

1943 Yarwood, G., Rao, S., Yocke, M., and Whitten, G.: Updates to the carbon bond chemical  
 1944 mechanism: CB05. Final report to the US EPA, EPA Report Number: RT-0400675, available  
 1945 at: www.camx.com, last access: 1 July 2014, 2005.

1946

	<b>MACCRA</b>	<b>CAMSiRA</b>
Period	01/2003–12/2012	01/2003–12/2015
Horizontal resolution	80 km (T255)	110 km (T159)
Vertical resolution	60 layers from surface to 0.1 hPa	as MACCRA
Anthropogenic Emissions	MACCity (trend: ACCMIP + RCP 8.5), AEROCOM	as MACCRA & CO emission upgrade (Stein et al., 2014)
Chemistry module	MOZART-3	C-IFS CB05 / Cariolle ozone
Assimilated CO observations	MOPITT (V4) & IASI (from 2008 onwards)	MOPITT (V5) & updated error statistics (Inness et al., 2015)
Assimilated ozone observations	SBUV-2, OMI, MLS, GOME-2, SCIAMACHY, GOME, MIPAS (01/2003– 06/2004)	as MACCRA & MIPAS (2003–2012)
Ozone MLS bias correction	On	Off
Assimilated AOD observations	MODIS (Aqua and Terra) + VarBC	as MACCRA
Fire emissions	GFED (2003–2008) and GFAS v0 (2009-2012 )	GFAS v 1.2 (2003–2015)
IFS model version	CY36R2	CY40R2
Assimilation method and model	ECMWF 4D-VAR	as MACCRA
Meteorological observations assimilated	ECMWF RD setup (satellites, sondes, surface )	as MACCRA

1947 *Table 1 Important commonalities and differences between MACCRA and CAMSiRA*

1948



<b>Instrument</b>	<b>References</b>	<b>Version</b>	<b>Period</b>	<b>Type</b>	<b>Data usage</b>
MOPITT Terra	Deeter et al. (2011)	V5 TIR NRT	20030101– 20121218 From 20121219	CO TC	65N–65S QC=0
GOME ERS-2	Munro et al. (1998)		20030101– 20030531	O3 profile	80N–80S SOE>15, QC=0
GOME-2 Metop A	Hao et al. (2014)	NRT GDP4.4 NRT GDP4.7	20120901– 20130714 From 20130715	O3 TC	SOE>10 QC=0
GOME-2 Metop B	Hao et al. (2014)	NRT GDP4.7	From 20140101	O3 TC	SOE>10 QC=0
MIPAS Envisat	von Clarmann et al. (2003, 2009)	NRT CCI	20030101– 20040326 20050127– 20120331	O3 profile	QC=0
MLS Aura	Froidevaux et al. (2008)	V2 NRT V3.4	20040808– 20121231 From 20130107	O3 profile	QC=0
OMI Aura	Liu et al. (2010)	V003 NRT	20041001– 20121231 From 20130101	O3 TC	SOE>10 QC=0
SBUV/2 NOAA- 16	Bhartia et al. (1996)	V8	20040101– 20081020	O3 PC 6 layers	SOE>6 QC=0
SBUV/2 NOAA- 17	Bhartia et al. (1996)	V8	20030101– 20121130	O3 PC 6 layers	SOE>6 QC=0
SBUV/2 NOAA- 18	Bhartia et al. (1996)	V8	20050604– 20121217	O3 PC 6 layers	SOE>6 QC=0
SBUV/2 NOAA- 19	Bhartia et al. (1996)	V8	From 20090100	O3 PC 6 layers	SOE>6 QC=0
SCIAMACHY Envisat	Eskes et al. (2012)	CCI	20030101– 20120408	O3 TC	SOE>6 QC=0
MODIS / Terra	Remer et al. (2005)	Col.5 NRT Col.5	20030101– 20080731 From 20080801	AOD 550nm	70N–70S
MODIS / Aqua	Remer et al. (2005)	Col.5 NRT Col.5	20030101– 20080731 From 20080801	AOD 550nm	70N–70S

Table 2 Assimilated satellite observations in CAMSiRA

1952

<b>Area</b>	<b>Coordinates</b>
North America	165°W–55°W, 25°N–75°N
Europe	10°W–45°E, 38°N–70°N
East Asia	90°E–150°E/10°N–55°N
South America	82°W–30°W/40°S–15°N
Tropical Africa	15°W–55°E/10°S–20°N
Northern Africa	15°W–55°E/20°N–35°N
Maritime South East Asia	90°E–150°E/10°S–10°N
Tropics	23°S–23°N
Arctic	60°N–90°N
Antarctica	90°S–60°S
NH mid latitudes	30°N–60°N
SH mid-latitudes	60°S–30°S

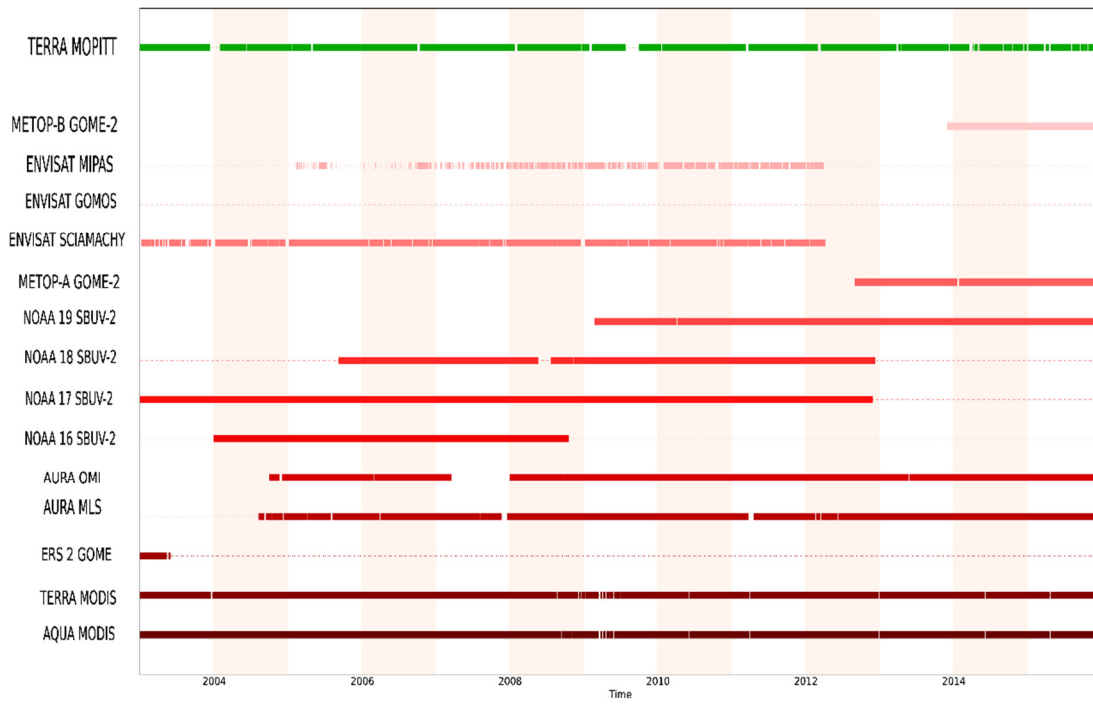
1953

*Table 3 Coordinates of regions*

1954

1955

1956



1957

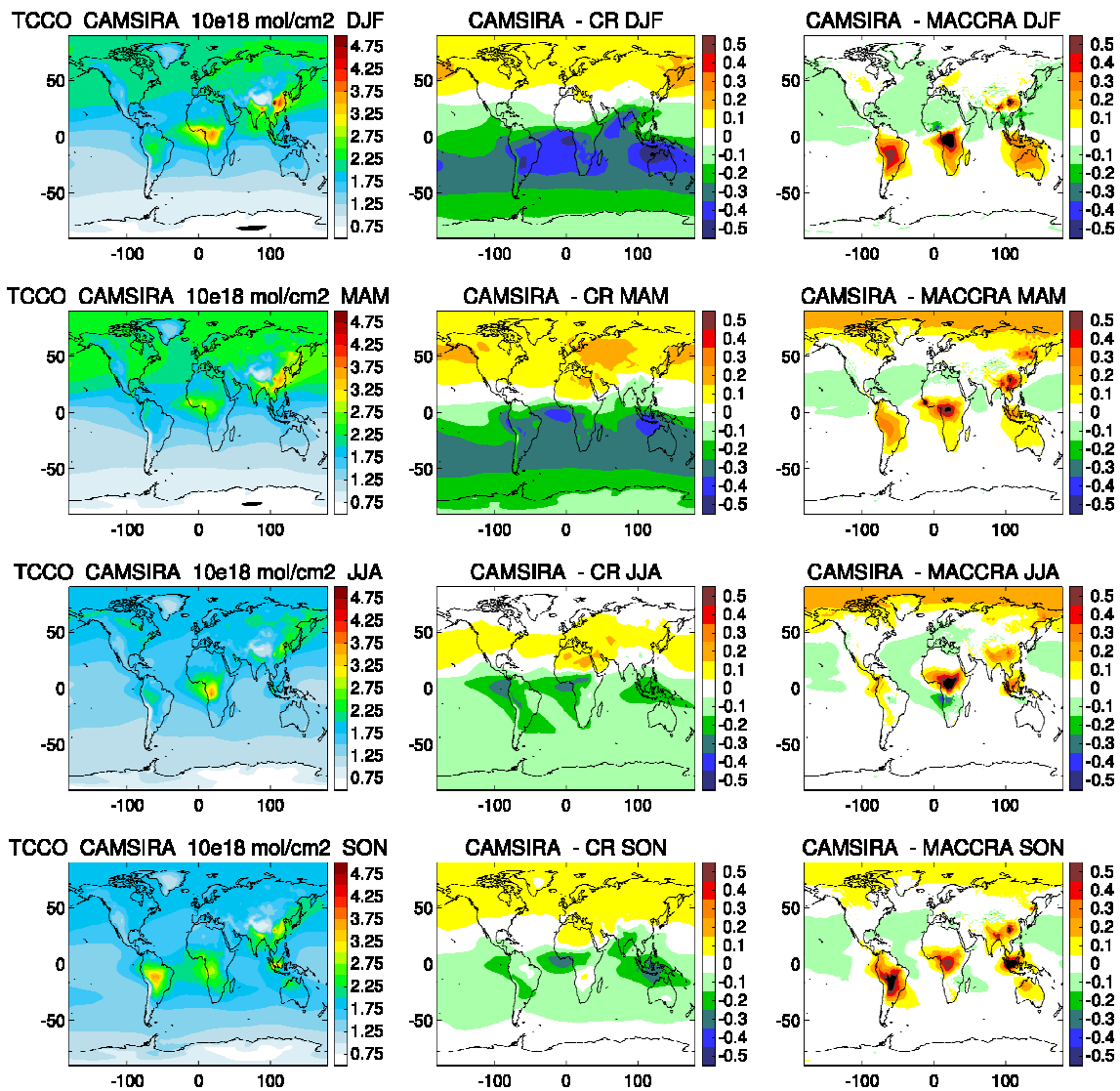
1958

1959

1960

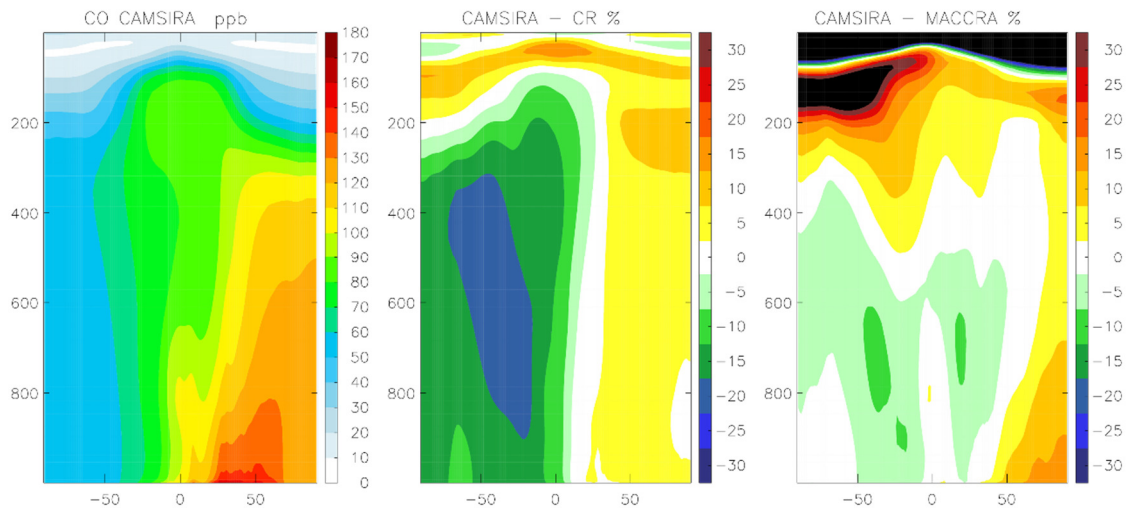
*Figure 1 Time line of assimilated AC satellite retrievals from different instruments assimilated in CAMSiRA (see Table 2)*





1961  
 1962  
 1963  
 1964  
  
 1965

Figure 2 Average TC CO ( $10^{18}$  molecules/cm<sup>2</sup>) of CAMSiRA (2003–2015, left) and difference against CR (2003–2015, middle) and MACCRA (2003–2012, right) for the seasons DJF (row 1), MAM (row 2), JJA (row 3) and SON (row 4).



1966

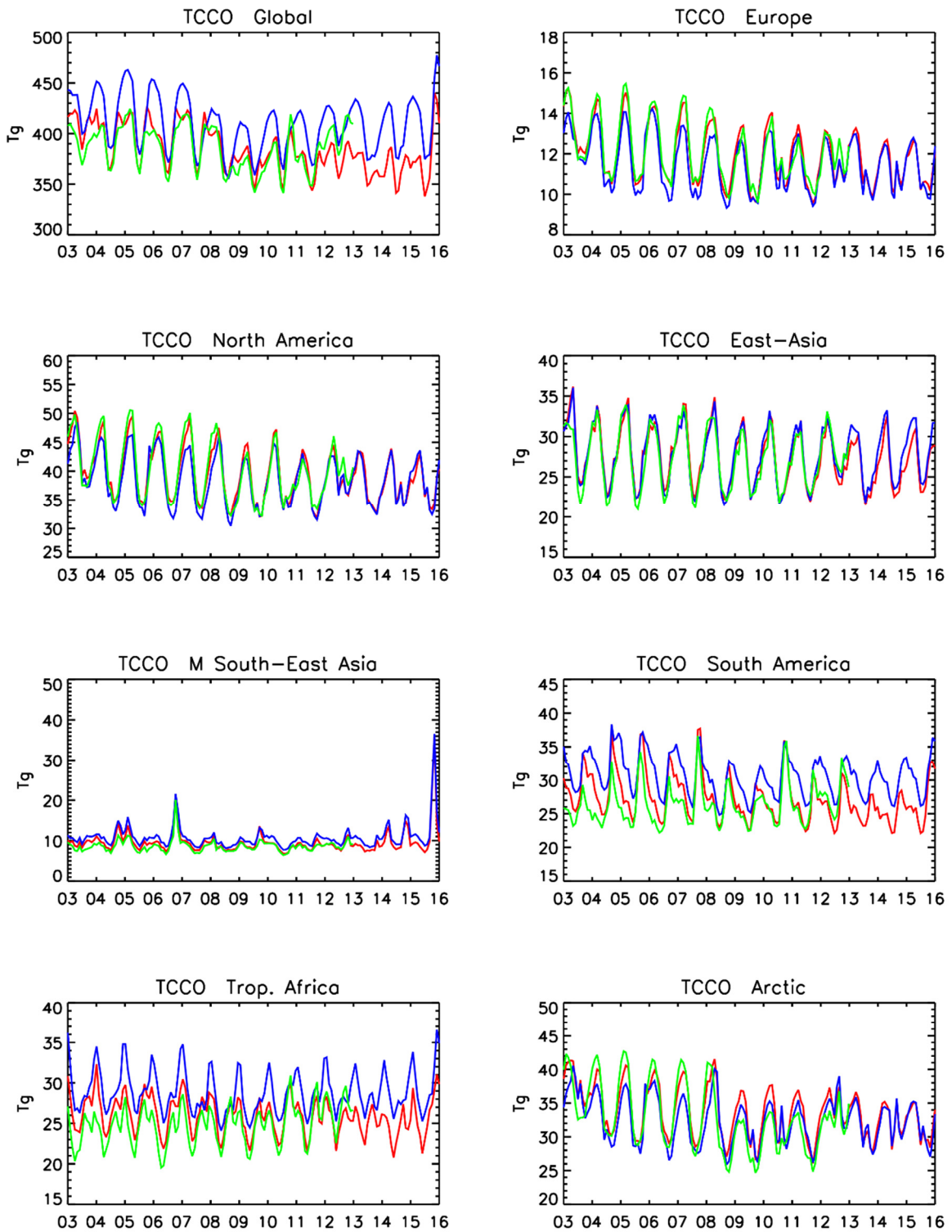
1967

1968

1969

*Figure 3 Zonally averaged CO cross section of CAMSiRA (ppb) (2003–2015, left) and relative difference (%) against CR (2003–2015, middle) and MACCRA (2003–2012, right).*

1970



1971

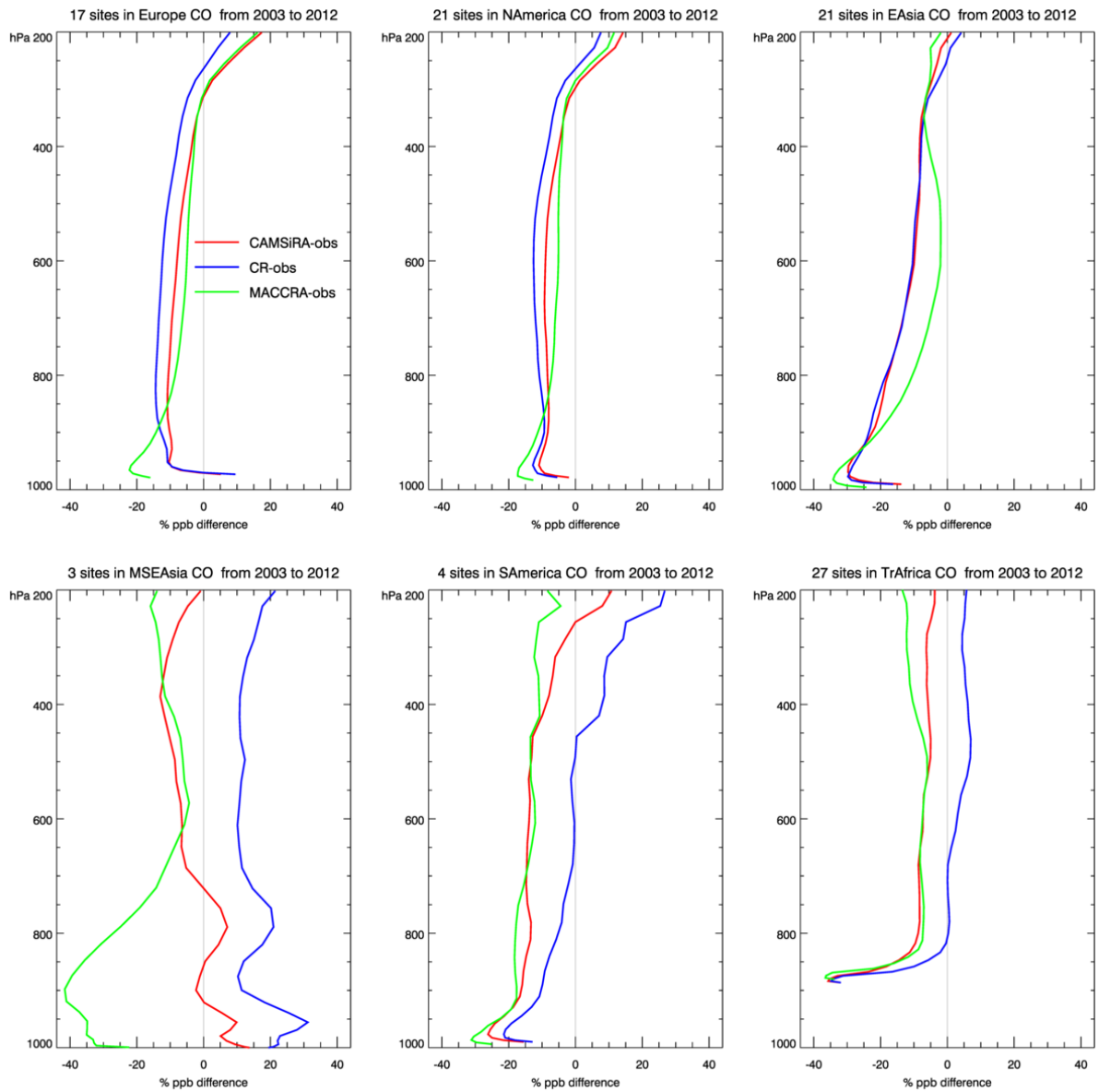
1972

1973

1974

1975

Figure 4 Time series of monthly mean CO burden ( $T_g$ ) over different regions (see Table 3) for the period 2003–2015 from CAMSiRA (red), CR (blue) and MACCRA (green, 2003–2012).



1976

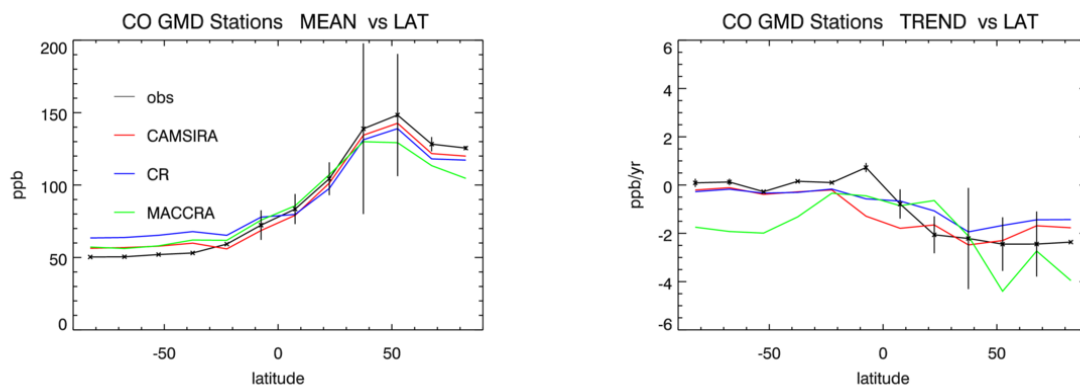
1977

1978

1979

1980

*Figure 5 Average relative bias (%) in CO of CAMSiRA, MACCRA and CR against MOZAIC / IGAOS flight profiles averaged over different regions (see Table 3) for the period 2003–2012.*



1981

1982

1983

1984

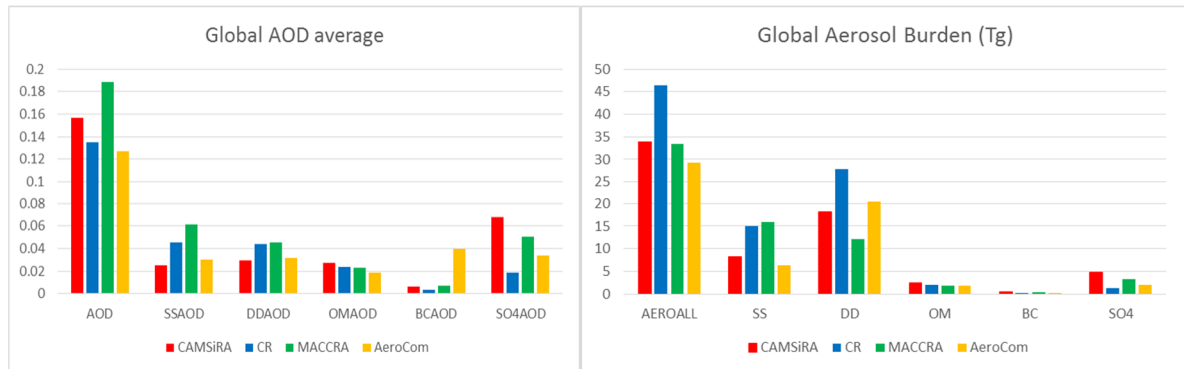
1985

1986

*Figure 6 Zonal average of mean surface CO in ppb observed at NOAA-GMD stations (2003–2014) and values from CAMSiRA, CR and MACCRA (2003–2012) (left) and zonal median of linear trend in ppb/yr (right). The error bars indicate the range of the observed values.*

1987

1988



1989

1990

1991

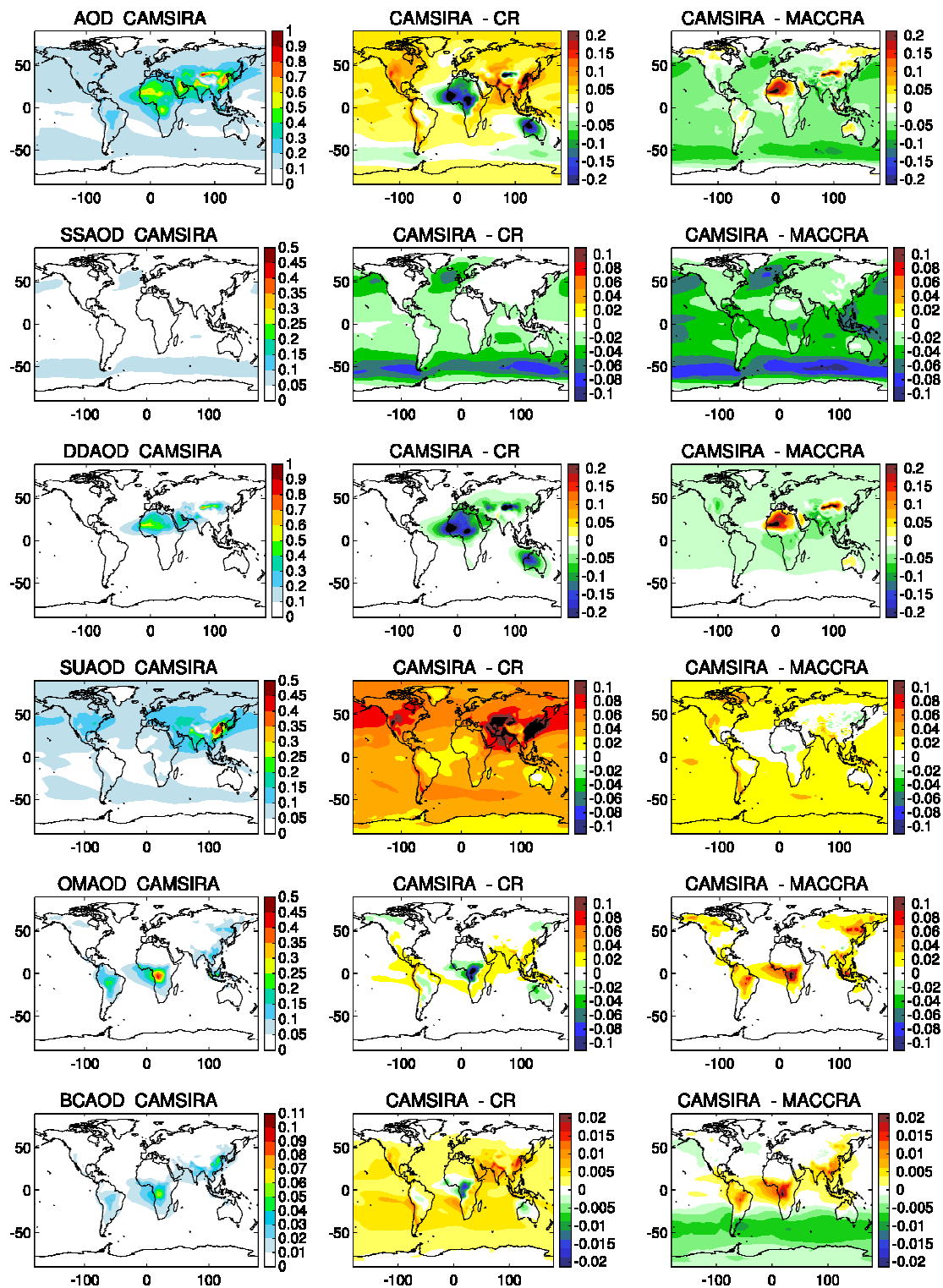
1992

1993

1994

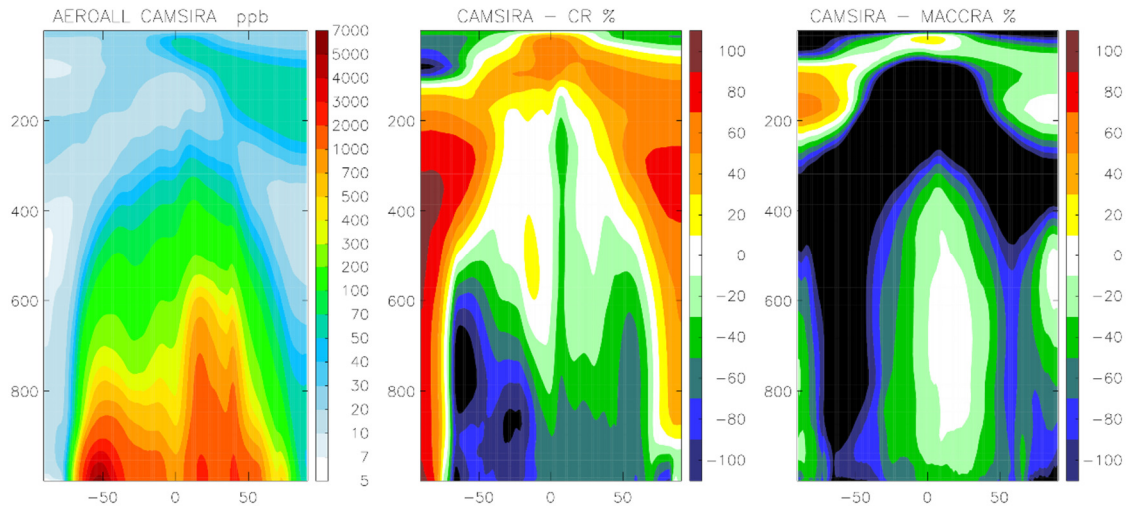
Figure 7 Globally average of total AOD (550 nm) and species AOD (left) and global total and species and burden in Tg (right) of sea salt (SS), desert dust (DD), organic matter (OM), black carbon (BC) and sulphate aerosol (SO<sub>4</sub>) for CAMSiRA (red), CR (blue) and MACCRA (green) and the median of the AeroCom model inter-comparison (yellow, Kinne et al., 2006 and Textor et al., 2006).

1995



1996  
 1997  
 1998  
 1999  
 2000

Figure 8 Total average AOD (row 1, scale max 1.0), AOD of desert dust (row 2, 1.0), sea salt (row 3, 0.5), sulphate (row 4, 0.5), organic matter (row 5, 0.5) and black carbon (row 6, 0.11) of CAMSIRA (average 2003–2015, left) and differences against CR (average 2003–2015, middle) and MACCRA (average 2003–2012, right).



2001

2002

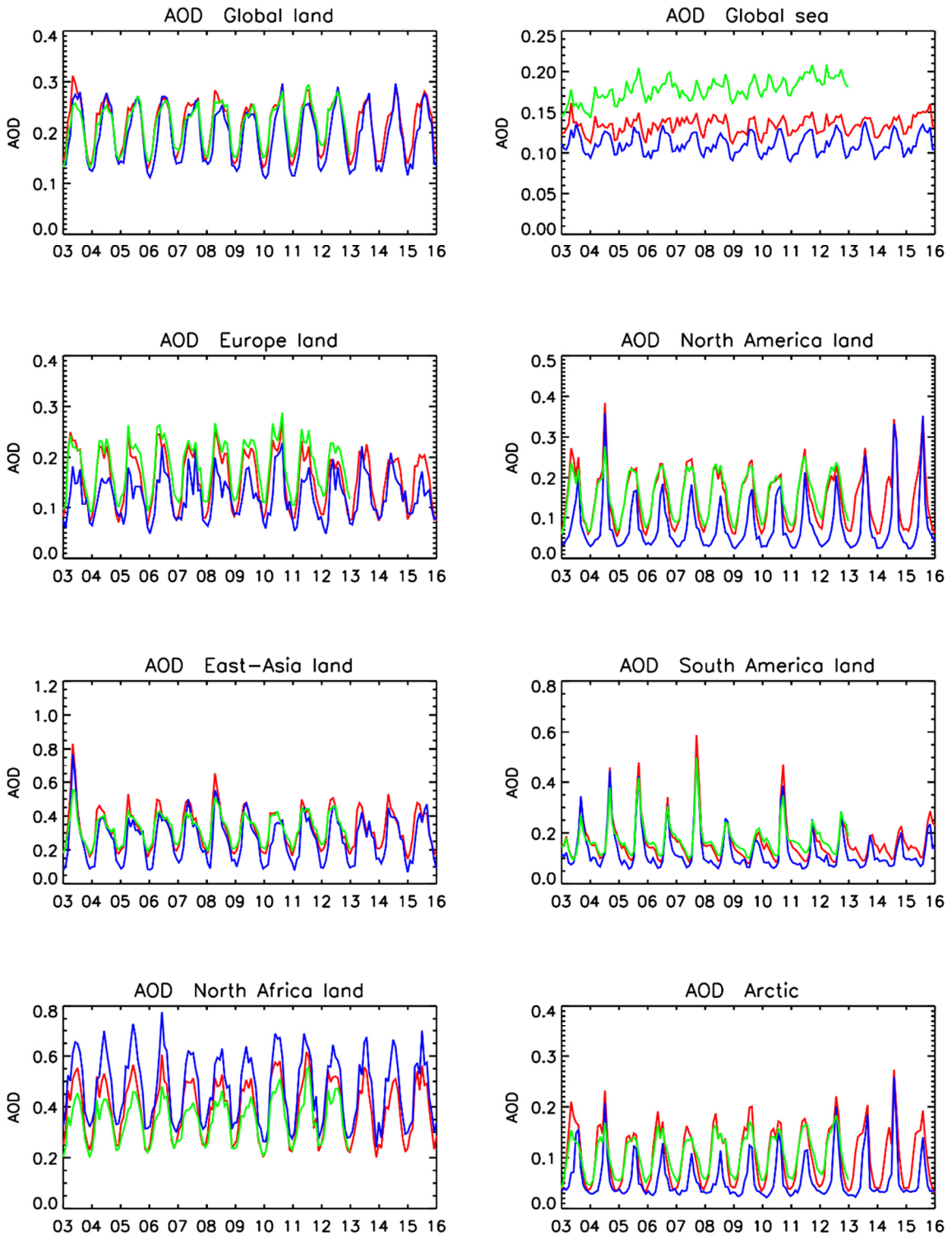
2003

2004

*Figure 9 Zonally averaged total aerosol mass mixing ratio ( $10^{-9}\text{kg/kg}$ ) of CAMSiRA (2003–2015, left) and relative difference (%) against CR (2003–2015, middle) and MACCRA (2003–2012, right).*

2005

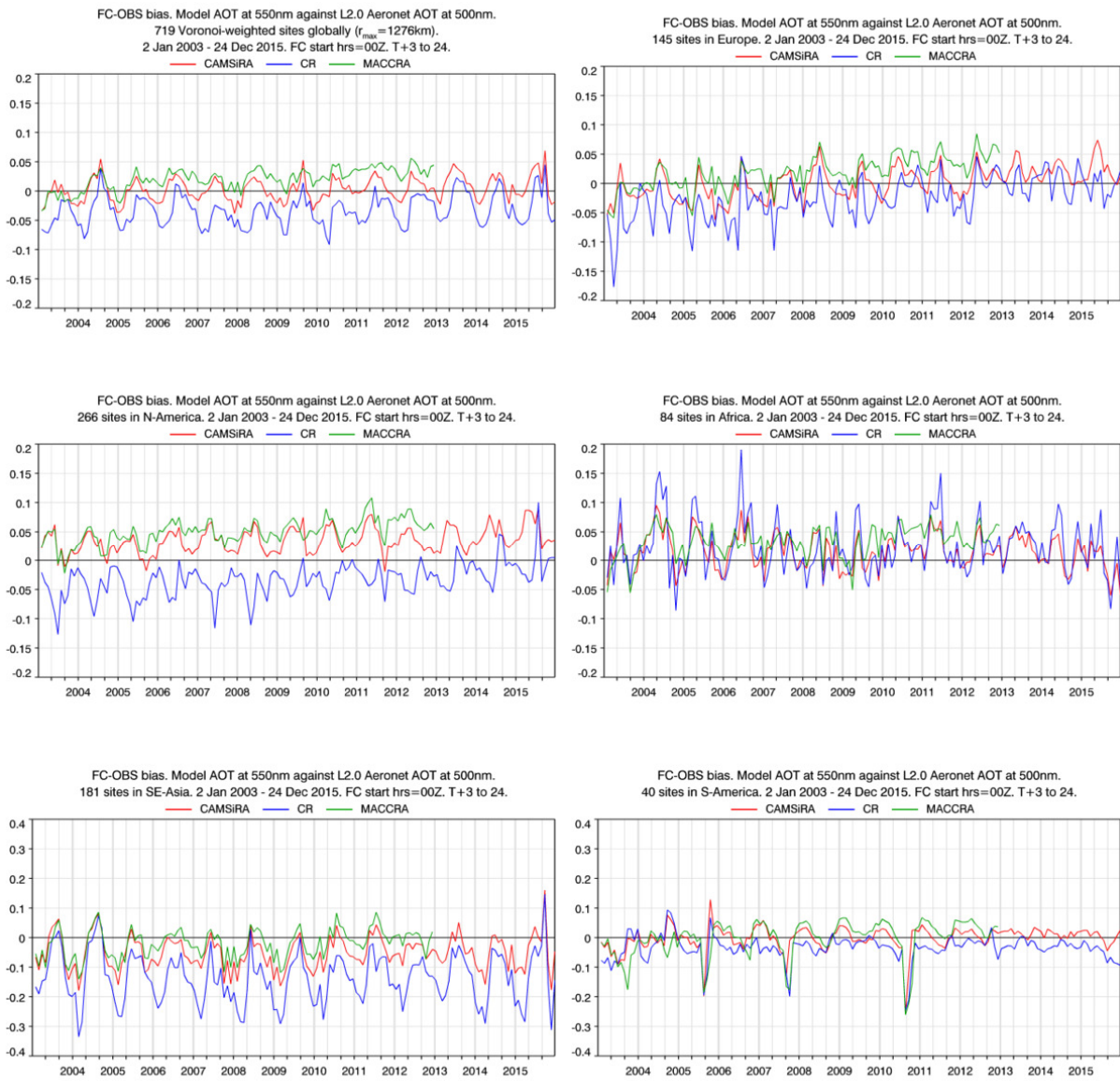




2006  
 2007  
 2008  
 2009  
 2010

Figure 10 Time series of monthly mean AOD over the whole globe (land or seas points) and for different regions (see Table 3) for the period 2003–2015 from CAMSiRA (red), CR(blue) and MACCRA(green, 2003–2012).

2011



2012

2013

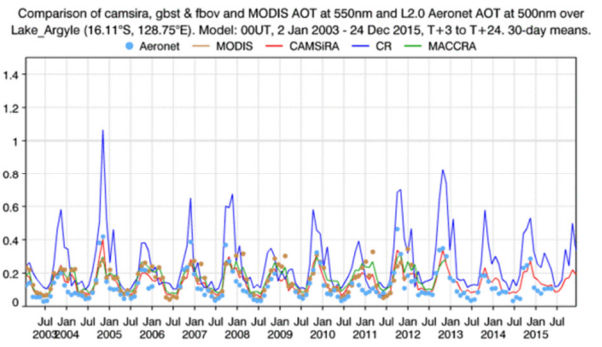
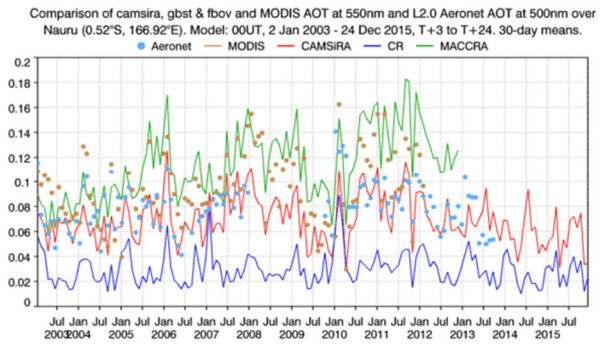
2014

2015

2016

*Figure 11 Time series of monthly mean bias against AERONET AOD observations averaged over the whole globe (top left), Europe (top right), North America (middle left), Africa (middle right), South East Asia (bottom left) and South America (bottom right) for CAMSiRA (red), CR (blue) and MACCRA (green).*

2017



2018

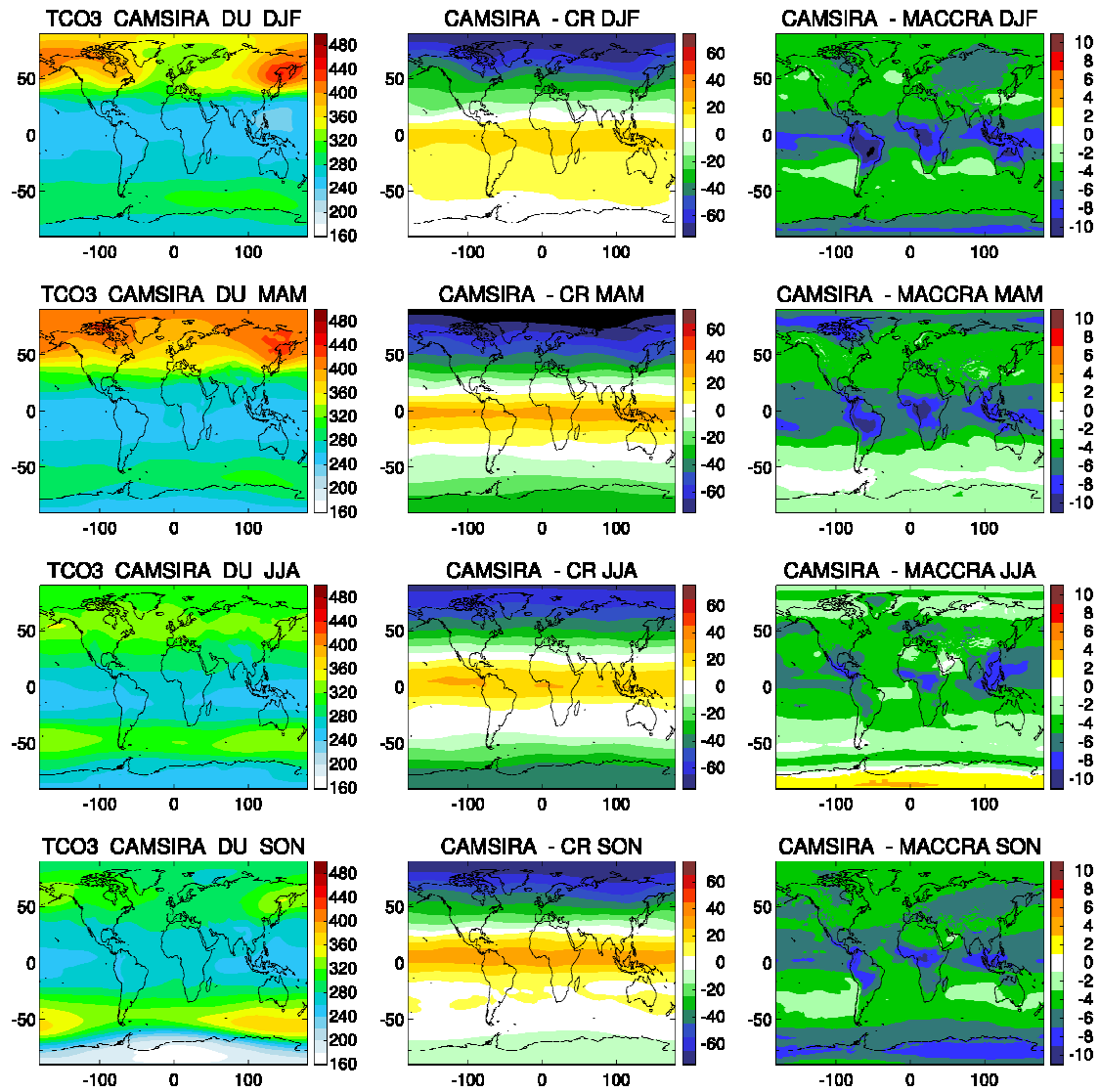
2019

2020

2021

*Figure 12 Time series of monthly mean AOD from AERONET observations (light blue dots), MODIS retrievals (brown dots) and from CAMSiRA (red), CR (blue) and MACCRA (green) at Nauru (left) and Lake Argyle (right).*

2022



2023

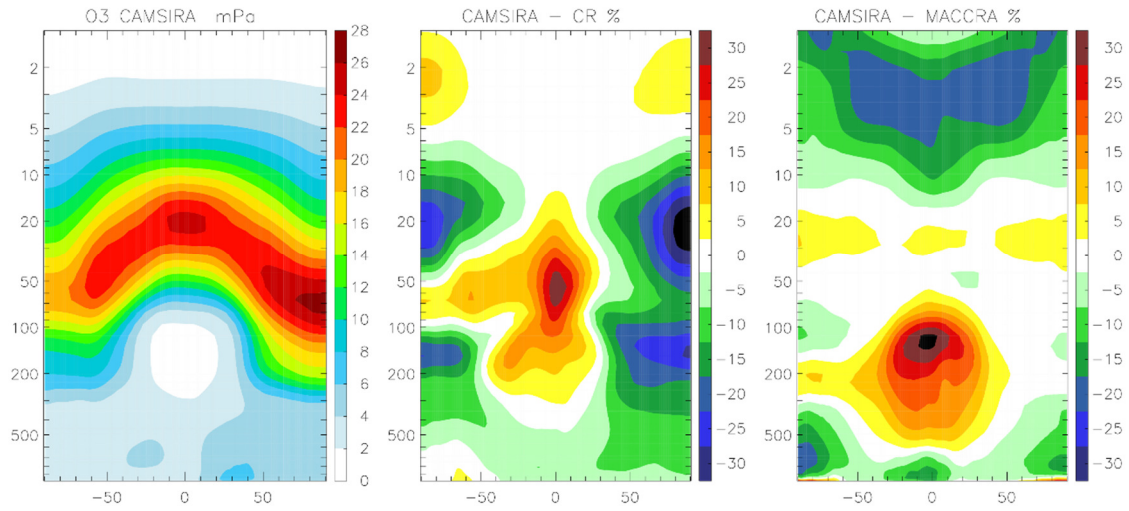
2024

2025

2026

Figure 13 Seasonal averaged TC ozone (DU) from CAMSiRA (left), difference between CAMSiRA and CR (middle) and CAMSiRA and MACCRA (right, 2003–2012, different scale) for the seasons DJF (row 1) MAM ( row 2), JJA (row 3) and SON (row 4).

2027



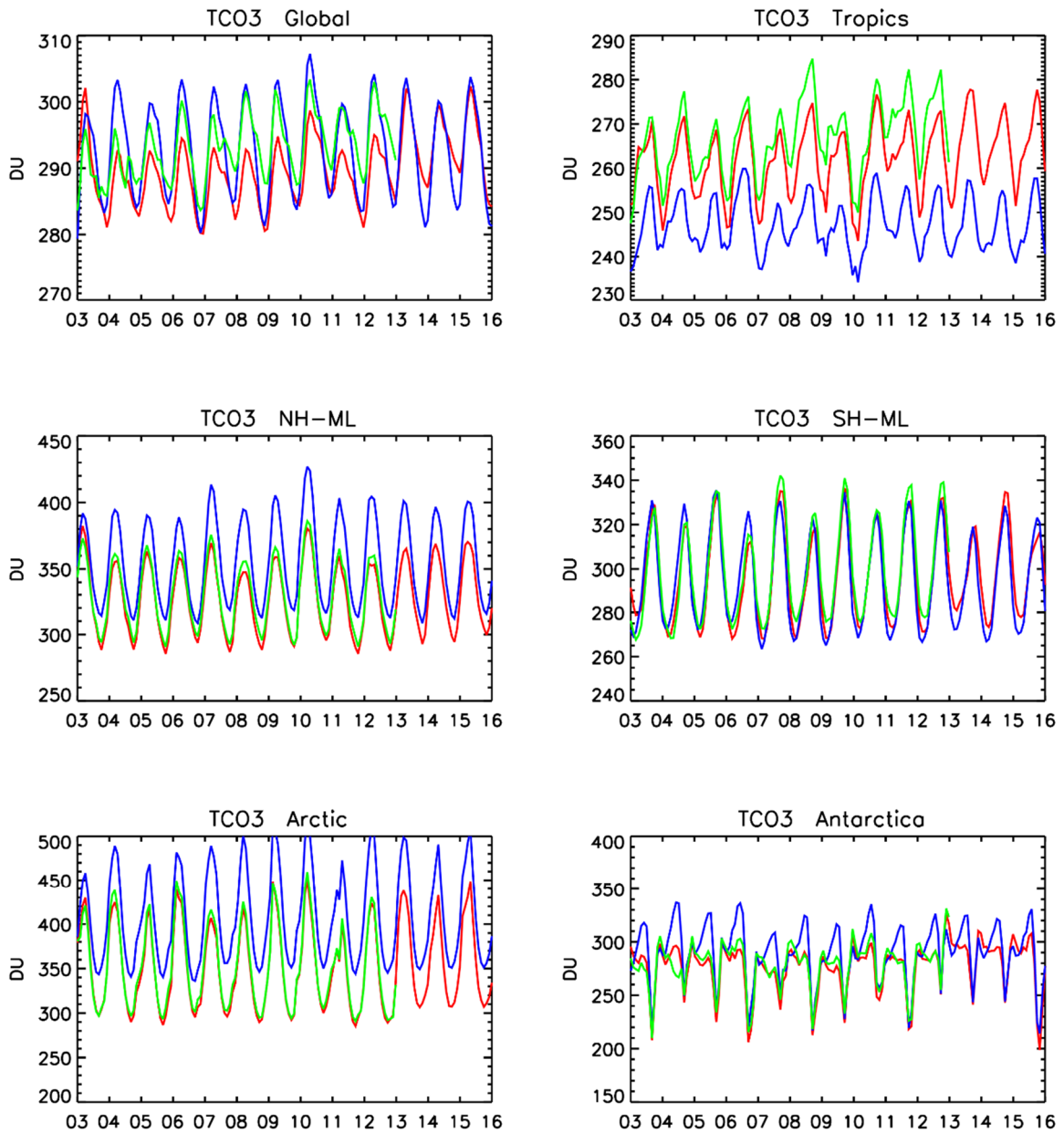
2028

2029

2030

*Figure 14 Zonally averaged ozone partial pressure (mPa) of CAMSiRA (2003–2015, left) and relative difference (%) against CR (2003–2015, middle) and MACCRA (2003–2012)*

2031



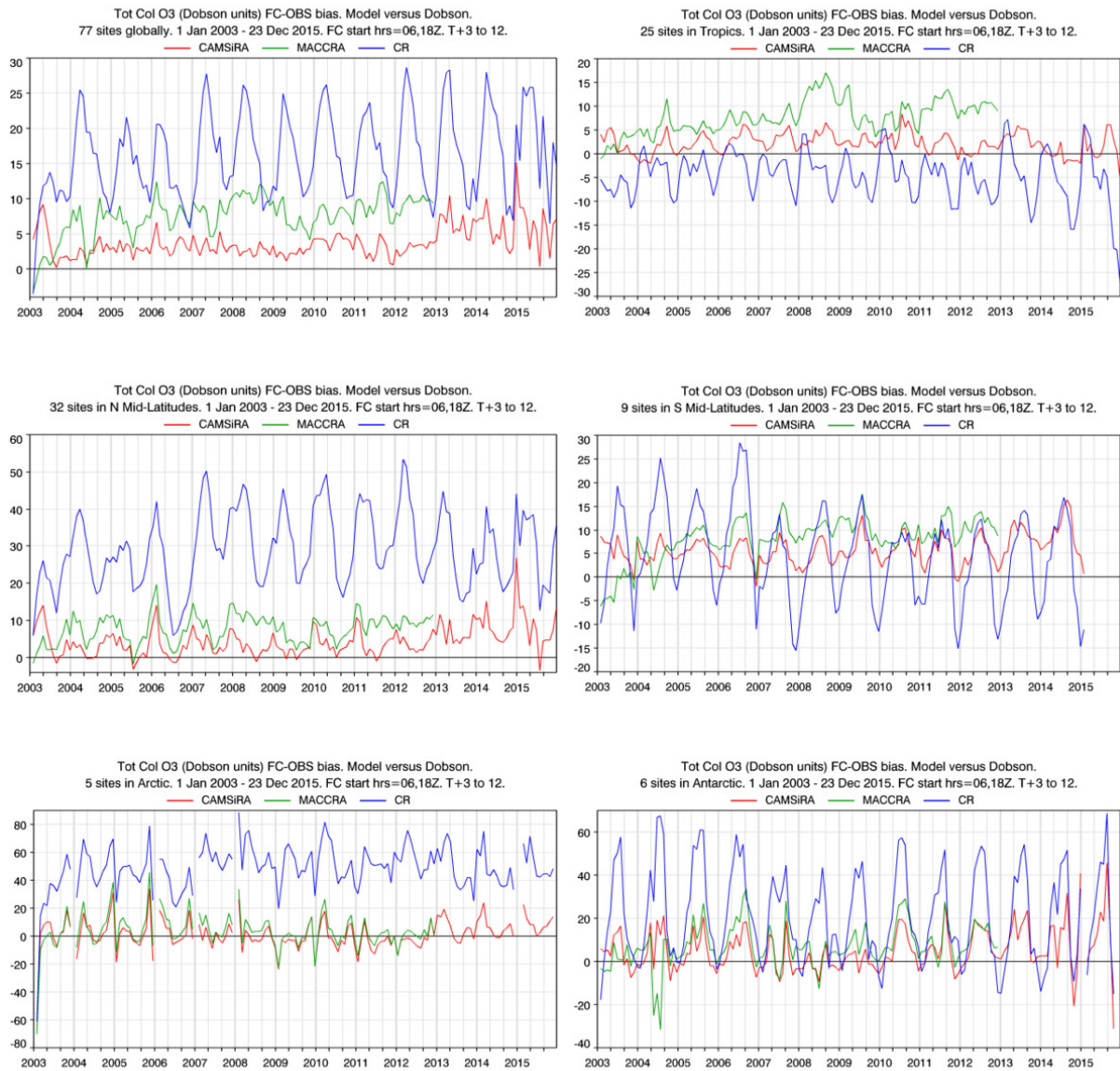
2032

2033

2034

*Figure 15 Monthly ozone TC (DU) area averaged over different regions (see Table 3) from CAMSiRA (black), CR (blue) and MACCRA (green) for 2003–2015.*

2035



2037

2038

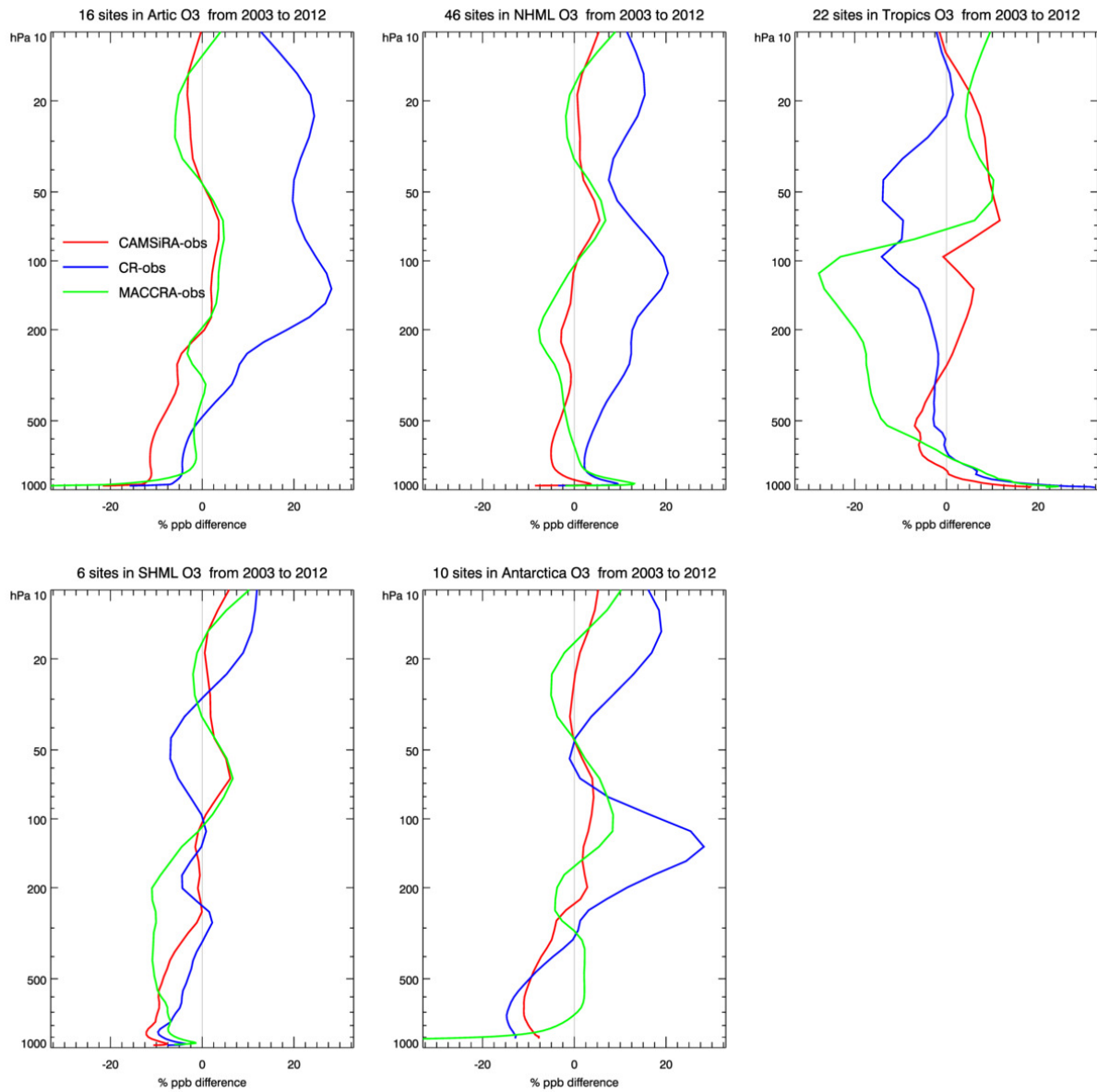
2039

2040

2041

Figure 16 Time series of monthly mean bias in DU against WOUDC Dobson sun photometers for the globe (top left), the tropics (top right), NH mid-latitudes (middle left), SH mid-latitudes (middle right), the Arctic (bottom left) and Antarctica (bottom right) for CAMSIRA (red), CR(blue) and MACCRA (green).

2042



2043

2044

2045

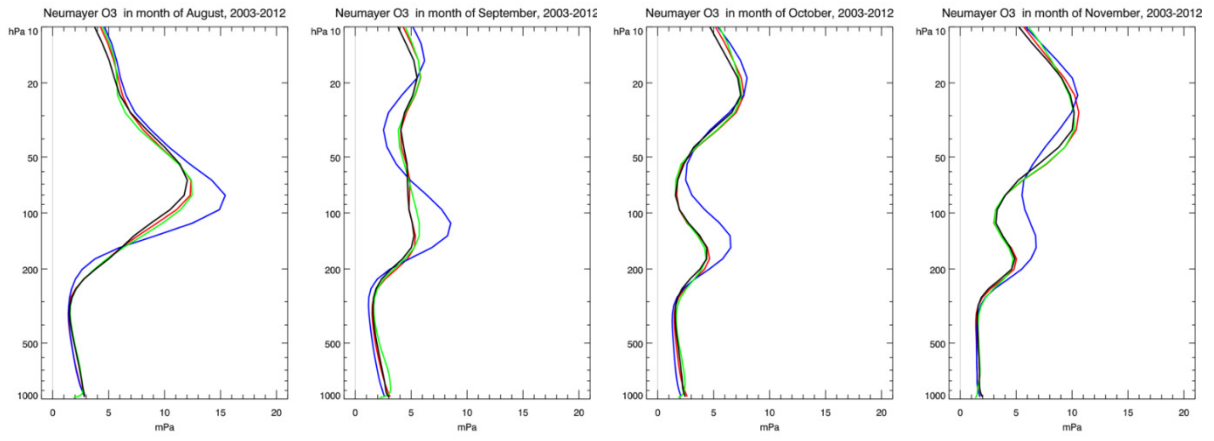
2046

2047

*Figure 17 Mean relative bias of CAMSiRA (red), MACCRA (green) and CR (blue) against ozone sondes in the Arctic (top left), NH mid-latitudes (top middle), Tropics (top right), SH-mod-latitudes (bottom left) and Antarctica (bottom middle) for the period 2003–2012.*

2048





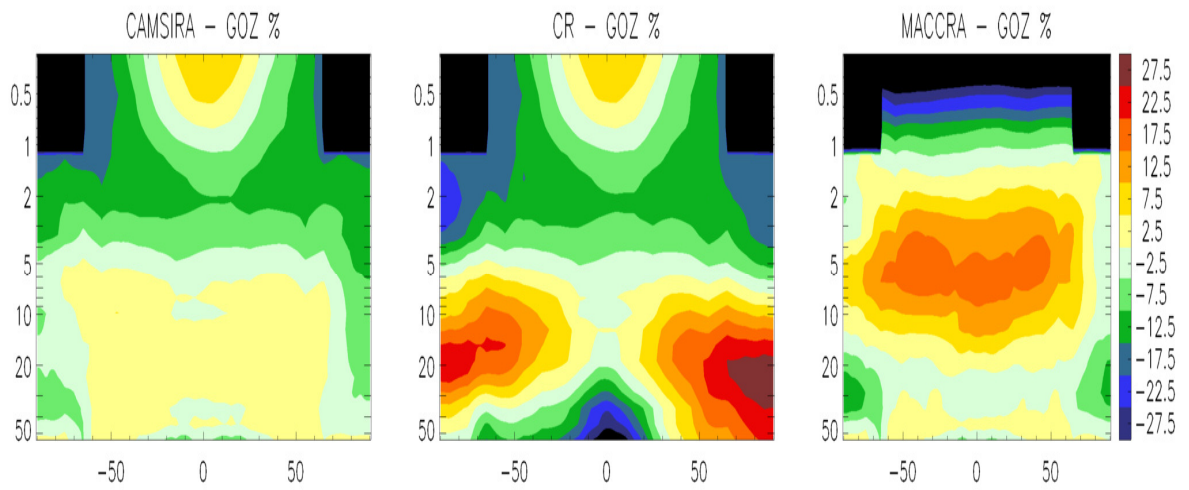
2049

2050

2051

*Figure 18 Monthly mean ozone profiles (mPa) at Neumayer Station from ozone sondes, of CAMSiRA (red), MACCRA (green) and CR (blue) for August to November (2003–20012).*

2052



2053

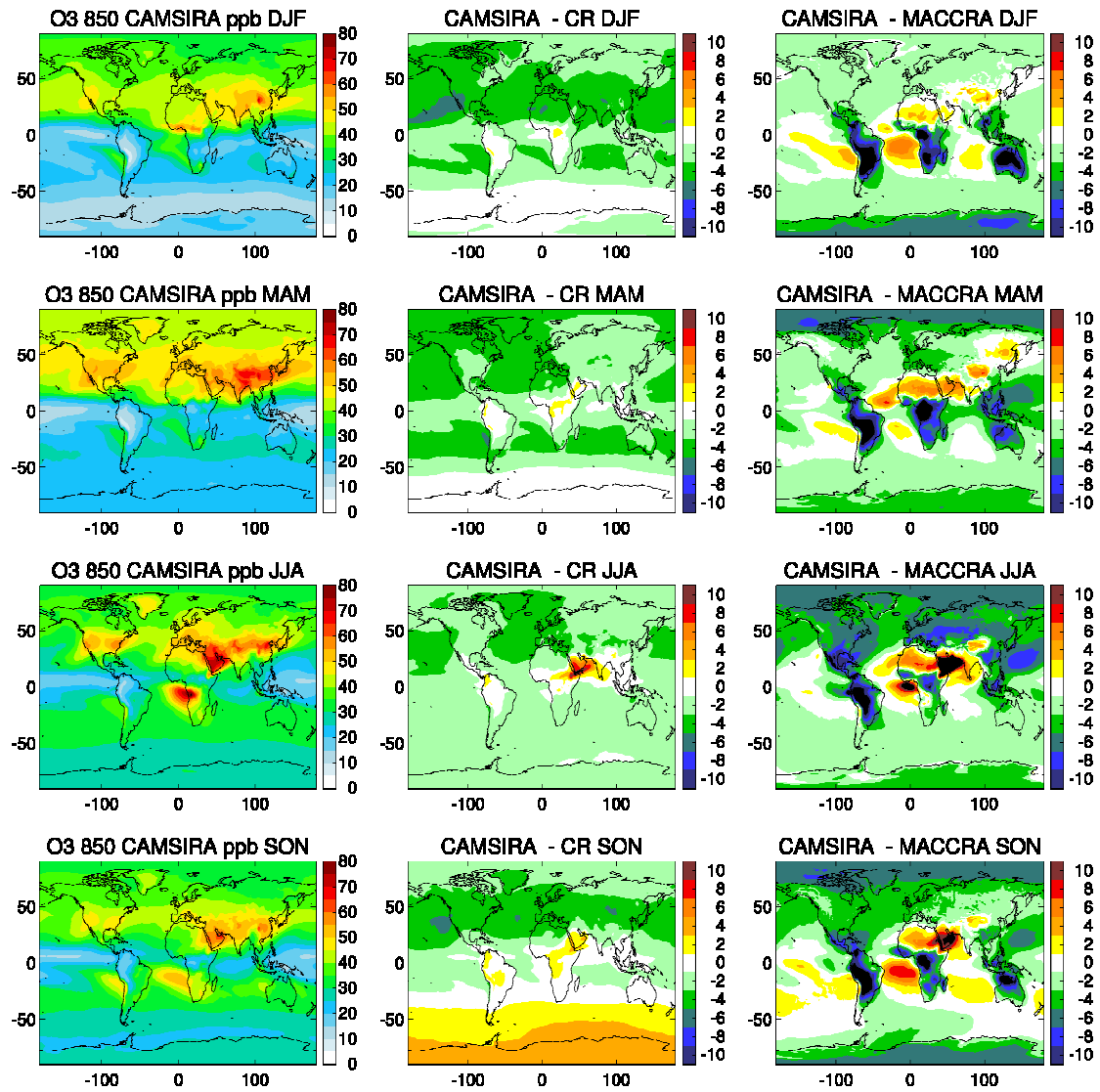
2054

*Figure 19 Cross sections (50–0.3 hPa) of the relative biases of zonally averaged ozone (%) of CAMSiRA (left), CR (middle) and MACCRA (right) against the GOZCARDS product (GOZ) for the period 2005–2012.*

2055

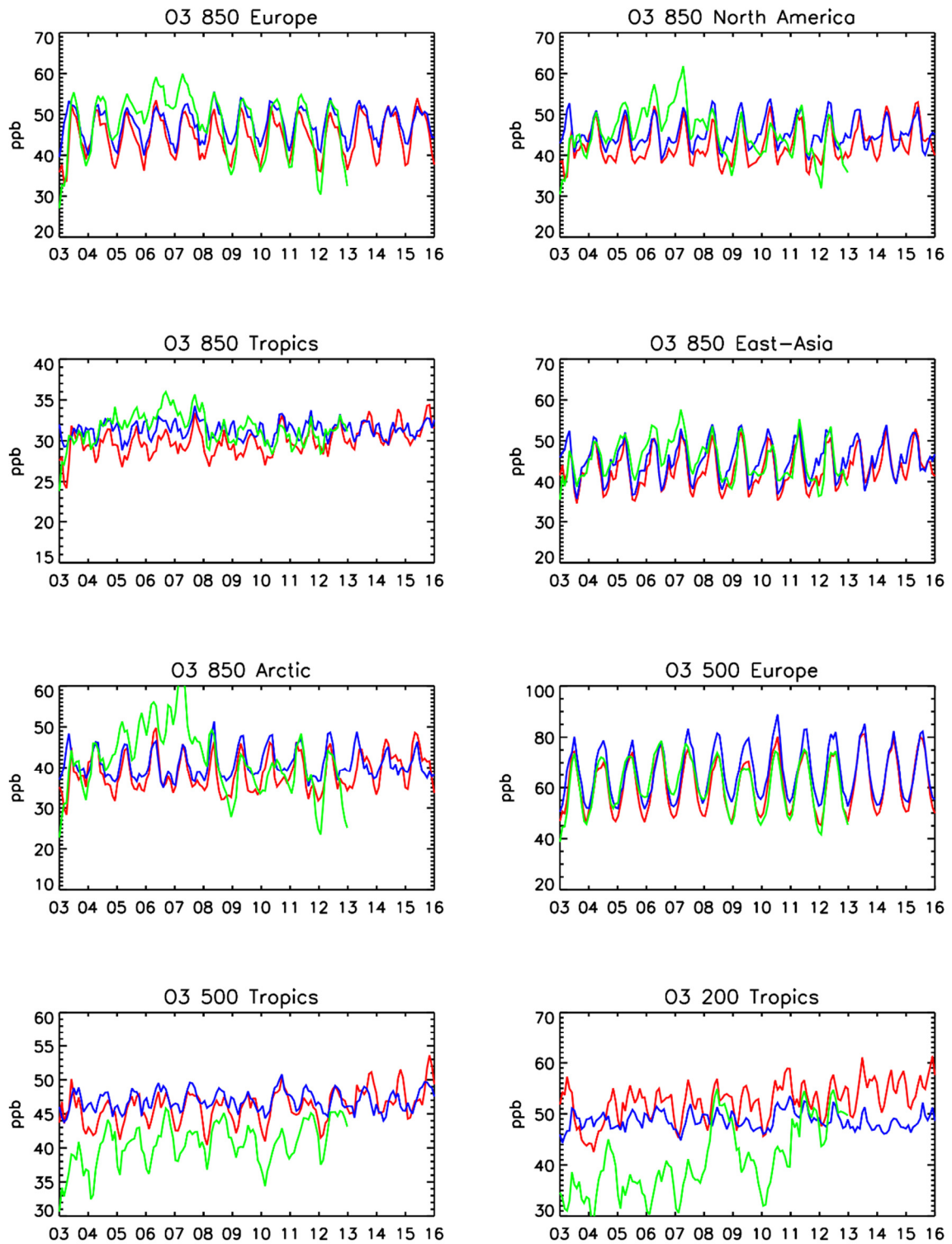
2056

2057



2058  
 2059  
 2060  
 2061

Figure 20 Seasonal averaged ozone at 850 hPa (ppb) from CAMSiRA (left), difference between CAMSIRA and CR (middle) and CAMSiRA and MACCRA (right, 2003–2012) for the season DJF (row 1), MAM ( row 2 ), JJA (row 3) and SON ( row 4).



2062

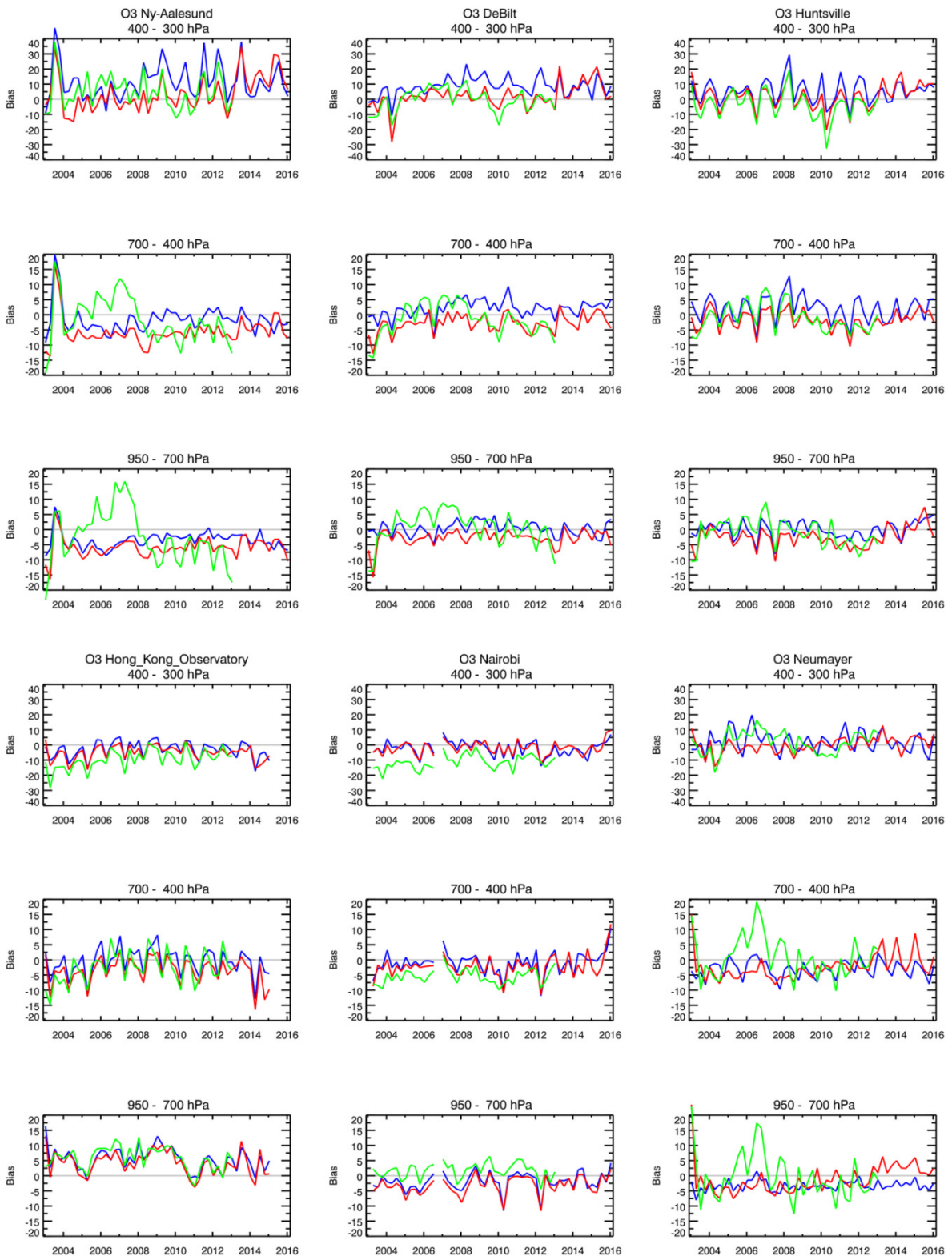
2063

2064

2065

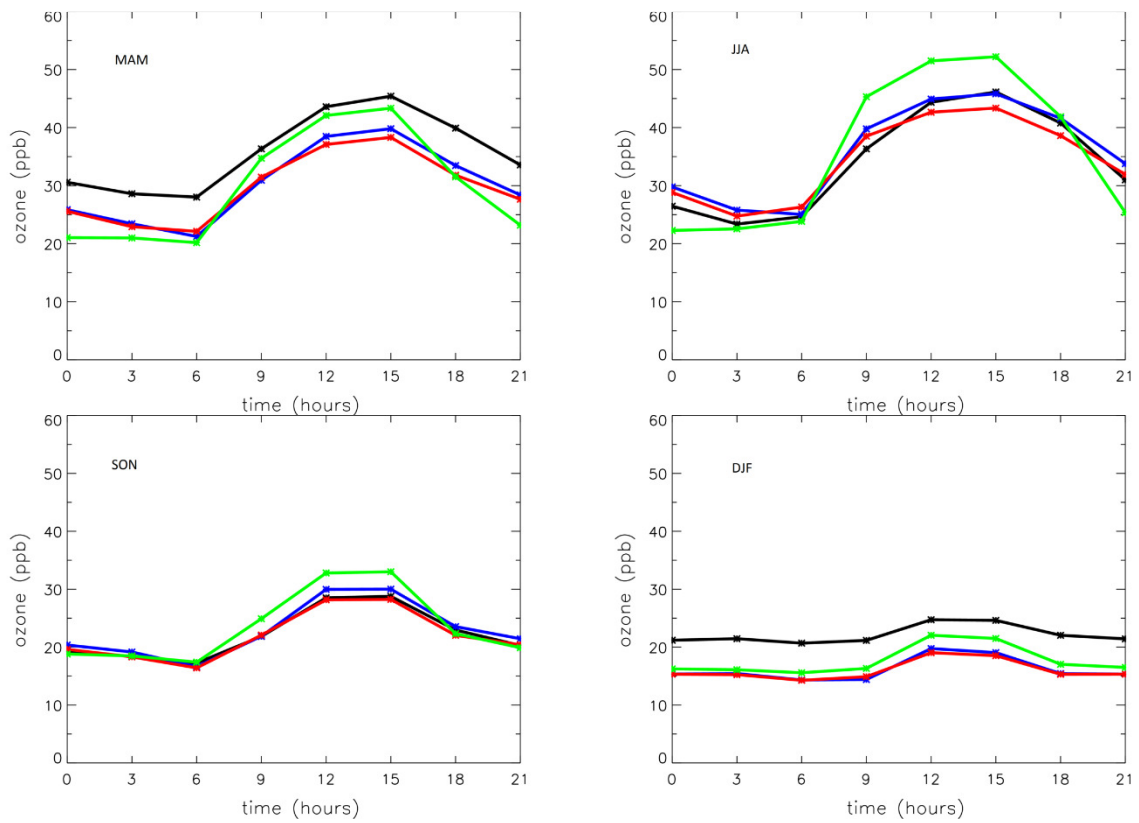
2066

Figure 21 Monthly ozone volume mixing ratio at 850, 500 and 200 hPa over different regions (see Table 3) from CAMSiRA (red), CR (blue) and MACCRA (green) for 2003–2015.



2067  
 2068  
 2069  
 2070  
 2071

Figure 22 Time series of seasonal mean ozone bias in ppb in the pressure ranges 950-700, 700-400 and 400-300 hPa against ozone sondes at Ny-Ålesund, DeBilt, Huntsville, Hong Kong Observatory, Nairobi and Neumayer station for CAMSiRA (red), CR (blue) and MACCRA (green).



2072

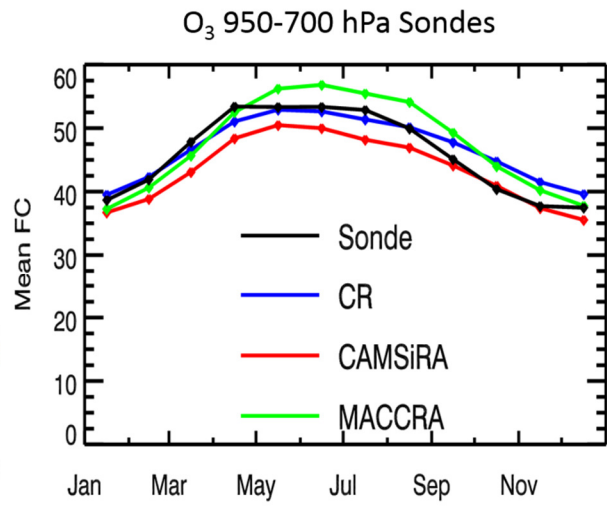
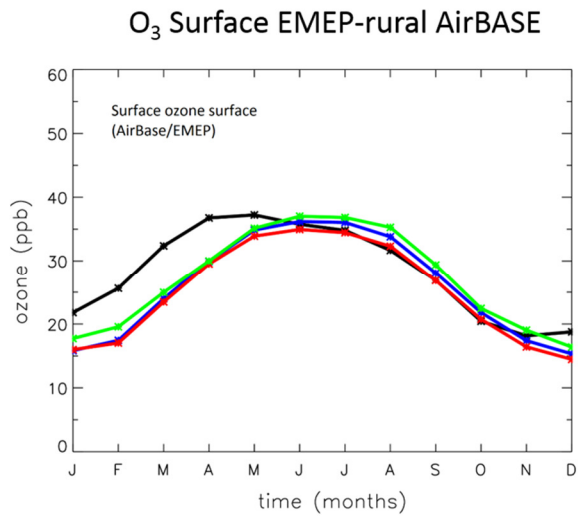
2073

2074

2075

*Figure 23 Average diurnal cycle of ozone at EMEP-AirBase stations in Europe (black) for the seasons MAM (top left), JJA (top right), SON (bottom left) and DJF (bottom right) for CAMSiRA (red), CR (blue) and MACCRA (green).*

2076



2077

2078

2079

2080

*Figure 24 Average seasonal cycle of surface ozone at EMEP-AirBase stations (left) and at European ozone sonde sites in the pressure range (950–700 hPa) for CAMSiRA (red), CR (blue) and MACCRA (green).*